Orbits of bright stars near the Galactic Center as a tool to test gravity theories

А.Ф. Захаров (Alexander F. Zakharov)
E-mail: zakharov@itep.ru

Bogoliubov Laboratory of Theoretical Physics
Joint Institute for Nuclear Research, Dubna, Russia

23.08.2021

Twentieth Lomonosov Conference on Elementary Particle Physics
MSU, Moscow, Russia

THE MATHEMATICAL THEORY OF BLACK HOLES

S. CHANDRASEKHAR
University of Chicago

Clarendon Press • Oxford
Oxford University Press • New York
1983

PROLOGUE

The black holes of nature are the most perfect macroscopic objects there are in the universe: the only elements in their construction are our concepts of space and time. And since the general theory of relativity provides only a single unique family of solutions for their descriptions, they are the simplest objects as well.

The unique two-parameter family of solutions which describes the space-time around black holes is the Kerr family discovered by Roy Patrick Kerr in July, 1963. The two parameters are the mass of the black hole and the angular momentum of the black hole. The static solution, with zero angular momentum, was discovered .by Karl Schwarzschild in December, 1915. A study of the black holes of nature is then a study of these solutions. It is to this study that this book is devoted.

EPILOGUE

There is no excellent beauty that hath not some strangeness in the proportion.
Francis Bacon
Beauty is the proper conformity of the parts to one another and to the whole.
Werner Heisenberg

The author had occasion to ask Henry Moore how one should view sculptures: from afar or from near by. Moore's response was that the greatest sculptures can be viewed—indeed, should be viewed—from all distances, since new aspects of beauty will be revealed at every scale. Moore cited the sculptures of Michelangelo as examples: from the excellence of their entire proportion to the graceful delicacy of the fingernails. The mathematical perfectness of the black holes of Nature is, similarly, revealed at every level by some strangeness in the proportion in conformity of the parts to one another and to the whole.

- Ya. B. Zeldovich: I dislike the no hair theorem

The Royal Swedish Academy of Sciences has decided to award the Nobel Prize in Physics 2020 to Roger Penrose, University of Oxford, UK, Reinhard Genzel, Max Planck Institute for Extraterrestrial Physics, Garching, Germany and University of California, Berkeley, USA, and Andrea Ghez, University of California, Los Angeles, USA.

With one half to **Roger Penrose**, University of Oxford, UK

*"**for the discovery that black hole formation is a robust prediction of the general theory of relativity"***

and the other half jointly to

Reinhard Genzel, Max Pla nck Institute for Extraterrestrial Physics, Garching, Germany and University of California, Berkeley, USA, and **Andrea Ghez**, University of California, Los Angeles, USA

*"**for the discovery of a supermassive compact object at the centre of our galaxy"***

Black holes and the Milky Way's darkest secret

Three Laureates share this year's Nobel Prize in Physics for their discoveries about one of the most exotic phenomena in the universe, the black hole. Roger Penrose showed that the general theory of relativity leads to the formation of black holes. Reinhard Genzel and Andrea Ghez discovered that an invisible and extremely heavy object governs the orbits of stars at the centre of our galaxy. A supermassive black hole is the only currently known explanation.

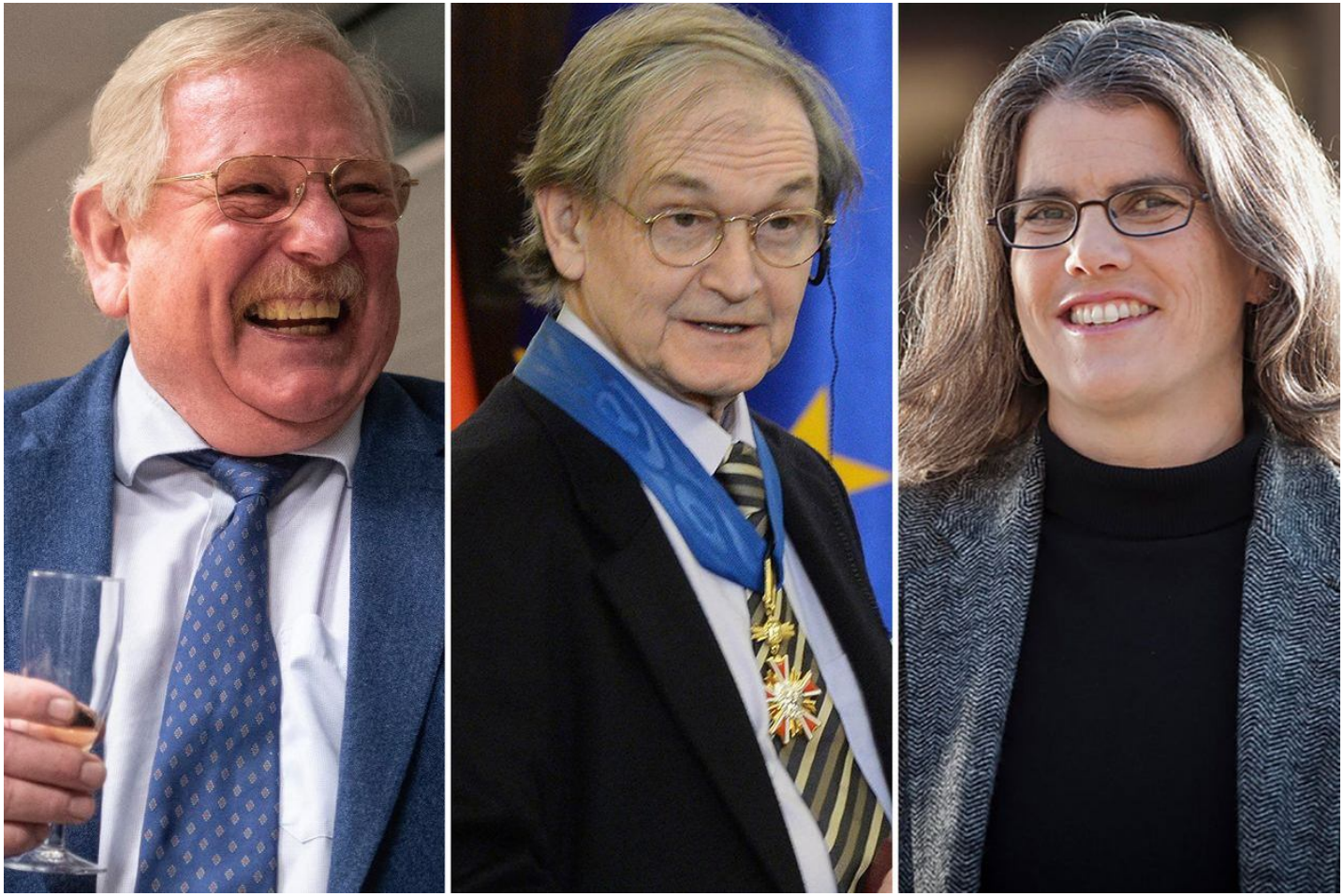

“The discoveries of this year’s Laureates have broken new ground in the study of compact and supermassive objects. But these exotic objects still pose many questions that beg for answers and motivate future research. Not only questions about their inner structure, but also questions about **how to test our theory of gravity under the extreme conditions in the immediate vicinity of a black hole**”, says David Haviland, chair of the Nobel Committee for Physics.

Outline of my talk

- Nobel prize in Physics in 2020
- Introduction
- Bright star trajectories around BH at GC as a tool to evaluate BH parameters and DM cluster
- Constraints on massive graviton theories
- Forecasts for graviton mass improvements
- Constraints on tidal charge
- Applications for current and forthcoming observations
- Conclusions

References

- AFZ, F. De Paolis, G. Ingrosso, and A. A. Nucita, New Astronomy Reviews, **56**, 64 (2012).
- D. Borka, P. Jovanovic, V. Borka Jovanovic and AFZ, Physical Reviews D, **85**, 124004 (2012).
- D. Borka, P. Jovanovic, V. Borka Jovanovic and AFZ, JCAP **11**, 050 (2013).
- AFZ, Physical Reviews D **90**, 062007 (2014).
- AFZ, D. Borka, P. Jovanovic, V. Borka Jovanovic, Advances in Space Research 54, 1108 (2014).
- AFZ, J Astrophys. Astron. **36**, 539 (2015)
- AFZ , P. Jovanovic, D. Borka, V. Borka Jovanovic, gr-qc: 1605.00913v; JCAP (2016)
- AFZ, P.Jovanovic, D. Borka, and V. Borka Jovanovic, JCAP (2018).
- AFZ, EPJ C (2018)
- AFZ, IJMPD (2019)
- P. Jovanovic, D. Borka, V. Borka Jovanovic, AFZ, EJPD (2021)

Three Nobel prizes in last four years (2017, 2019, 2020)

- LIGO-Virgo: BBHs, BNS (kilonova) GW 170817;
- GRAVITY, Keck and new tests of GR (gravitational redshift for S2 near its periapsis passage)
- EHT and M87* images
- The confirmation of relativistic precession for S2 (GRAVITY)

Reinhard Genzel, Prof. Dr.
Max Planck Institute for Extraterrestrial Physics, Garching

Curriculum Vitae

Born on March 24, 1952 in Bad Homburg v.d.H. Study of physics Bonn Univ., doctorate Max Planck Institute for Radioastronomy Bonn (1978), Postdoctoral Fellow, Harvard-Smithsonian Center for Astrophysics (1978-1980), Cambridge, MA, Associate Professor of Physics and Associate Research Astronomer, Space Sciences Laboratory, University of California, Berkeley (1981- 1985), Full Professor of Physics, University of California, Berkeley (1985-1986), Director and Scientific Member at the Max Planck Institute for Extraterrestrial Physics (since 1986), Honorary Professor Munich Univ. (since 1988), Full Professor of Physics University of California Berkeley (since 1999).

American citizen. Born 1965 in New York City, NY, USA. Ph.D. 1992 at California Institute of Technology, Pasadena, CA, USA. Professor at University of California, Los Angeles, CA, USA.

Four woman against more than 200 men

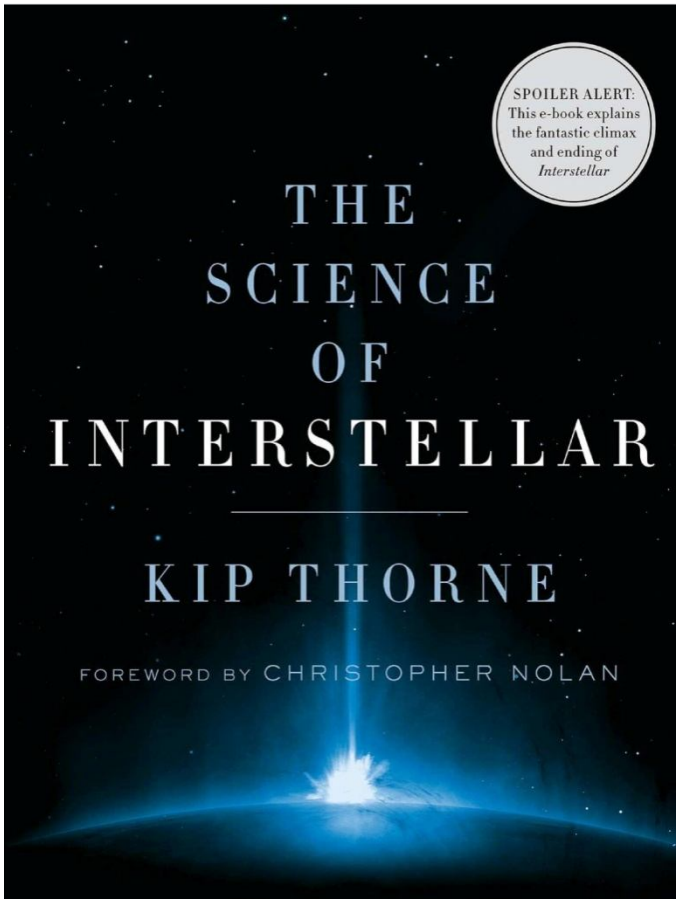
SPOILER ALERT:
This e-book explains
the fantastic climax
and ending of
Interstellar
THE
SCIENCE
OF
INTERSTELLAR
KIP THORNE
FOREWORD BY CHRISTOPHER NOLAN

deduced the spinning hole's "Kerr metric." And in the early 1970s Stephen Hawking and others deduced a set of laws that black holes must obey when they swallow stars, collide and merge, and feel the tidal forces of other objects.

Black holes surely do exist. Einstein's relativistic laws insist that, when a massive star exhausts the nuclear fuel that keeps it hot, then the star must implode. In 1939, J. Robert Oppenheimer and his student Hartland Snyder used Einstein's laws to discover that, if the implosion is precisely spherical, the imploding star *must* create a black hole around itself, and then create a singularity at the hole's center, and then get swallowed into the singularity. No matter is left behind. None whatsoever. The resulting black hole is made entirely from warped space and time. Over the decades since 1939, physicists using Einstein's laws have shown that if the imploding star is deformed and spinning, it will also produce a black hole. Computer simulations reveal the full details.

Astronomers have seen compelling evidence for many black holes in our universe. The most beautiful example is a massive black hole at the center of our Milky Way galaxy. Andrea Ghez of UCLA, with a small group of astronomers that she leads, has monitored the motions of stars around that black hole (Figure 5.8). Along each orbit, the dots are the star's position at times separated by one year. I marked the black hole's location by a white, five-pointed symbol. From the stars' observed motions, Ghez has deduced the strength of the hole's gravity. Its gravitational pull, at a fixed distance, is 4.1 million times greater than the Sun's pull at that distance. This means the black hole's mass is 4.1 million times greater than the Sun's!

Fig 5.7. Black-hole scientists. *Left to right*: Karl Schwarzschild (1873–1916), Roy Kerr (1934–), Stephen W. Hawking (1942–), J. Robert Oppenheimer (1904–1967), and Andrea Ghez (1965–).

Figure 5.9 shows where this black hole is on the night sky in summer. It is to the lower right of the constellation Sagittarius, the teapot, at the × labeled "Galactic Center."

A massive black hole inhabits the core of nearly every big galaxy in our

Home
News
Features
Columns & blogs
Archive Archive
Specials
In focus
X chromosome
Future computing
Stem cells
Bird flu
Mars
GM crops
Stories by subject

NEWS CHANNELS
My news
Biotechnology
Careers
Drug discovery
Earth and environment
Medical Research
Physical Sciences

Feedback
About this site
About us
For librarians

TOP STORIES

Air pollution influences crop disease
04 April 2005
Hunters win hike in polar bear quota
04 April 2005
Genetic patch treats 'bubble-boy' disease
03 April 2005
Transgenic cows have

NEWS

Published online: 31 March 2005; | doi:10.1038/news050328-8

Black holes 'do not exist'

Philip Ball

These mysterious objects are dark-energy stars, physicist claims.

Black holes are staples of science fiction and many think astronomers have observed them indirectly. But according to a physicist at the Lawrence Livermore National Laboratory in California, these awesome breaches in space-time do not and indeed cannot exist.

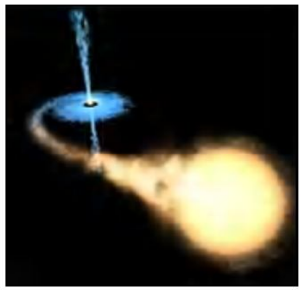

Black holes, such as the one pictured in this artist's impression, may in fact be pockets of 'dark energy'.

Over the past few years, observations of the motions of galaxies have shown that some 70% the Universe seems to be composed of a strange 'dark energy' that is driving the Universe's accelerating expansion.

George Chapline thinks that the collapse of the massive stars, which was long believed to generate black holes, actually leads to the formation of stars that contain dark energy. "It's a near certainty that black holes don't exist," he claims.

Black holes are one of the most celebrated predictions of Einstein's general theory of relativity, which explains gravity as the warping of space-time caused by massive objects. The theory suggests that

ANNALS OF MATHEMATICS
Vol. 40, No. 4, October, 1939

ON A STATIONARY SYSTEM WITH SPHERICAL SYMMETRY CONSISTING OF MANY GRAVITATING MASSES

BY ALBERT EINSTEIN

(Received May 10, 1939)

If one considers Schwarzschild's solution of the static gravitational field of spherical symmetry

$$(1) \qquad ds^2 = -\left(1 + \frac{\mu}{2r}\right)^4 (dx_1^2 + dx_2^2 + dx_3^2) + \left(\frac{1 - \frac{\mu}{2r}}{1 + \frac{\mu}{2r}}\right)^2 dt^2$$

it is noted that

$$g_{44} = \left(\frac{1 - \frac{\mu}{2r}}{1 + \frac{\mu}{2r}}\right)^2$$

vanishes for $r = \mu/2$. This means that a clock kept at this place would go at the rate zero. Further it is easy to show that both light rays and material particles take an infinitely long time (measured in "coördinate time") in order to reach the point $r = \mu/2$ when originating from a point $r > \mu/2$. In this sense the sphere $r = \mu/2$ constitutes a place where the field is singular. (μ represents the gravitating mass.)

There arises the question whether it is possible to build up a field containing such singularities with the help of actual gravitating masses, or whether such regions with vanishing g_{44} do not exist in cases which have physical reality. Schwarzschild himself investigated the gravitational field which is produced by an incompressible liquid. He found that in this case, too, there appears a region with vanishing g_{44} if only, with given density of the liquid, the radius of the field-producing sphere is chosen large enough.

This argument, however, is not convincing; the concept of an incompressible liquid is not compatible with relativity theory as elastic waves would have to travel with infinite velocity. It would be necessary, therefore, to introduce a compressible liquid whose equation of state excludes the possibility of sound signals with a speed in excess of the velocity of light. But the treatment of any such problem would be quite involved; besides, the choice of such an equation of state would be arbitrary within wide limits, and one could not be sure that thereby no assumptions have been made which contain physical impossibilities.

One is thus led to ask whether matter cannot be introduced in such a way that questionable assumptions are excluded from the very beginning. In fact this can be done by choosing, as the field-producing mass, a great number of

The following table gives μ and $2r_0$ for $M = 1$ as functions of σ_0 (approximately):

σ_0	μ	$2r_0$
0.	1.	∞
.05	.988	19.76
.1	.948	9.48
.15	.97	6.56
.2	1.13	5.65
.23	1.32	5.63
.25	1.82	7.40
.26	2.63	10.1
.268	∞	∞

When the cluster is contracted from an infinite diameter its mass decreases at the most about 5%. This minimal mass will be reached when the diameter $2r_0$ is about 9. The diameter can be further reduced down to about 5.6, but only by adding enormous amounts of energy. It is not possible to compress the cluster any more while preserving the chosen mass distribution. A further addition of energy enlarges the diameter again. In this way the energy content, i.e. the gravitating mass of the cluster, can be increased arbitrarily without destroying the cluster. To each possible diameter there belong two clusters (when the number of particles is given) which differ with respect to the particle velocity.

Of course, these paradoxical results are not represented by anything in physical nature. Only that branch belonging to smaller σ_0 values contains the cases bearing some resemblance to real stars, and this branch only for diameter values between ∞ and $9M$.

The case of the cluster of the shell type, discussed earlier in this paper, behaves quite similarly to this one, despite the different mass distribution. The shell type cluster, however, does not contain a case with infinite μ, given a finite M.

The essential result of this investigation is a clear understanding as to why the "Schwarzschild singularities" do not exist in physical reality. Although the theory given here treats only clusters whose particles move along circular paths it does not seem to be subject to reasonable doubt that more general cases will have analogous results. The "Schwarzschild singularity" does not appear for the reason that matter cannot be concentrated arbitrarily. And this is due to the fact that otherwise the constituting particles would reach the velocity of light.

This investigation arose out of discussions the author conducted with Professor H. P. Robertson and with Drs. V. Bargmann and P. Bergmann on the mathematical and physical significance of the Schwarzschild singularity. The problem quite naturally leads to the question, answered by this paper in the negative, as to whether physical models are capable of exhibiting such a singularity.

THE INSTITUTE FOR ADVANCED STUDY

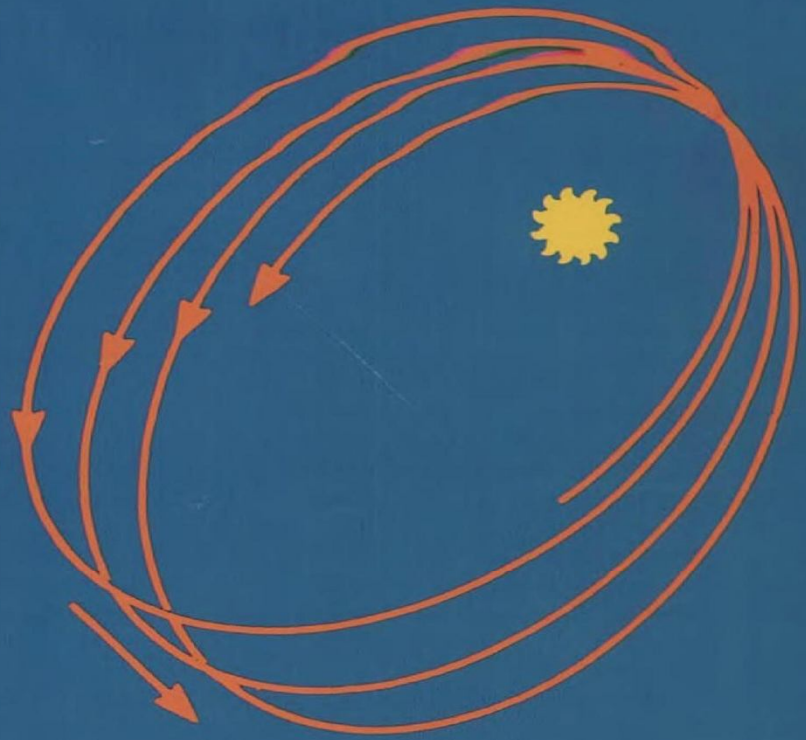

Introduction to the THEORY OF RELATIVITY

Peter Gabriel Bergmann

With a Foreword by Albert Einstein

In nature, mass is never sufficiently concentrated to permit a Schwarzschild singularity to occur in empty space. Einstein investigated the field of a system of many mass points, each of which is moving along a circular path, $r = \text{const.}$, under the influence of the field created by the ensemble.[3] If the axes of the circular paths are assumed to be oriented at random, the whole system or cluster is spherically symmetric. The purpose of the investigation was to find out whether the constituent particles can be concentrated toward the center so strongly that the total field exhibits a Schwarzschild singularity. The investigation showed that even before the critical concentration of particles is reached, some of the particles (those on the outside) begin to move with the velocity of light, that is, along zero world lines. It is, therefore, impossible to concentrate the particles of the cluster to such a degree that the field has a singularity. (The singularities connected with each individual mass point are, of course, not considered.)

Einstein chose this example so that he would not have to consider thermodynamical questions, or to introduce a pressure, for the particles of his cluster do not undergo collisions, and their individual paths are explicitly known. In this respect, Einstein's cluster has properties which are nowhere encountered in nature. Nevertheless, it appears reasonable to believe that Einstein's result can be extended to conglomerations of particles where the motions of the individual particles are not artificially restricted as in Einstein's example.

The field of an electrically charged mass point. We shall now treat a mass point which carries an electric charge. The electrostatic field will be characterized by a scalar potential φ_4, which is a function of r. The covariant components of the electromagnetic field are

$$\varphi_{4\alpha} = \varphi_{4,\alpha} = \varphi_4' x_\alpha , \qquad \varphi_{r\alpha} = 0. \tag{13.26}$$

The components of the electromagnetic stress-energy tensor are

$$\left.\begin{aligned} M_{\mu\nu} &= \frac{1}{4\pi}\left[\tfrac{1}{4} g_{\mu\nu}\varphi_{\rho\sigma}\varphi^{\rho\sigma} - \varphi_{\mu\rho}\varphi_{\nu}^{\ \rho}\right], \\ M_{44} &= -\frac{1}{8\pi}\varphi_{4\alpha}\varphi_{4\tau}g^{\alpha\tau} = \frac{1}{8\pi}(\varphi_4')^2 e^{-\sigma}, \\ M_{4\alpha} &= 0 \\ M_{r\alpha} &= \frac{1}{4\pi}\left[\tfrac{1}{2} g_{r\alpha}\varphi_{4\lambda}\varphi^{4\lambda} - \varphi_{r4}\varphi_{\alpha}^{\ 4}\right] \end{aligned}\right\} \tag{13.27}$$

Ho1

Ho2

Black holes in centers of galaxies

(L.Ho,ApJ 564,120 (2002))

Coevolution (Or Not) of Supermassive Black Holes and Host Galaxies

John Kormendy[1] and Luis C. Ho[2]

[1]Department of Astronomy, University of Texas at Austin,
2515 Speedway C1400, Austin, TX 78712-1205; email: kormendy@astro.as.utexas.edu

[2]The Observatories of the Carnegie Institution for Science,
813 Santa Barbara Street, Pasadena, CA 91101; email: lho@obs.carnegiescience.edu

Abstract

Supermassive black holes (BHs) have been found in 87 galaxies by dynamical modeling of spatially resolved kinematics. The *Hubble Space Telescope* revolutionized BH research by advancing the subject from its proof-of-concept phase into quantitative studies of BH demographics. Most influential was the discovery of a tight correlation between BH mass $M_\bullet$ and the velocity dispersion σ of the bulge component of the host galaxy. Together with similar correlations with bulge luminosity and mass, this led to the widespread belief that BHs and bulges coevolve by regulating each other's growth. Conclusions based on one set of correlations from $M_\bullet \sim 10^{9.5}\ M_\odot$ in brightest cluster ellipticals to $M_\bullet \sim 10^6\ M_\odot$ in the smallest galaxies dominated BH work for more than a decade.

New results are now replacing this simple story with a richer and more plausible picture in which BHs correlate differently with different galaxy components. A reasonable aim is to use this progress to refine our understanding of BH – galaxy coevolution. BHs with masses of $10^5 - 10^6\ M_\odot$ are found in many bulgeless galaxies. Therefore, classical (elliptical-galaxy-like) bulges are not necessary for BH formation. On the other hand, while they live in galaxy disks, BHs do not correlate with galaxy disks. Also, any $M_\bullet$ correlations with the properties of disk-grown pseudobulges and dark matter halos are weak enough to imply no close coevolution.

The above and other correlations of host galaxy parameters with each other and with $M_\bullet$ suggest that there are four regimes of BH feedback. (1) Local, secular, episodic, and stochastic feeding of small BHs in largely bulgeless galaxies involves too little energy to result in coevolution. (2) Global feeding in major, wet galaxy mergers rapidly grows giant BHs in short-duration, quasar-like events whose energy feedback does affect galaxy evolution. The resulting hosts are classical bulges and coreless-rotating-disky ellipticals. (3) After these AGN phases and at the highest galaxy masses, maintenance-mode BH feedback into X-ray-emitting gas has the primarily negative effect of helping to keep baryons locked up in hot gas and thereby keeping galaxy formation from going to completion. This happens in giant, core-nonrotating-boxy ellipticals. Their properties, including their tight correlations between $M_\bullet$ and core parameters, support the conclusion that core ellipticals form by dissipationless major mergers. They inherit coevolution effects from smaller progenitor galaxies. Also, (4) independent of any feedback physics, in BH growth modes (2) and (3), the averaging that results from successive mergers plays a major role in decreasing the scatter in $M_\bullet$ correlations from the large values observed in bulgeless and pseudobulge galaxies to the small values observed in giant elliptical galaxies.

Table 1 Mass measurements of supermassive black holes in our Galaxy, M 31, and M 32

Galaxy	D (Mpc)	σ_e (km s^{-1})	$M_\bullet$ ($M_{\rm low}, M_{\rm high}$) ($M_\odot$)	$r_{\rm infl}$ (arcsec)	σ_* (arcsec)	$r_{\rm infl}/\sigma_*$	Reference
(1)	(2)	(3)	(4)	(5)	(6)	(7)	(8)
Galaxy			4.41(3.98–4.84) e6		0.0146	2868.	Meyer et al. 2012
Galaxy			4.2 (3.9 –4.6) e6		0.0139	3013.	Yelda et al. 2011
Galaxy	0.00828	105	4.30(3.94–4.66) e6	41.9	0.0146	2868.	Genzel, Eisenhauer & Gillessen 2010
Galaxy	0.00828	105	4.30(3.94–4.66) e6	41.9	0.0146	2868.	Gillessen et al. 2009a
Galaxy			4.09(3.74–4.43) e6		0.0148	2829.	Gillessen et al. 2009b
Galaxy			4.25(3.44–4.79) e6		0.0139	3013.	Ghez et al. 2008
Galaxy			3.80(3.60–4.00) e6		0.0056	7478.	Ghez et al. 2005
Galaxy			3.7 (3.3 –4.1) e6		0.0075	5583.	Ghez et al. 2003
Galaxy			3.8 (2.3 –5.4) e6		0.0155	2702.	Schödel et al. 2002
Galaxy			2.1 (1.3 –2.8) e6		0.113	371.	Chakrabarty & Saha 2001
Galaxy			3.1 (2.6 –3.6) e6		0.26	161.	Genzel et al. 2000
Galaxy			2.7 (2.5 –2.9) e6		0.39	107.	Ghez et al. 1998
Galaxy			2.70(2.31–3.09) e6		0.39	107.	Genzel et al. 1997
Galaxy			2.55(2.12–2.95) e6		0.39	107.	Eckart & Genzel 1997
Galaxy			2.8 (2.5 –3.1) e6		2.4	17.4	Genzel et al. 1996
Galaxy			2.0 (0.9 –2.9) e6		4.9	8.5	Haller et al. 1996
Galaxy			2.9 (2.0 –3.9) e6		3.4	12.3	Krabbe et al. 1995
Galaxy			2. e6		5	8.4	Evans & de Zeeuw 1994
Galaxy			3. e6		5	8.4	Kent 1992
Galaxy			5.4 (3.9 –6.8) e6		15	2.8	Sellgren et al. 1990
M 31	0.774	169	1.4 (1.1–2.3) e8	5.75	0.053	109.	Bender et al. 2005
M 31			1.0 e8		0.297	19.4	Peiris & Tremaine 2003
M 31			6.1 (3.6–8.7) e7		0.052	111.	Bacon et al. 2001
M 31			3.3 (1.5–4.5) e7		0.297	19.4	Kormendy & Bender 1999
M 31			6.0 (5.8–6.2) e7		0.297	19.4	Magorrian et al. 1998
M 31			9.5 (7 – 10) e7		0.42	13.7	Emsellem & Combes 1997
M 31			7.5 e7		0.56	10.3	Tremaine 1995
M 31			8.0 e7		0.42	13.7	Bacon et al. 1994
M 31			5 (4.5–5.6) e7		0.59	9.7	Richstone, Bower & Dressler 1990
M 31			3.8 (1.1– 11) e7		0.56	10.3	Kormendy 1988a
M 31			5.6 (3.4–7.8) e7		0.59	9.7	Dressler & Richstone 1988
M 32	0.805	77	2.45(1.4–3.5) e6	0.46	0.052	8.76	van den Bosch & de Zeeuw 2010
M 32			2.9 (2.7–3.1) e6		0.052	8.76	Verolme et al. 2002
M 32			3.5 (2.3–4.6) e6		0.052	8.76	Joseph et al. 2001
M 32			2.4 (2.2–2.6) e6		0.23	1.98	Magorrian et al. 1998
M 32			3.9 (3.1–4.7) e6		0.050	9.11	van der Marel et al. 1998a
M 32			3.9 (3.3–4.5) e6		0.050	9.11	van der Marel et al. 1997a, 1997b
M 32			3.2 (2.6–3.7) e6		0.23	1.98	Bender, Kormendy & Dehnen 1996
M 32			2.1 (1.8–2.3) e6		0.34	1.34	Dehnen 1995
M 32			2.1 e6		0.34	1.34	Qian et al. 1995
M 32			2.1 (1.7–2.4) e6		0.34	1.34	van der Marel et al. 1994a
M 32			2.2 (0.8–3.5) e6		0.59	0.77	Richstone, Bower & Dressler 1990
M 32			9.3 e6		0.59	0.77	Dressler & Richstone 1988
M 32			7.5 (3.5–11.5) e6		0.76	0.60	Tonry 1987
M 32			5.8 e6		1.49	0.31	Tonry 1984

Lines based on HST spectroscopy are in red. Column 2 is the assumed distance. Column 3 is the stellar velocity dispersion inside the "effective radius" that encompasses half of the light of the bulge. Column 4 is the measured BH mass with the one-sigma range that includes 68 % of the probability in parentheses. Only the top four $M_\bullet$ values for the Galaxy include distance uncertainties in the error bars. Column 5 is the radius of the sphere of influence of the BH; the line that lists $r_{\rm infl}$ contains the adopted $M_\bullet$. Column 6 is the effective resolution of the spectroscopy, estimated as in Kormendy (2004). It is a radius that measures the blurring effects of the telescope point-spread function or "PSF," the slit width or aperture size, and the pixel size. The contribution of the telescope is estimated by the dispersion $\sigma_{*\rm tel}$ of a Gaussian fitted to the core of the average radial brightness profile of the PSF. In particular, the HST PSF has $\sigma_{*\rm tel} \simeq 0''.036$ from a single-Gaussian fit to the PSF model in van der Marel, de Zeeuw & Rix (1997a).

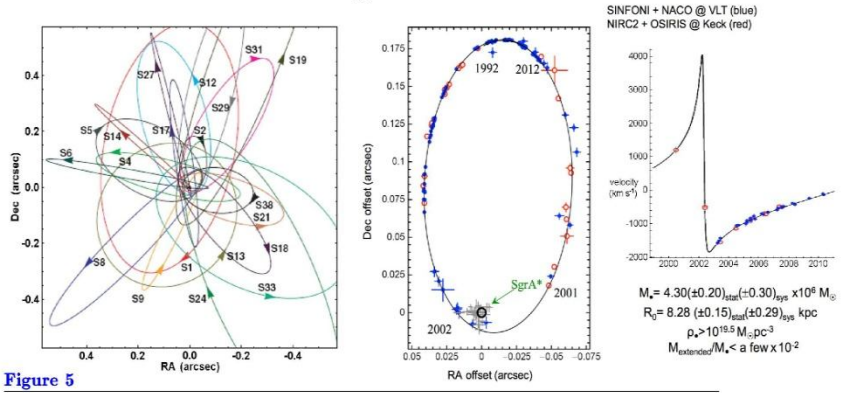

Figure 5

(*left*) Orbits of individual stars near the Galactic center. (*right*) Orbit of star S2 around the BH and associated radio source Sgr A* based on observations of its position from 1992 to 2012. Results from the Ghez group using the Keck telescope and from the Genzel group using the Europen Very Large Telescope (VLT) are combined. This figure is updated from Genzel, Eisenhauer & Gillessen (2010) and is kindly provided by Reinhard Genzel.

These results establish the existence and mass of the central dark object beyond any reasonable doubt. They also eliminate astrophysical plausible alternatives to a BH. These include brown dwarfs and stellar remnants (e. g., Maoz 1995, 1998; Genzel et al. 1997, 2000; Ghez et al. 1998, 2005) and even fermion balls (Ghez et al. 2005; GEG10). Boson balls (Torres et al. 2000; Schunck & Mielke 2003; Liebling & Palenzuela 2012) are harder to exclude; they are highly relativistic, they do not have hard surfaces, and they are consistent with dynamical mass and size constraints. But a boson ball is like the proverbial elephant in a tree: it is OK where it is, but how did it ever get there? GEG10 argue that boson balls are inconsistent with astrophysical constraints based on AGN radiation. Also, the Sołtan (1982) argument implies that at least most of the central dark mass observed in galaxies grew by accretion in AGN phases, and this quickly makes highly relativistic objects collapse into BHs. Finally (Fabian 2013), X-ray AGN observations imply that we see, in some objects, material interior to the innermost stable circular orbit of a non-rotating BH; this implies that these BHs are rotating rapidly and excludes boson balls as alternatives to all central dark objects. Arguments against the most plausible BH alternatives – failed stars and dead stars – are also made for other galaxies in Maoz (1995, 1998) and in Bender et al. (2005). Exotica such as sterile neutrinos or dark matter WIMPs could still have detectable (small) effects, but we conclude that they no longer threaten the conclusion that we are detecting supermassive black holes.

KR95 was titled "Inward Bound – The Search for Supermassive Black Holes in Galactic Nuclei." HST has taken us essentially one order of magnitude inward in radius. A few other telescopes take us closer. But mostly, we are still working at 10^4 to 10^5 Schwarzschild radii. In our Galaxy, we have observed individual stars in to $\sim$ 500 Schwarzschild radii. Only the velocity profiles of relativistically broadened Fe Kα lines (e. g., Tanaka et al. 1995; Fabian 2013) probe radii that are comparable to the Schwarzschild radius. So we are still inward bound. Joining up our measurements made at thousands of r_S with those probed by Fe Kα emission requires that we robustly integrate into our story the rich and complicated details of AGN physics; that is, the narrow– and broad–emission-line regions. That journey still has far to go.

R. Hooke's "proof" that F ~$1/r^2$ could explain Kepler's laws, German Aerospace Center (Robert Hooke Strasse, 7)

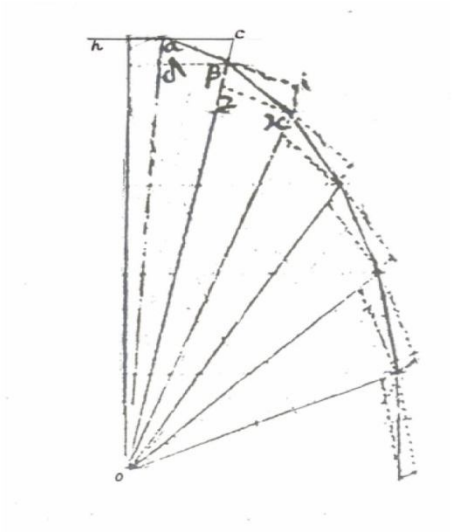

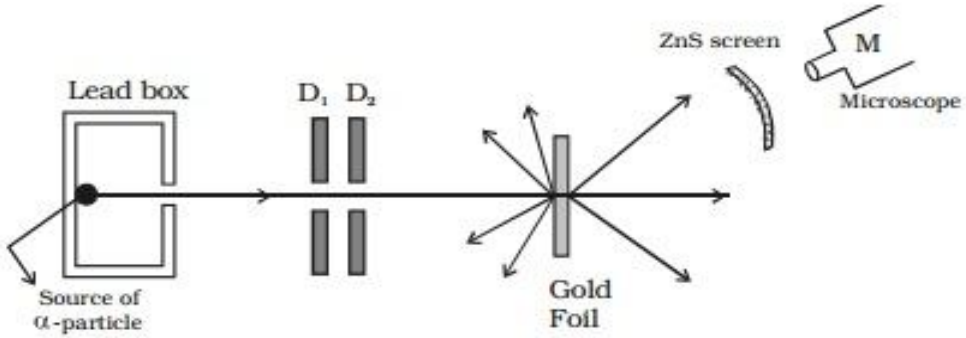

Fig Rutherford's α - particle scattering experiment

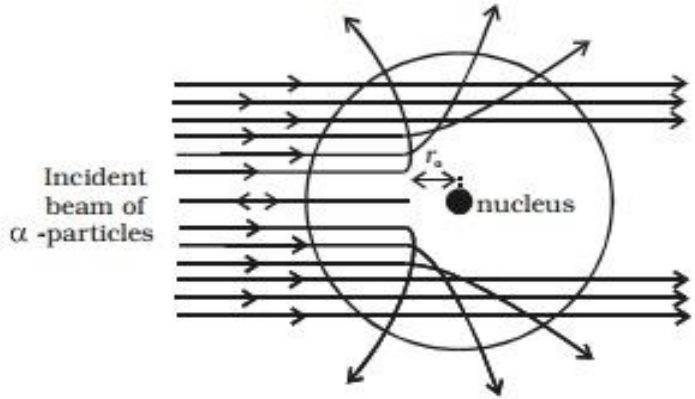

Fig Scattering of α – rays

THE COMPACT SOURCE AT THE GALACTIC CENTER

Martin J. Rees
Institute of Astronomy, Madingley Rd., Cambridge, U.K.

ABSTRACT

Various circumstantial arguments for (and against) the presence of a massive black hole ($\lesssim 5 \times 10^6 M_\odot$) are mentioned and assessed; in particular, the upper limits to the hole's mass based on considerations of stellar disruption and swallowing are shown to be very uncertain. If a massive black hole indeed lurks at the Galactic Center a compact radio source resembling the one actually observed would be a natural (indeed, almost inevitable) consequence of low-level accretion onto it. Related processes could account for an ionizing flux up to $\sim 10^{41}$ erg s^{-1}, and perhaps also for the observed $e^+ - e^-$ annihilation, but these latter aspects of the model involve physical uncertainties (particularly with regard to particle acceleration) which cannot be reliably quantified.

INTRODUCTION

Are there any phenomena at the Galactic Center which resemble - in a muted form - those which we observe in external galaxies with active nuclei? This question is interesting if we are aiming to understand the data presented at this meeting. But it bears also on the general interpretation of galactic nuclei - whether, in particular, the Seyfert galaxies are just ordinary spirals undergoing a flaring phase.

The conjecture that there might be a massive black hole at the Galactic Center goes back at least 10 years[1]. The infra-red data from the Berkeley group[2,3] and recombination line observations[4] have in the last few years allowed us to rule out any mass above $\sim 5 \times 10^6 M_\odot$. There is no straight dynamical evidence <u>for</u> a massive black hole - part at least of the central mass concentration could take some more conventional form (e.g. a star cluster), and in any case the observed gas may be flowing outward[5]. But the present data on the IR emission and on the unresolved radio source increasingly suggest that there is <u>some</u> unique object right at the Center, even if much of the activity and structure outside the central parsec can be accounted for in conventional terms. Bailey[6] has shown that, if IRS 16 were simply a star cluster, then within a radius 0.1 pc the stars would be so closely packed that runaway dynamical evolution would take $\lesssim 10^9$ yrs. Unless we are observing at a special epoch in the history of our Galactic nucleus, this supports the idea that a massive central object may already have formed. A further suggestive argument is based on the conjecture that all normal galaxies pass intermittently through Seyfert phases. A massive black hole could then exist as a relic of earlier Seyfert-style outbursts, being "reactivated" whenever the fuelling rate is boosted[7]. If a massive black hole <u>is</u> present in the central region of our galaxy, then dynamical friction would cause it to settle quickly into the true dynamical centre.

0094-243X/82/830166-11$3.00

at relativistic energies by synchrotron absorption (unless coherent emission allows them to cool more efficiently); the cross section for annihilation would then be small

Relation to the nuclei of other galaxies

The distinctive pre-requisite for this type of quasi-stationary radio source is a low level of accretion (cf. eqn (10)). Qualitatively similarly behaviour may occur in other galactic nuclei. I would conjecture that those cases which do not display rapid variability may all be of this type, but that the variable nuclear components may involve "jets". The jets would be energised by extraction of the spin energy of the hole, coupled electromagnetically to the surrounding torus[17].

I have benefitted from discussions with a number of colleagues, and would particularly like to thank Mitch Begelman, Roger Blandford, Bob Brown, Juhan Frank and Sterl Phinney. I am grateful also to Guenter Riegler for the invitation to participate in the Galactic Center conference.

REFERENCES

1. D. Lynden-Bell and M.J. Rees. MNRAS, 152, 461 (1971).
2. E.R. Woolman, T.R. Geballe, J.H. Lacy, & C.H. Townes. Astrophys.J. (Lett), 218, 103 (1977).
3. J.H. Lacy, F. Baas, C.H. Townes & T.R. Geballe. Astrophys.J.(Lett), 227, L17 (1979).
4. L.F. Rodriguez & E.J. Chaisson. Astrophys.J., 228, 734 (1979).
5. R. Brown. Astrophys.J. (submitted).
6. M.E. Bailey. MNRAS, 190, 217 (1980).
7. R.H. Sanders, Nature, 294, 427 (1981) and references cited therein.
8. L.M. Ozernoi in "Large-Scale Characteristics of the Galaxy", ed. W.B. Burton, p. 395 (Reidel, Holland, 1979).
9. V.I. Dokuchaev and L.M. Ozernoi. Sov.Astron.- A.J., 3, 209 (1977).
10. V.G. Gurzadyan & L.M. Ozernoi. Astron. Astrophys., 86, 315 (1980).
11. V.G. Gurzadyan & L.M. Ozernoi. Astron.Astrophys., 95, 39 (1981) and earlier references cited therein.
12. J.G. Hills. Nature, 254, 295 (1975).
13. J. Frank & M.J. Rees. MNRAS, 176, 633 (1976).
14. B. Carter & J. Luminet. Preprint (1981).
15. J. Frank. MNRAS, 187, 833 (1979).
16. A.C. Fabian, J.E. Pringle & M.J. Rees. MNRAS, 172, 15P (1975).
17. M.J. Rees, M.C. Begelman, R.D. Blandford & E.S. Phinney. Nature, 295, 17 (1982).
18. D.M. Eardley & A.P. Lightman. Astrophys.J., 200, 187 (1975).
19. S.P. Reynolds & C.F. McKee. Astrophys.J., 239, 893 (1980).
20. D.B. Wilson & M.J. Rees. MNRAS, 185, 297 (1978).
21. R.W. Bussard, R. Ramaty & R.J. Drachman. Astrophys.J., 228, 928 (1979).

A. N. Kolmogorov, A.M. Obukhov, V. I. Tatarskii developed mathematical foundations of AO (based on conversations with Paul Hickson (University of British Columbia))

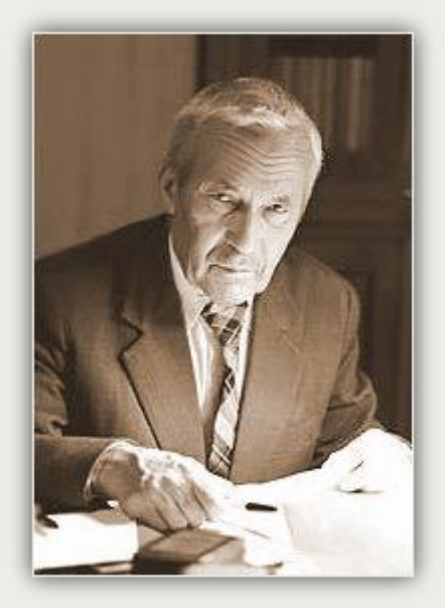

P. L. Kapitsa (1946): "A large number of the largest engineering initiatives were born in our country. We have almost never been able to develop them ourselves... Often the reason for not using innovation is that we usually underestimated our own and overestimated foreign ones. Usually, organizational shortcomings prevented our technical pioneer work from developing and influencing the world technology. Many of these shortcomings exist to this day, and one of the main ones is the underestimation of their own and overestimation of foreign forces.”

In 2003, Nobel laureate Reinhard Genzel, right, posed with his mentor, Charles Townes, who won a Nobel Prize in Physics for invention of the laser. Townes, who died in 2015, and Genzel collaborated on some of the first observations of the galactic center, later shown by Genzel and Nobel co-winner Andrea Ghez to host a supermassive black hole. (2003 UC Berkeley photo)

“Charlie Townes’ dream was to do this experiment we have done, already in the 1970s,” he said. “And he, in fact, did these fantastic, pioneering experiments. But (when he saw) the results, he knew he would never get to the galactic center, which was a real disappointment to him.”

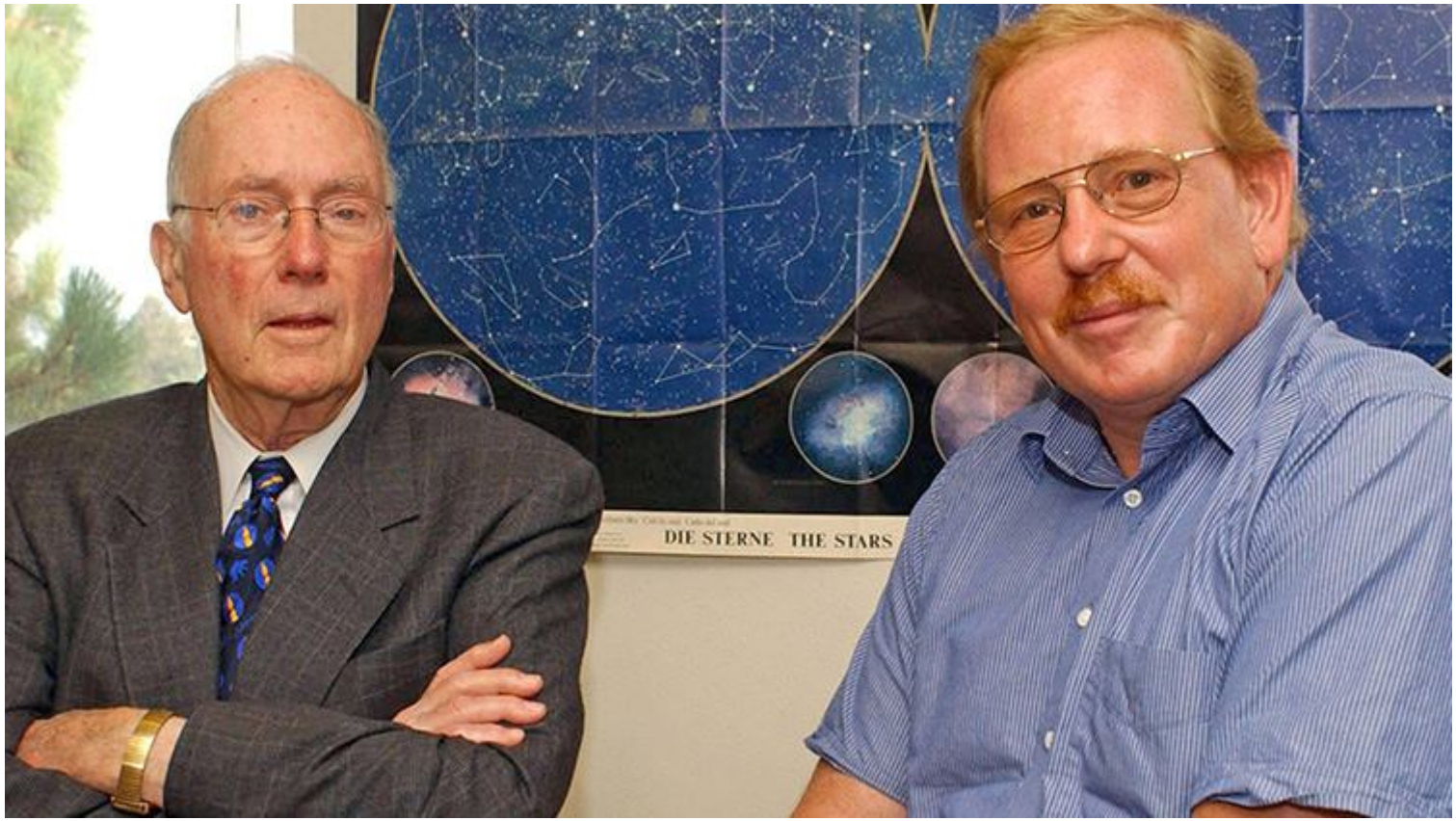

Ch. H. Townes

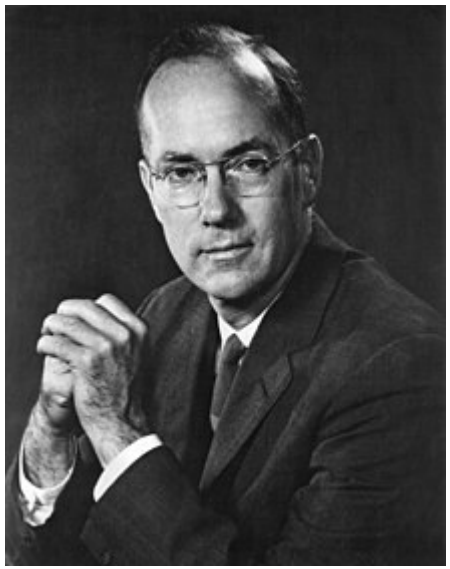

Rep. Prog. Phys. 57 (1994) 417–479. Printed in the UK

The nucleus of our Galaxy

Reinhard Genzel†, David Hollenbach‡ and Charles H Townes§

† Max-Planck Institut für Extraterrestrische Physik, Garching, Germany
‡ NASA Ames Research Center, Moffett Field, CA, USA
§ Department of Physics, University of California, Berkeley, CA, USA

Abstract

The subject of this review is the central 100 parsecs of our Galaxy, with a strong focus on the central few parsecs. Observations of the electromagnetic spectrum over 13 orders of magnitude in wavelength show a broad range of phenomena involving a number of physical processes. We discuss the stellar and interstellar components, the importance of magnetic and gravitational forces, the evidence for stellar formation and a central massive black hole, and the origin and nature of ionization, outflows and interstellar gas dynamics.

The density of stars is approximately proportional to R^{-2} from Galactocentric radii of a few tenths to more than one hundred parsecs, the central density perhaps being more than 10^7 times as large as in the solar vicinity. On all scales one finds massive stars that must have formed within the last 10^7 years. On scales $\geqslant 10$ pc there are a number of compact x-ray sources, including a spectacular black hole candidate exhibiting time variable, hard x-ray/γ-ray emission and a twin radio jet. In the central regions stellar collisions are probably frequent and may affect the stellar populations.

The Galactic nucleus contains a remarkable concentration of dense and excited interstellar matter. The average density of gas and dust and the average thermal pressures are 10^2–10^5 times those found in the solar neighbourhood. A component of very hot (10^7–10^8 K) gas may be the result of a few hundred supernova explosions that occurred in the central 10^2 pc during the last 10^4–10^5 years. The coronal gas escapes the disk as a Galactic wind. The region between 3 and 30 pc shows evidence for poloidal magnetic fields out of the plane of the disk of the Galaxy, of strength 0.1 to a few mGauss. A circum-nuclear disk or torus of dense molecular gas orbits the centre between 1.5 and 5 pc and probably is fed with gas from massive molecular clouds at $R \geqslant 10$ pc. The central parsec has a relatively low average gas density, but contains a number of predominantly atomic and ionized streamers.

The luminosity of the central few parsecs appears to be dominated by a cluster of hot stars, whose ultraviolet radiation and winds excite, photoionize and perturb the gas streamers. These massive stars may be the products of a small burst of star formation that occurred a few million years ago when there may have been a much greater nuclear concentration of interstellar gas than is presently observed. Alternatively, or additionally, massive stars in the central core may form as the result of mergers of low mass stars if the central stellar density in fact significantly exceeds $10^7\ M_\odot\ \mathrm{pc}^{-3}$.

0034-4885/94/050417+63$59.50

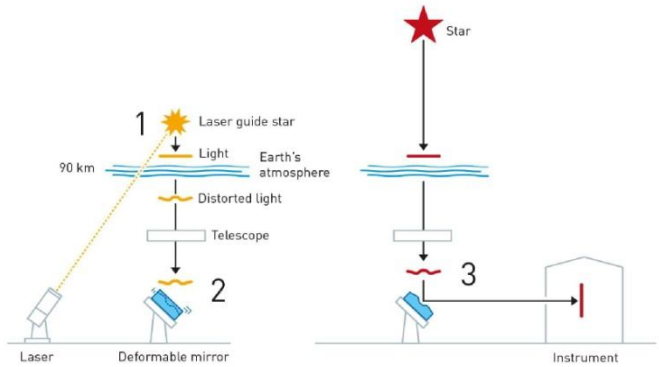

Figure 7. *The principle of adaptive optics. A laser system is used to make artificial guide stars that sense the blurring in the Earth's atmosphere. The images of the bright spots generated by the laser [1] are used in a feedback loop to introduce fast deformations of a secondary mirror [2] that effectively correct for the atmospheric turbulence in the science images [3].*

The discovery of a compact object in the Galactic centre

One of the stars, labelled as S2 by Genzel's group (called S02 by the team led by Ghez), was shown to have a very short orbiting period around Sgr A*, just under 16 years (Schödel et al. 2002, Ghez et al. 2003). For comparison, it takes over 200 million years for the Sun to complete a full orbit around the Galactic centre. This star has a highly elliptical orbit with eccentricity e = 0.88. Its pericentre distance from Sgr A* in the spring of 2002 was a mere 17 light hours, or 1,400 R_s, for a black hole of mass $4 \times 10^6 M_\odot$ (see figure 8). The plane of the orbit has an inclination of about 46° with respect to the plane of the sky.

The agreement between the data from the NTT/VLT and Keck telescopes was excellent. The analysis of the combined data sets showed that the extended mass component (visible stars, stellar remnants and, possibly, dark matter) within the orbit of S2, gave a negligible contribution to the estimation of the central mass (Ghez et al. 2008, Gillessen et al. 2009b). The work of the two teams together established that the Galactic centre contains a highly concentrated mass of ~4 million solar masses within the pericentre of S2, i.e. within 125 AU. This requires a minimum density of $5 \times 10^{15} M_\odot pc^{-3}$. The mass centroid lies within ±2 milliarcseconds of the position of the compact radio source Sgr A*, which itself has an apparent size of <1 AU (Shen et al. 2005, Bower et al. 2006, Doeleman et al. 2008) and lacks detectable proper motion (Reid & Brunthaler, 2004).

A robust interpretation of these observations is that the compact object at the Galactic centre is compatible with being a supermassive black hole. Further support for this conclusion comes from the fact that near-infrared and X-ray flares are observed from the same position, which can be naturally ascribed to variations in the accretion flow towards a massive black hole.

Large telescopes, AO and bright stars in IR

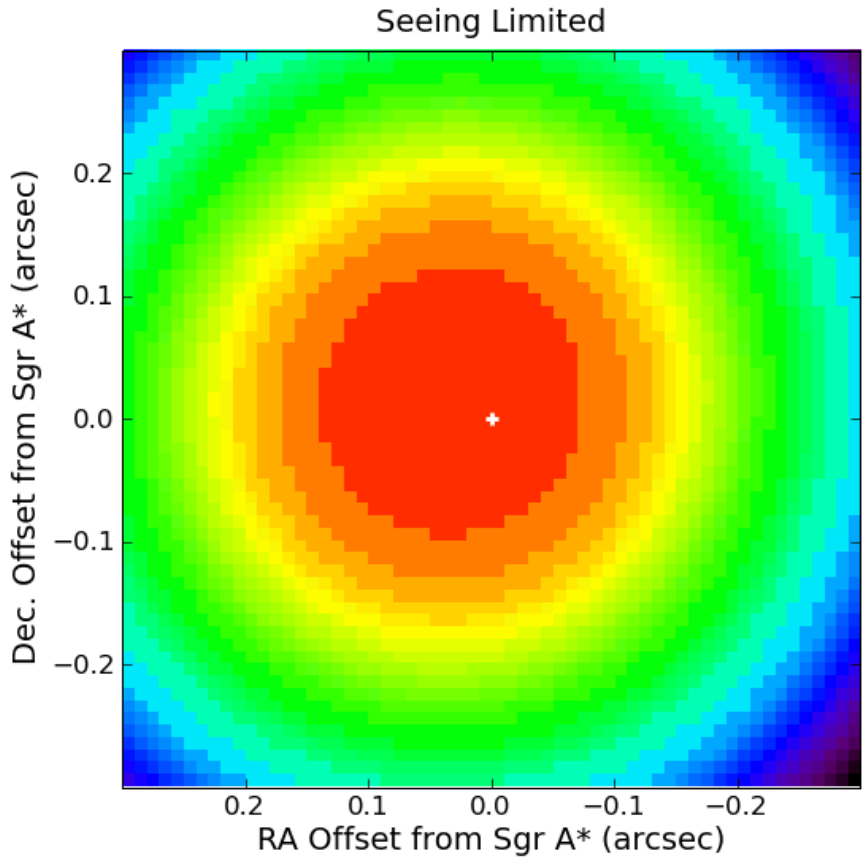

http://www.astro.ucla.edu/~ghezgroup/gc/pictures/Future_GCorbits.shtml

Keck Telecopes

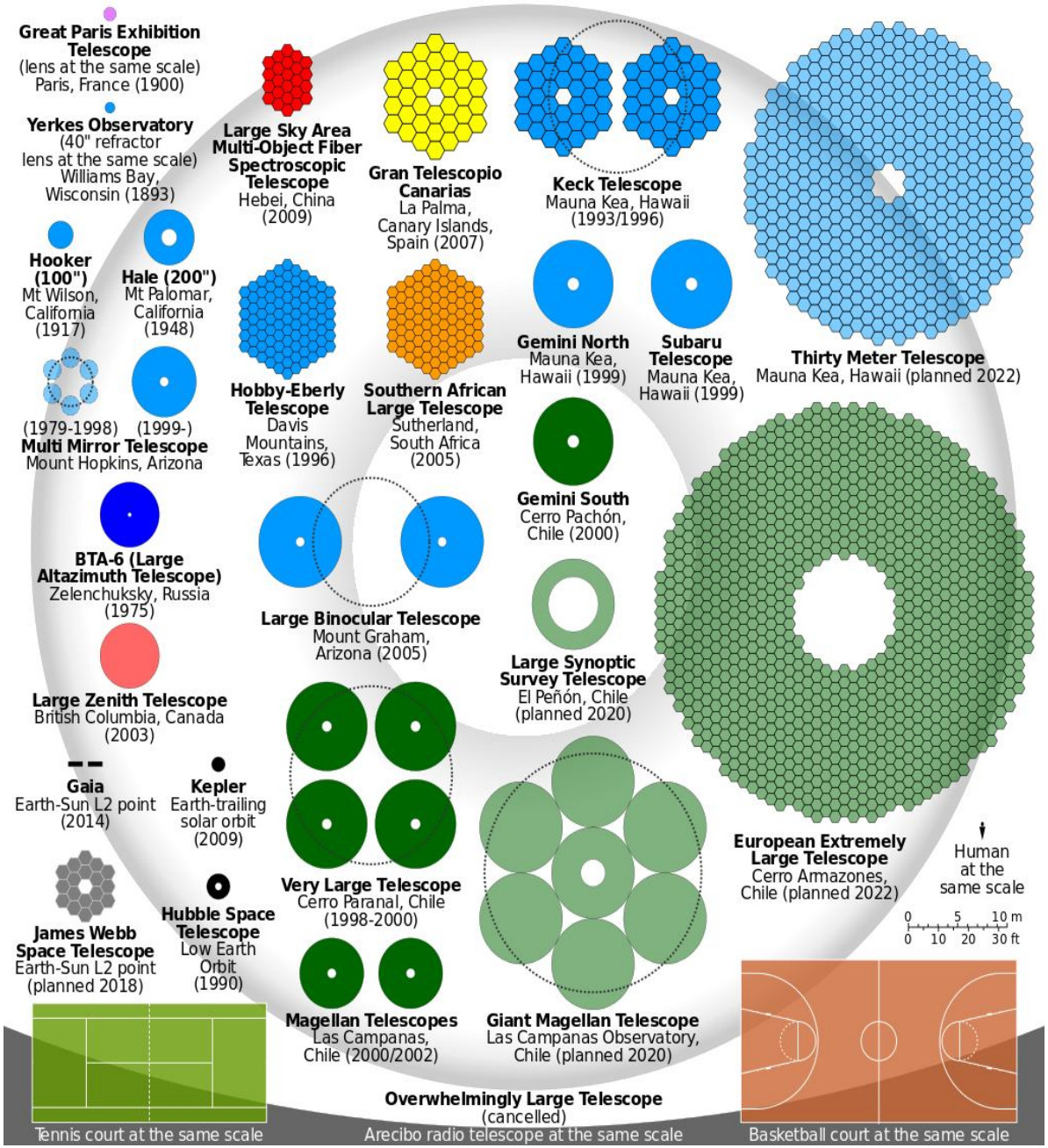
Great Paris Exhibition Telescope
(lens at the same scale)
Paris, France (1900)
Yerkes Observatory
(40" refractor
lens at the same scale)
Williams Bay,
Wisconsin (1893)
Hooker (100")
Mt Wilson,
California
(1917)
Hale (200")
Mt Palomar,
California
(1948)
(1979-1998)
(1999-)
Multi Mirror Telescope
Mount Hopkins, Arizona
BTA-6 (Large Altazimuth Telescope)
Zelenchuksky, Russia
(1975)
Large Zenith Telescope
British Columbia, Canada
(2003)
Gaia
Earth-Sun L2 point
(2014)
Kepler
Earth-trailing
solar orbit
(2009)
James Webb Space Telescope
Earth-Sun L2 point
(planned 2018)
Hubble Space Telescope
Low Earth
Orbit
(1990)
Large Sky Area Multi-Object Fiber Spectroscopic Telescope
Hebei, China
(2009)
Gran Telescopio Canarias
La Palma,
Canary Islands,
Spain (2007)
Keck Telescope
Mauna Kea, Hawaii
(1993/1996)
Hobby-Eberly Telescope
Davis
Mountains,
Texas (1996)
Southern African Large Telescope
Sutherland,
South Africa
(2005)
Gemini North
Mauna Kea,
Hawaii (1999)
Subaru Telescope
Mauna Kea,
Hawaii (1999)
Thirty Meter Telescope
Mauna Kea, Hawaii (planned 2022)
Gemini South
Cerro Pachón,
Chile (2000)
Large Binocular Telescope
Mount Graham,
Arizona (2005)
Large Synoptic Survey Telescope
El Peñón, Chile
(planned 2020)
European Extremely Large Telescope
Cerro Armazones,
Chile (planned 2022)
Human at the same scale
0 5 10 m
0 10 20 30 ft
Very Large Telescope
Cerro Paranal, Chile
(1998-2000)
Magellan Telescopes
Las Campanas,
Chile (2000/2002)
Giant Magellan Telescope
Las Campanas Observatory,
Chile (planned 2020)
Overwhelmingly Large Telescope
(cancelled)
Tennis court at the same scale
Arecibo radio telescope at the same scale
Basketball court at the same scale

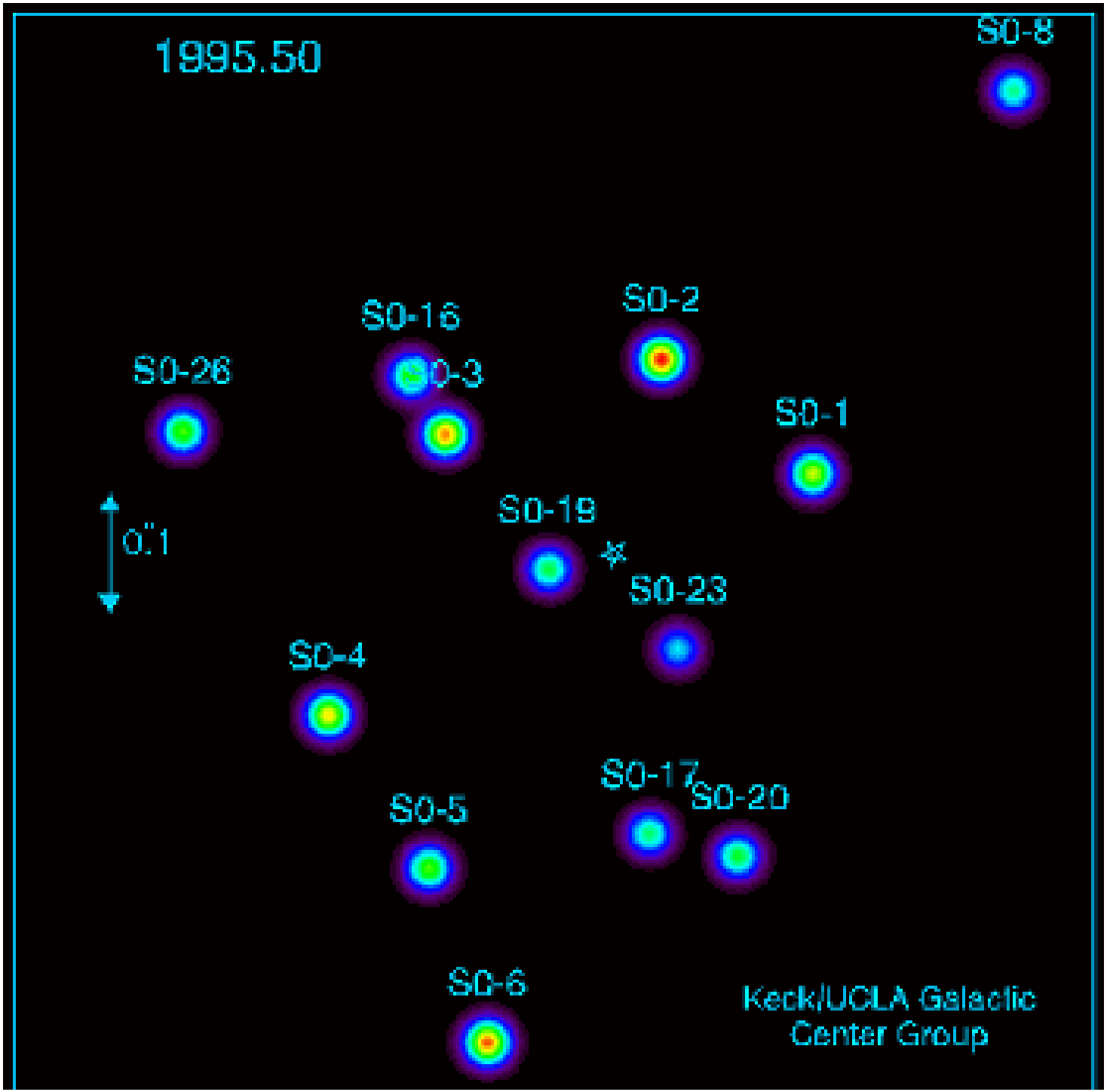
1995.50
S0-8
S0-16
S0-2
S0-26
S0-3
S0-1
0.1
S0-19
S0-23
S0-4
S0-17
S0-20
S0-5
S0-6
Keck/UCLA Galactic
Center Group

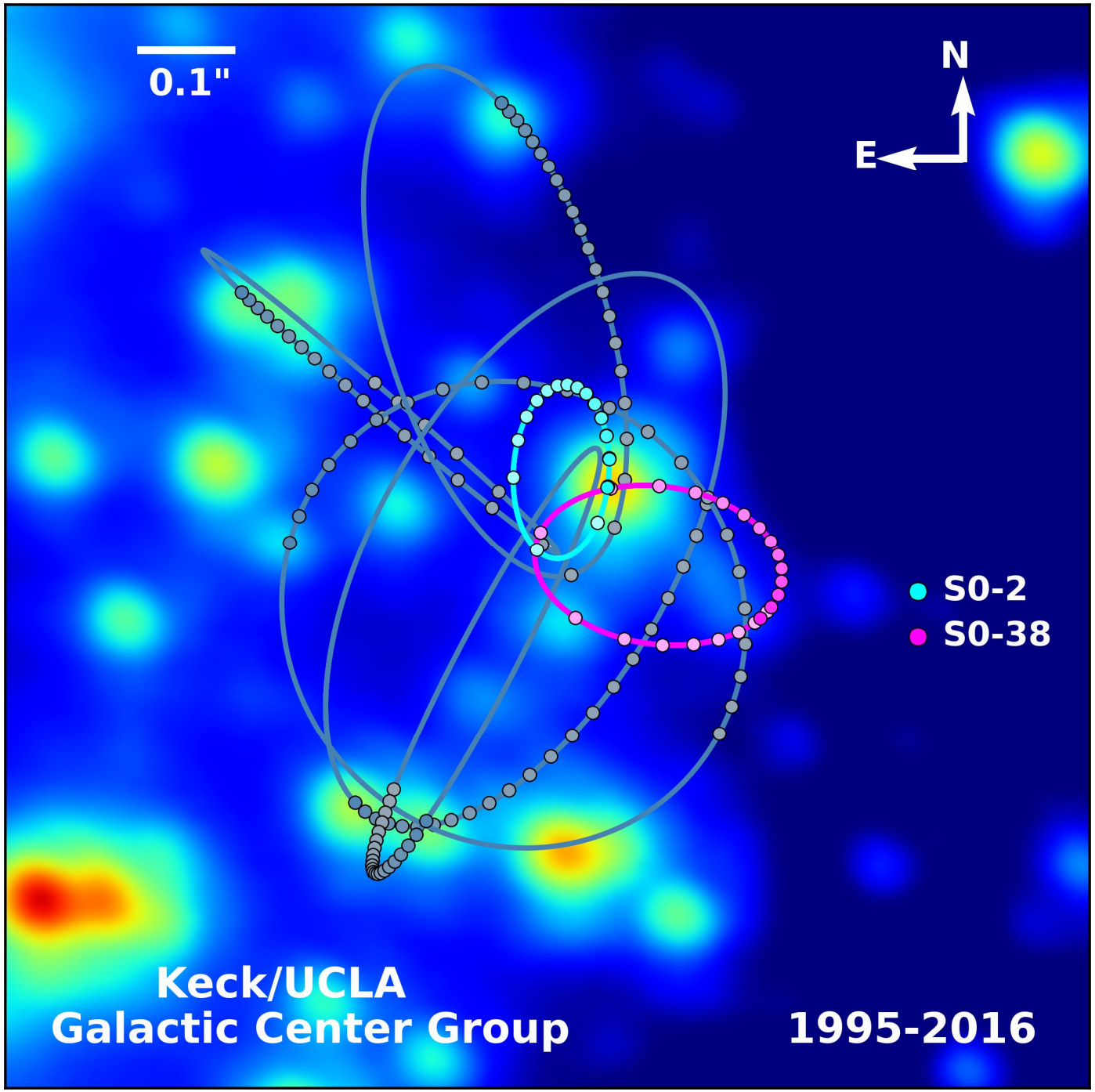
0.1"
N
E
S0-2
S0-38
Keck/UCLA
Galactic Center Group
1995-2016

An Expanded View of the Universe

Science with the European Extremely Large Telescope

Black Holes

Black holes are some of the most bizarre objects in the Universe, challenging the imaginations of even the most creative scientists. They are places where gravity trumps all other forces in the Universe, pushing our understanding of physics to the limit. Even more strangely, supermassive black holes seem to play a key role in the formation of galaxies and structures in the Universe.

Galactic Centre

Over the last 15 years or so, an enormous amount of work has gone into improving our understanding of the closest supermassive black hole — Sagittarius A* at the centre of the Milky Way.

Technological progress, in particular in the areas of adaptive optics and high angular resolution with ground-based 8-metre-class telescopes, has allowed impressive progress in understanding supermassive black holes and their surroundings. Key progress was made in proving the very existence of a supermassive black hole at the centre of the Milky Way, in refining our knowledge of how matter falls into black holes, and in identifying gas discs and young stars in the immediate vicinity of the black hole. The Galactic Centre was thus established as the most important laboratory for the study of supermassive black holes and their surroundings.

But its potential for progress in fundamental physics and astrophysics is far from being fully exploited. The Galactic Centre remains the best place to test general relativity directly in a strong gravitational field. The E-ELT will enable extremely accurate measurements of the positions of stars (at the 50–100 microarcsecond level over fields of tens of arcseconds), as well as radial velocity measurements with about 1 km/s precision, pushing our observations ever closer to the black hole event horizon. Stars can then be discovered at 100 Schwarzschild radii, where orbital velocities approach a tenth of the speed of light. This is more than ten times closer than can be achieved with the current generation of telescopes. Such stellar probes will allow us to test the predicted relativistic signals of black hole spin and the gravitational redshift caused by the black hole, and even to detect gravitational wave effects. Further out, the dark matter distribution around the black hole, predicted by cold dark matter cosmologies (ΛCDM), can be explored. The distance to the Galactic Centre can be measured to 0.1 %, constraining in turn the size and shape of the galactic halo and the Galaxy's local rotation speed to unprecedented levels. Crucial progress in our understanding of the interaction of the black hole with its surroundings will be made. The puzzling stellar cusp around the Galactic Centre, as well as the observed star formation in the vicinity of the black hole will be studied in detail for the first time.

Left: Very Large Telescope (VLT) observations have revealed that the supermassive black hole closest to us is located in the centre of the Milky Way.

The Milky Way's central supermassive black hole has been weighed by measuring the proper motions of stars in its vicinity.

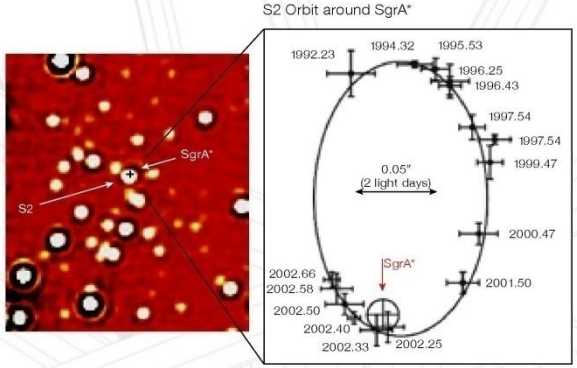

The VLT, *Very Large Telescope*
4 european 8 m telescopes at Cerro Paranal in Chili

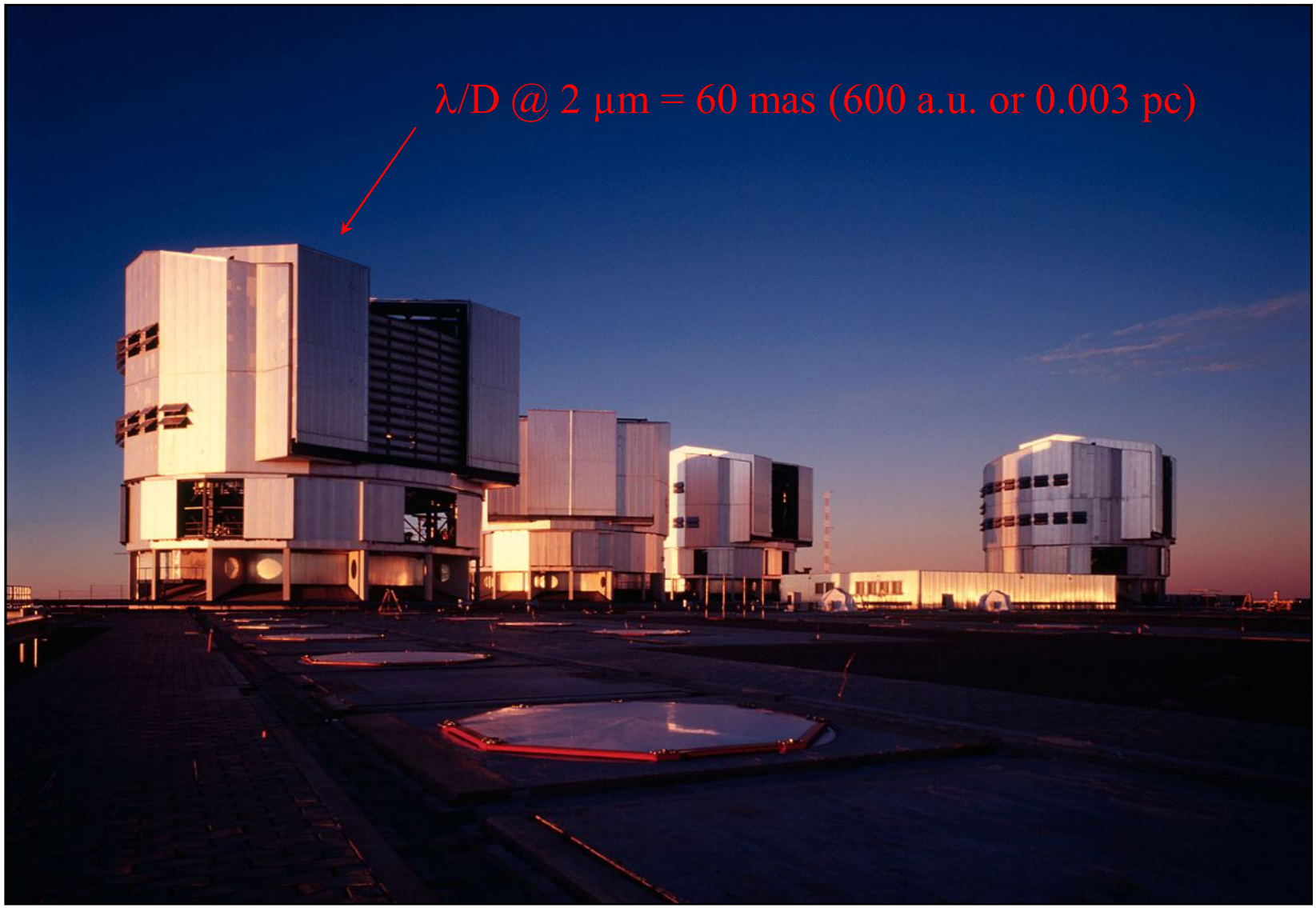

Going beyond boundaries thanks to accurate spatial information

- Bring the ultimate evidence that Sgr A* is a black hole: the mass is contained in the Schwarzschild radius.
- Understand the nature of flares.
- Use the black hole as a tool to study general relativity in the strong field regime

Scale ~ 1 R_s 10 μas

- Study relativistic effects on nearby stars
- Understand the nature of S stars and their distribution

Scale ~ 100 R_s 1 mas

AFZ, A.A. Nucita, F. De Paolis, G. Ingrosso, PRD 76, 062001 (2007)

The mass concentration at the Galactic Center

Recent advancements in infrared astronomy are allowing to test the scale of the mass profile at the center of our galaxy down to tens of AU. With the Keck 10 m telescope, the proper motion of several stars orbiting the Galactic Center black hole have been monitored and almost entire orbits, as for example that of the S2 star, have been measured allowing an unprecedent description of the Galactic Center region. Measurements of the amount of mass $M(< r)$ contained within a distance r from the Galactic Center are continuously improved as more precise data are collected. Recent observations (Ghez et al. (2003)) extend down to the periastron distance ($\simeq 3 \times 10^{-4}$ pc) of the S16 star and they correspond to a value of the enclosed mass within $\simeq 3 \times 10^{-4}$ pc of $\simeq 3.67 \times 10^{6}$ $M_{\odot}$. Several authors have used these observations to model the Galactic Center mass concentration. Here and in the following, we use the three component

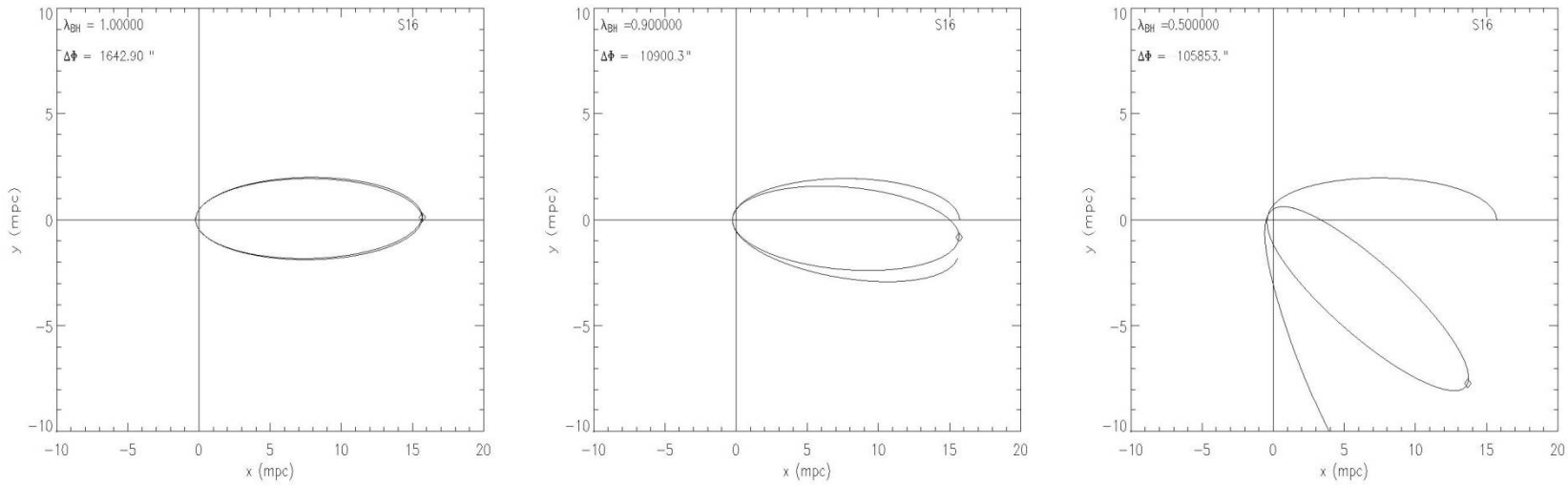

Figure 21: The same as in Figure 20 but for the S16–Sgr A* binary system. In this case, the binary system orbital parameters were taken from Ghez et al. (2005) assuming for the S16 mass a conservative value of $\simeq 10$ $M_{\odot}$.

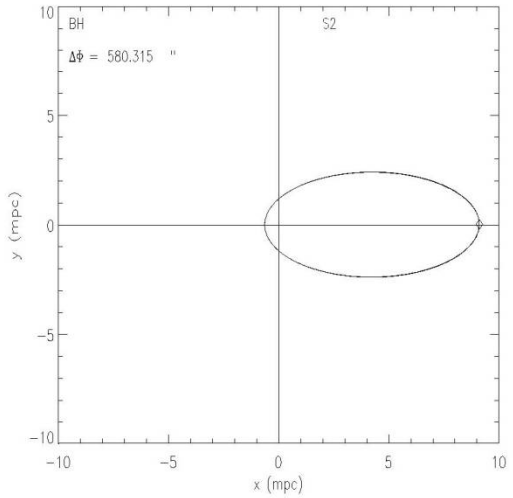
BH
S2
Δϕ = 580.315 "
y (mpc)
x (mpc)

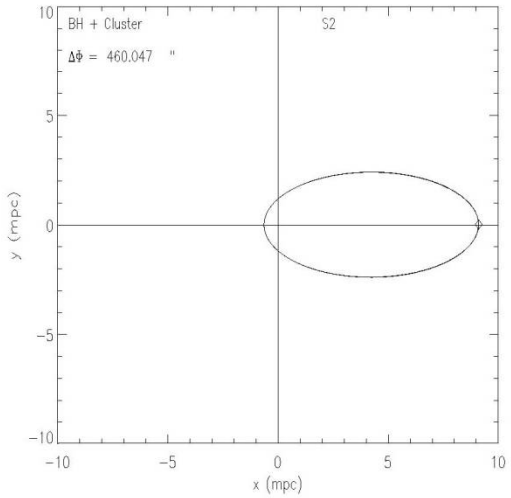
BH + Cluster
S2
Δϕ = 460.047 "
y (mpc)
x (mpc)

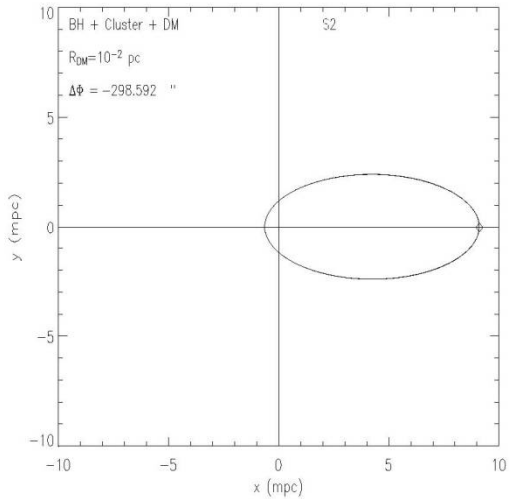
BH + Cluster + DM
S2
R_DM=10^-2 pc
Δϕ = −298.592 "
y (mpc)
x (mpc)

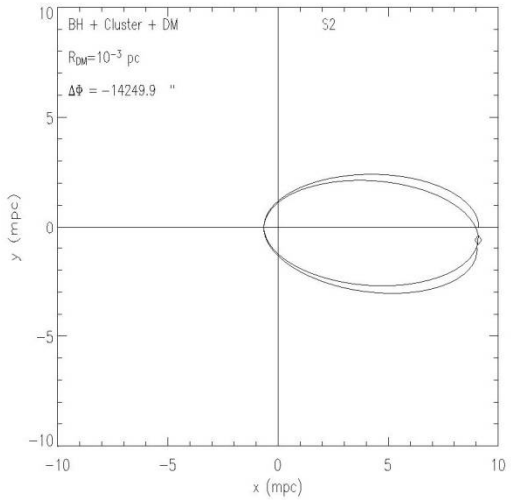
BH + Cluster + DM
S2
R_DM=10^-3 pc
Δϕ = −14249.9 "
y (mpc)
x (mpc)

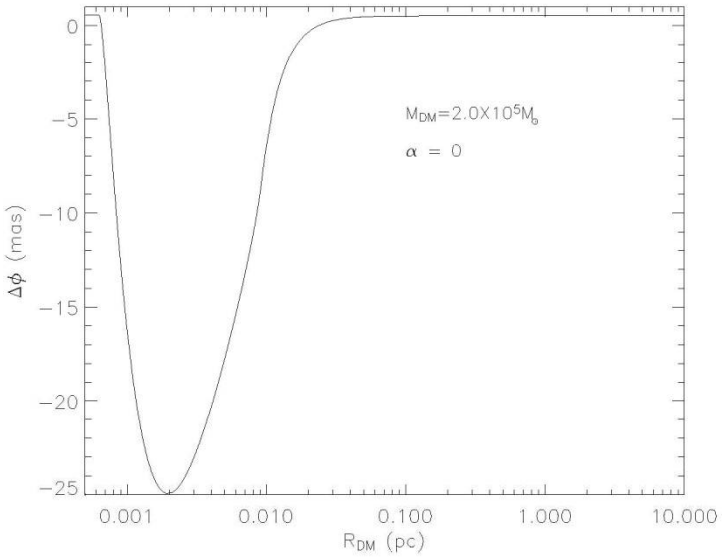

Figure 32: Apoastron shift as a function of the DM radius R_{DM} for $\alpha = 0$ and $M_{DM} \simeq 2 \times 10^5$ $M_\odot$. Taking into account present day precision for the apoastron shift measurements (about 10 mas) one can say that DM radii R_{DM} in the range $8 \times 10^{-4} - 10^{-2}$ pc are not acceptable.

D. Borka, P. Jovanovic, V. Borka Jovanovic and AFZ, PRD, **85**, 124004 (2012).

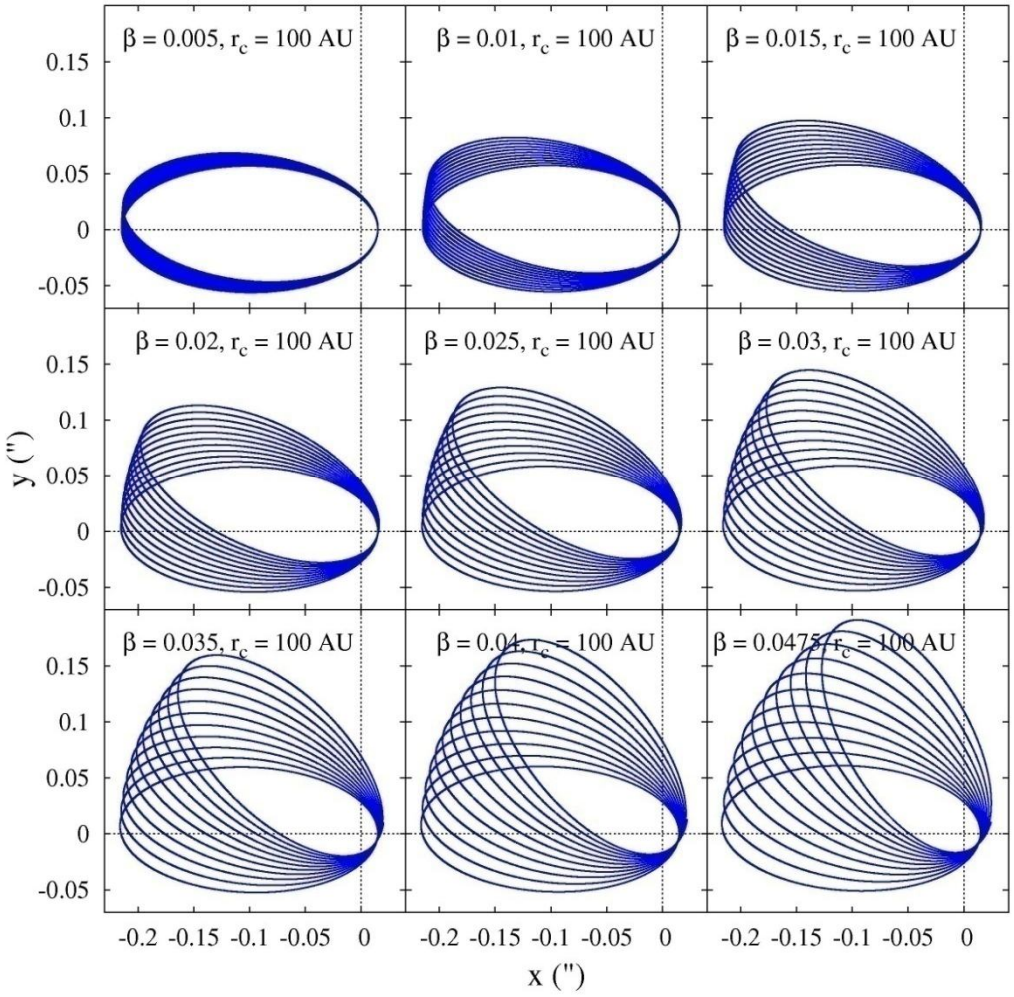

capabilities. They showed that the orbital precession can occur due to relativistic effects, resulting in a prograde shift and due to a possible extended mass distribution, producing a retrograde shift. Both prograde relativistic and retrograde Newtonian periastron shifts will result in rosette-shaped orbits. Weinberg *et al.* [12] discussed physical experiments achievable via the monitoring of stellar dynamics near the massive black hole at the Galactic center with a diffraction-limited, next-generation, extremely large telescope. They demonstrated that the lowest order relativistic effects, such as the prograde precession, will be detectable if the astrometric precision becomes less than 0.5 mas.

In this paper we continue to investigate constraints on the parameters of this class of gravity theories using S2-like star orbits under the uncertainty of 10 mas. In Sec. II the type of gravitational potential we use is given. In Sec. III we present the S2-like star orbits, gravity parameters, and angles of orbital precession, and also compare theoretical results with observations. The main conclusions are pointed out in Sec. IV.

II. THEORY

R^n gravity belongs to power-law fourth-order theories of gravity obtained by replacing the scalar curvature R with $f(R) = f_0 R^n$ in the gravity Lagrangian [1,2]. As a result, in the weak field limit [13], the gravitational potential is found to be [1,2]

$$\Phi(r) = -\frac{GM}{2r}\left[1 + \left(\frac{r}{r_c}\right)^{\beta}\right], \tag{1}$$

where r_c is an arbitrary parameter, depending on the typical scale of the considered system, and β is a universal parameter:

$$\beta = \frac{12n^2 - 7n - 1 - \sqrt{36n^4 + 12n^3 - 83n^2 + 50n + 1}}{6n^2 - 4n + 2}. \tag{2}$$

This formula corresponds to a modification of the gravity action in the form

$$A = \int d^4x\sqrt{-g}(f(R) + L_m), \tag{3}$$

where $f(R)$ is a generic function of the Ricci scalar curvature and L_m is the standard matter Lagrangian.

For $n = 1$ and $\beta = 0$ the R^n potential reduces to the Newtonian one, as expected. Parameter β controls the shape of the correction term and is related to n, which is part of the gravity Lagrangian. Since it is the same for all gravitating systems, as a consequence, β must be the same for all of them and therefore it is a universal parameter [2]. The parameter r_c is the scale length parameter, and it is related to the boundary conditions and the mass of the system [2].

III. RESULTS

A. Orbits of S2-like stars and parameters of R^n gravity

In order to study the effects of R^n gravity on the motion of S2, we performed two-body calculations of its orbit in the R^n potential [Eq. (1)] during two periods. We assumed the following input parameters taken from the paper of Zakharov *et al.* [10]: orbital eccentricity of the S2-like star, $e = 0.87$; major semiaxis $a = 919$ AU; mass of the S2-like star, $M_\star = 1M_\odot$; mass of the central black hole, $M_{\rm BH} = 3.4 \times 10^6 M_\odot$ (where $M_\odot$ is the solar mass); and orbital period of the S2-like star is 15 years. We calculated the S2-like star orbit during two periods using Newtonian and R^n potentials. We also investigated the constraints on the parameters β and r_c for which the deviations between the S2-like star orbits in the R^n gravity potential [Eq. (1)] and its Keplerian orbit will stay within the maximum precision of the current instruments (about 10 mas), during one orbital period.

In Fig. 1 we present the trajectory of the S2-like star around a massive black hole in R^n gravity (blue solid line) and in Newtonian gravity (red dashed line) for $r_c =$ 100 AU and for the following nine values of parameter β: 0.005, 0.01, 0.015, 0.02, 0.025, 0.03, 0.035, 0.04, 0.0475. The black hole is assumed to be located at the coordinate origin. We fix a value of parameter r_c at 100 AU, because this value corresponds to the maximal value of parameter β in the parameter space (see Fig. 3), and vary values of parameter β. All nine orbits presented fulfill the request that the R^n orbit and the corresponding Newtonian orbit differ by less than 10 mas (i.e. within the maximum precision of the current observations) during one orbital period. We can see that if parameter β increases, the R^n orbit differs more from the corresponding Newtonian orbit since the precession angle becomes larger. This indicates that the value of β should be small, as inferred from Solar System data [9] and in contrast to the value $\beta = 0.817$ (obtained by [2], which gives excellent agreement between theoretical and observed rotation curves). In the future, with improvements in observational facilities, the precision on constraints on values of parameters β and r_c will increase, as will the accuracy of the S2 orbit.

The corresponding distances between the S2-like star and the black hole as a function of time for the same values of parameters r_c and β as in Fig. 1 are presented in Fig. 2. There is an additional requirement on parameter space: the period of the S2-like star orbit has to remain $\approx$ 15 ± 0.2 yr. Like in the previous case, with increasing observational accuracy of the period, the precision on constraints on values of parameters β and r_c will also increase.

In Fig. 3 we present the parameter space for R^n gravity under the constraint that, during one orbital period, S2-like star orbits under R^n gravity differ by less than ε from their orbits under Newtonian gravity for ten values of parameter ε: 0.001, 0.002, 0.003, 0.004, 0.005, 0.006, 0.007, 0.008,

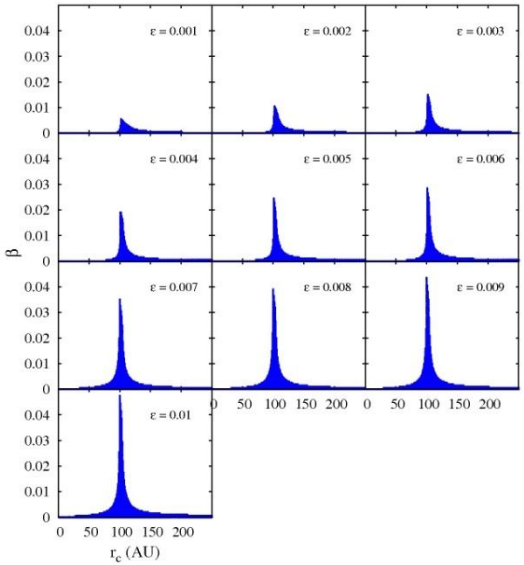

FIG. 3 (color online). The parameter space for R^n gravity under the constraint that, during one orbital period, the S2-like star orbits in R^n gravity differ by less than ε from the corresponding orbits in Newtonian gravity, for the following ten values of parameter ε: 0.001, 0.002, 0.003, 0.004, 0.005, 0.006, 0.007, 0.008, 0.009, and $0''.01$.

The exact expression (7) is inappropriate for practical applications. However, it can be easily approximated for $\beta \approx 0$ and $\beta \approx 1$. In the case of $\beta \approx 0$ expansion in Eq. (7) in Taylor's series over β, up to first order, leads to the following expression for the precession angle:

$$\Delta\theta = \frac{\pi^{\mathrm{rad}}\beta(\sqrt{1-e^2}-1)}{e^2} = \frac{180^\circ\beta(\sqrt{1-e^2}-1)}{e^2}. \quad (8)$$

The above expression in the case of the S2-like star orbit is presented in Fig. 9 as a blue dash-dotted line. Similarly, the expansion of Eq. (7) in power series for $\beta \approx 1$ leads to the following expression for the precession angle (red dotted line in Fig. 9):

$$\Delta\theta = \frac{\pi^{\mathrm{rad}}a(\beta-1)(\sqrt{1-e^2}-1+e^2)}{r_c e^2} = \frac{180^\circ a(\beta-1)(\sqrt{1-e^2}-1+e^2)}{r_c e^2}. \quad (9)$$

One can expect that, in general, the precession angle depends on the semimajor axis and eccentricity of the orbit (see e.g. Iorio and Ruggiero [17]), as well as on both potential parameters β and r_c. This is indeed the case for $\beta \approx 1$ in Eq. (9). But as it can be seen from formula (8), the precession angle in the case when β is small ($\beta \approx 0$) depends only on the eccentricity and the universal constant β itself.

In order to test if the approximation from Eq. (8) is satisfactory in the case of the S2-like star, we derived its precession angle in two ways:

(i) analytically from the approximative formula (8),
(ii) numerically from the calculated orbits presented in Fig. 8.

Comparison of the obtained precession angles by these two methods is presented in Table I. As it can be seen from this table, the approximative formula (8) can be used for estimating the precession angle for all values of β from Fig. 8.

The above analysis indicates that R^n gravity results in the retrograde shift of the S2-like star orbit. Rubilar and Eckart [11] showed that the orbital precession can be due to relativistic effects, resulting in a prograde shift, or due to an extended mass distribution, producing a retrograde shift. We can conclude that the perturbing potential $V(r)$ has an

D. Borka, V. Borka Jovanovic, P. Jovanovic, AFZ

From an analysis of S2 orbit one can find signatures of Yukawa gravity (JCAP, 2013)

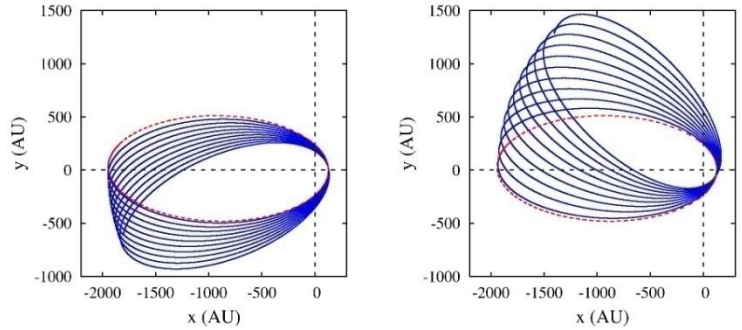

Figure 1. Comparisons between the orbit of S2 star in Newtonian gravity (red dashed line) and Yukawa gravity during 10 orbital periods (blue solid line) for $\Lambda = 2.59 \times 10^3$ AU. In the left panel $\delta = +1/3$, and in the right $\delta = -1/3$.

5. the reduced χ^2 is minimized and the final values of initial positions and velocities are obtained.

Finally, we kept the value of Λ which resulted with the smallest value of minimized reduced χ^2.

In order to obtain some more general constraints on the parameters of Yukawa gravity, we also varied both δ and Λ and studied the simulated orbits of S2 star which give at least the same or better fits than the Keplerian orbit. For each pair of these parameters the reduced χ^2 of the best fit is obtained and used for generating the χ^2 maps over the $\Lambda - \delta$ parameter space. These maps are then used to study the confidence regions in $\Lambda - \delta$ parameter space.

3 Results and discussion

The simulated orbits of S2 star around the central object in Yukawa gravity (blue solid line) and in Newtonian gravity (red dashed line) for $\Lambda = 2.59 \times 10^3$ AU and $\delta = +1/3$ (left panel) and $\delta = -1/3$ (right panel) during 10 periods, are presented in Fig. 1. We can notice that for $\delta = -1/3$ the precession has negative direction and when $\delta = +1/3$ the precession has positive direction. Our analysis shows that the Yukawa gravity potential induces precession of S2 star orbit in the same direction as General Relativity for $\delta > 0$ and for $\delta < -1$, and in the opposite direction for $-1 < \delta < 0$ as in the case of extended mass distribution or in R^n gravity [22].

We used these simulated orbits to fit the observed orbits of S2 star. The best fit (according to NTT/VLT data) is obtained for the scale parameter: $\Lambda = 2.59 \times 10^3$ AU, for which even a significant strength of Yukawa interaction could be expected according to the planetary and Lunar Laser Ranging constraints [32].

In Fig. 2 we presented two comparisons between the fitted orbits in Yukawa gravity for $\delta = +1/3$ through the astrometric observations of S2 star by NTT/VLT alone (left) and NTT/VLT+Keck combination (right). In order to combine NTT/VLT and Keck data sets,

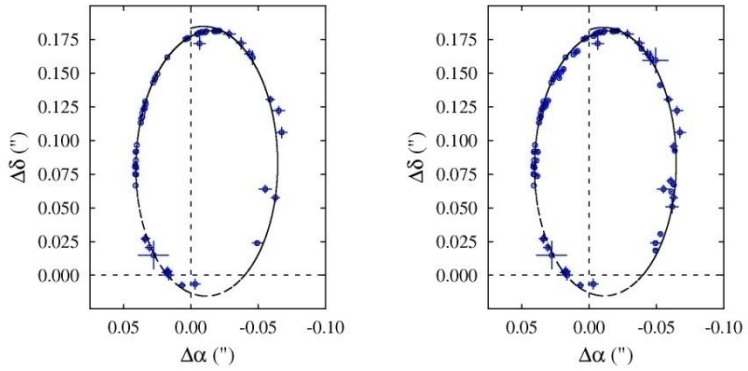

Figure 2. The fitted orbits in Yukawa gravity for $\delta = +1/3$ through the astrometric observations of S2 star (denoted by circles), obtained by NTT/VLT alone (left panel) and NTT/VLT+Keck (right panel). The best fits are obtained for $\Lambda = 2.59 \times 10^3$ AU and $\Lambda = 3.03 \times 10^3$ AU, respectively.

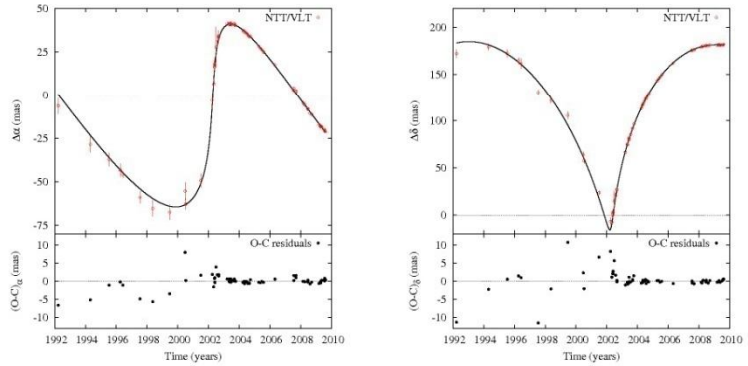

Figure 3. The comparisons between the observed (open circles with error bars) and fitted (solid lines) coordinates of S2 star (top), as well as the corresponding O-C residuals (bottom). The left panel shows the results for $\Delta\alpha$ and right panel for $\Delta\delta$ in the case of NTT/VLT observations and Yukawa gravity potential with $\delta = +1/3$ and $\Lambda = 2.59 \times 10^3$ AU.

the position of the origin of Keck observations is first shifted by $\Delta x = 3.7$ and $\Delta y = 4.1$ mas, following the suggestion given in [39]. In the first case the best fit is obtained for $\Lambda = 2.59 \times 10^3$ AU, resulting with reduced $\chi^2 = 1.54$, and in the second case for $\Lambda = 3.03 \times 10^3$ AU with reduced $\chi^2 = 3.24$. As one can see from these figures, in both cases there is a good agreement between the theoretical orbits and observations, although the higher value of reduced χ^2 in

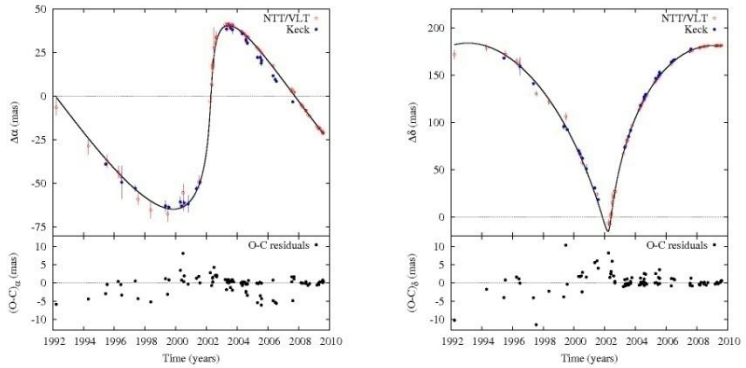

Figure 4. The same as in Fig. 3, but for NTT/VLT+Keck combined observations and for Yukawa gravity potential with $\Lambda = 3.03 \times 10^3$ AU.

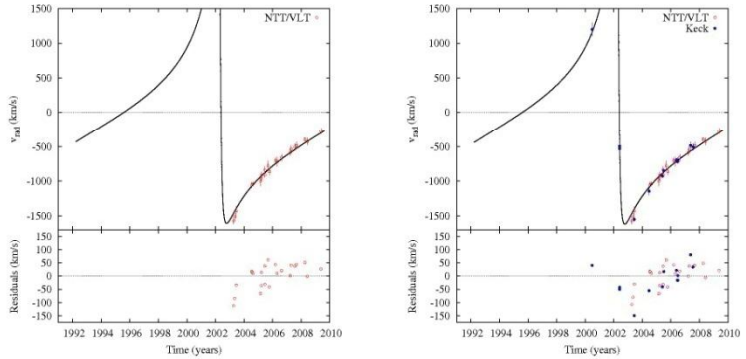

Figure 5. The comparisons between the observed (circles with error bars) and fitted (solid lines) radial velocities of S2 star (top), as well as the corresponding O-C residuals (bottom). The left panel shows the results in the case of NTT/VLT observations and Yukawa gravity potential with $\Lambda = 2.59 \times 10^3$ AU, while the right panel shows the results for NTT/VLT+Keck combined observations and for Yukawa gravity potential with $\Lambda = 3.03 \times 10^3$ AU. In both cases $\delta = +1/3$.

the second case indicates possibly larger positional difference between the two coordinate systems, as also noted in [39]. These figures also show that the simulated orbits of S2 are not closed in vicinity of apocenter, indicating a possible orbital precession.

In Figs. 3 and 4 we presented the comparisons between the observed and fitted coordinates of S2 star and their O-C residuals in the case of NTT/VLT observations, as well as NTT/VLT+Keck combined data set, respectively. One can notice that in both cases, O-C

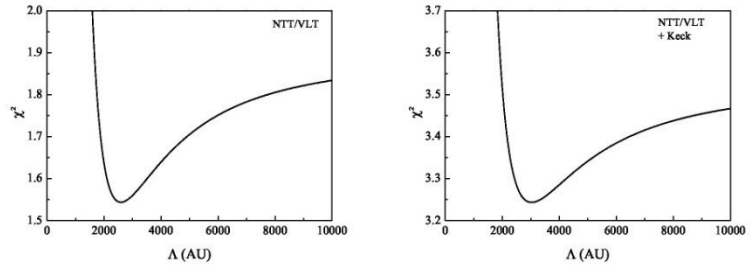

Figure 6. The reduced χ^2 for δ=1/3 as a function of Λ in case of NTT/VLT alone (left) and combined NTT/VLT+Keck (right) observations.

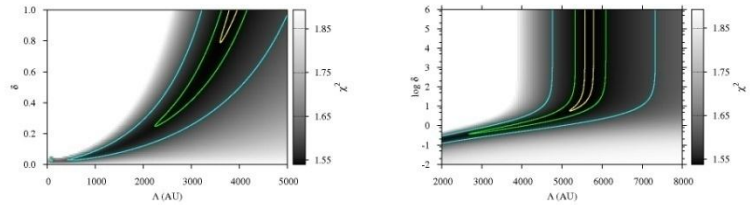

Figure 7. The maps of reduced χ^2 over the Λ δ parameter space in case of NTT/VLT observations. The left panel corresponds to $\delta \in [0, 1]$, and the right panel to the extended range of $\delta \in [0.01, 10^6]$. The shades of gray color represent the values of the reduced χ^2 which are less than the corresponding value in the case of Keplerian orbit, and three contours (from inner to outer) enclose the confidence regions in which the difference between the current and minimum reduced χ^2 is less than 0.0005, 0.005 and 0.05, respectively.

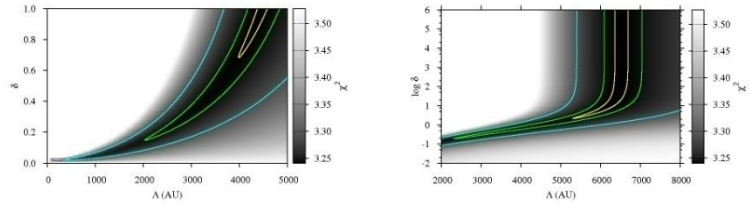

Figure 8. The same as in Fig. 7, but for the combined NTT/VLT+Keck observations.

residuals are higher in the first part of observing interval (up to the 12 mas) and much less in its second part (less than 2 mas). Due to adopted merit function given by expression (2.7), our fitting procedure assigned greater weight to these latter, more precise observations. Also, the O-C residuals are larger in the case of the combined NTT/VLT+Keck observations most likely due to the shift of the origin of the coordinate system, which was necessary in order to

Massive graviton theories

- M. Fierz and W.Pauli-1939
- Zakharov; Veltman, van Dam – 1970
- Vainshtein - 1972
- Boulware, Deser -- 1972
- Logunov, Mestvirishvili, Gershtein et al.
- Visser – 1998 (review on such theories)
- Rubakov, Tinyakov – 2008
- DeRham --2016

Observation of Gravitational Waves from a Binary Black Hole Merger

B. P. Abbott *et al.*[*]
(LIGO Scientific Collaboration and Virgo Collaboration)
(Received 21 January 2016; published 11 February 2016)

On September 14, 2015 at 09:50:45 UTC the two detectors of the Laser Interferometer Gravitational-Wave Observatory simultaneously observed a transient gravitational-wave signal. The signal sweeps upwards in frequency from 35 to 250 Hz with a peak gravitational-wave strain of 1.0×10^{-21}. It matches the waveform predicted by general relativity for the inspiral and merger of a pair of black holes and the ringdown of the resulting single black hole. The signal was observed with a matched-filter signal-to-noise ratio of 24 and a false alarm rate estimated to be less than 1 event per 203 000 years, equivalent to a significance greater than 5.1σ. The source lies at a luminosity distance of 410^{+160}_{-180} Mpc corresponding to a redshift $z = 0.09^{+0.03}_{-0.04}$. In the source frame, the initial black hole masses are $36^{+5}_{-4}M_{\odot}$ and $29^{+4}_{-4}M_{\odot}$, and the final black hole mass is $62^{+4}_{-4}M_{\odot}$, with $3.0^{+0.5}_{-0.5}M_{\odot}c^2$ radiated in gravitational waves. All uncertainties define 90% credible intervals. These observations demonstrate the existence of binary stellar-mass black hole systems. This is the first direct detection of gravitational waves and the first observation of a binary black hole merger.

DOI: 10.1103/PhysRevLett.116.061102

I. INTRODUCTION

In 1916, the year after the final formulation of the field equations of general relativity, Albert Einstein predicted the existence of gravitational waves. He found that the linearized weak-field equations had wave solutions: transverse waves of spatial strain that travel at the speed of light, generated by time variations of the mass quadrupole moment of the source [1,2]. Einstein understood that gravitational-wave amplitudes would be remarkably small; moreover, until the Chapel Hill conference in 1957 there was significant debate about the physical reality of gravitational waves [3].

Also in 1916, Schwarzschild published a solution for the field equations [4] that was later understood to describe a black hole [5,6], and in 1963 Kerr generalized the solution to rotating black holes [7]. Starting in the 1970s theoretical work led to the understanding of black hole quasinormal modes [8–10], and in the 1990s higher-order post-Newtonian calculations [11] preceded extensive analytical studies of relativistic two-body dynamics [12,13]. These advances, together with numerical relativity breakthroughs in the past decade [14–16], have enabled modeling of binary black hole mergers and accurate predictions of their gravitational waveforms. While numerous black hole candidates have now been identified through electromagnetic observations [17–19], black hole mergers have not previously been observed.

The discovery of the binary pulsar system PSR B1913+16 by Hulse and Taylor [20] and subsequent observations of its energy loss by Taylor and Weisberg [21] demonstrated the existence of gravitational waves. This discovery, along with emerging astrophysical understanding [22], led to the recognition that direct observations of the amplitude and phase of gravitational waves would enable studies of additional relativistic systems and provide new tests of general relativity, especially in the dynamic strong-field regime.

Experiments to detect gravitational waves began with Weber and his resonant mass detectors in the 1960s [23], followed by an international network of cryogenic resonant detectors [24]. Interferometric detectors were first suggested in the early 1960s [25] and the 1970s [26]. A study of the noise and performance of such detectors [27], and further concepts to improve them [28], led to proposals for long-baseline broadband laser interferometers with the potential for significantly increased sensitivity [29–32]. By the early 2000s, a set of initial detectors was completed, including TAMA 300 in Japan, GEO 600 in Germany, the Laser Interferometer Gravitational-Wave Observatory (LIGO) in the United States, and Virgo in Italy. Combinations of these detectors made joint observations from 2002 through 2011, setting upper limits on a variety of gravitational-wave sources while evolving into a global network. In 2015, Advanced LIGO became the first of a significantly more sensitive network of advanced detectors to begin observations [33–36].

A century after the fundamental predictions of Einstein and Schwarzschild, we report the first direct detection of gravitational waves and the first direct observation of a binary black hole system merging to form a single black hole. Our observations provide unique access to the

[*]Full author list given at the end of the article.

properties of space-time in the strong-field, high-velocity regime and confirm predictions of general relativity for the nonlinear dynamics of highly disturbed black holes.

II. OBSERVATION

On September 14, 2015 at 09:50:45 UTC, the LIGO Hanford, WA, and Livingston, LA, observatories detected the coincident signal GW150914 shown in Fig. 1. The initial detection was made by low-latency searches for generic gravitational-wave transients [41] and was reported within three minutes of data acquisition [43]. Subsequently, matched-filter analyses that use relativistic models of compact binary waveforms [44] recovered GW150914 as the most significant event from each detector for the observations reported here. Occurring within the 10-ms intersite

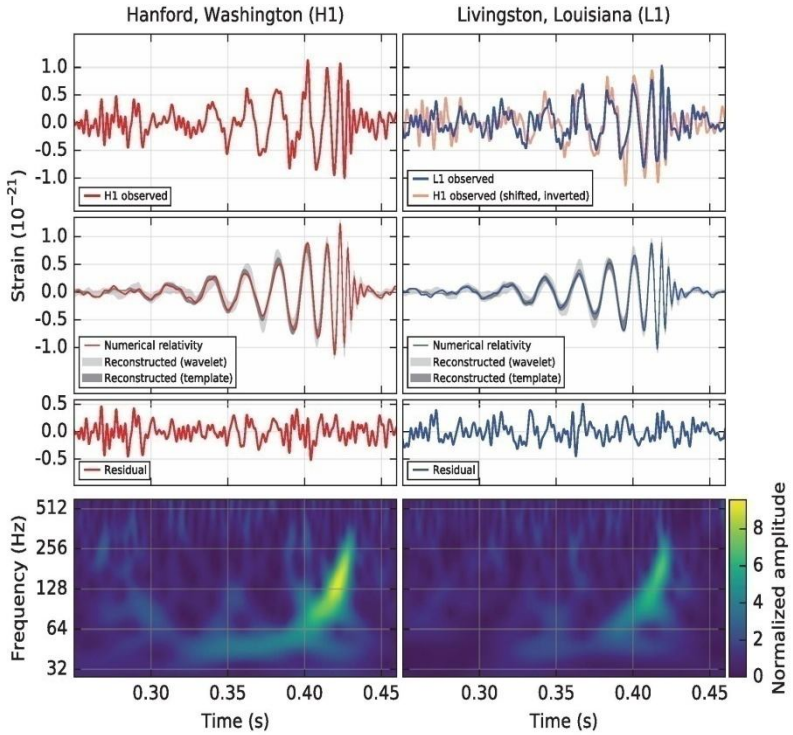

FIG. 1. The gravitational-wave event GW150914 observed by the LIGO Hanford (H1, left column panels) and Livingston (L1, right column panels) detectors. Times are shown relative to September 14, 2015 at 09:50:45 UTC. For visualization, all time series are filtered with a 35–350 Hz bandpass filter to suppress large fluctuations outside the detectors' most sensitive frequency band, and band-reject filters to remove the strong instrumental spectral lines seen in the Fig. 3 spectra. *Top row, left:* H1 strain. *Top row, right:* L1 strain. GW150914 arrived first at L1 and $6.9^{+0.5}_{-0.4}$ ms later at H1; for a visual comparison, the H1 data are also shown, shifted in time by this amount and inverted (to account for the detectors' relative orientations). *Second row:* Gravitational-wave strain projected onto each detector in the 35–350 Hz band. Solid lines show a numerical relativity waveform for a system with parameters consistent with those recovered from GW150914 [37,38] confirmed to 99.9% by an independent calculation based on [15]. Shaded areas show 90% credible regions for two independent waveform reconstructions. One (dark gray) models the signal using binary black hole template waveforms [39]. The other (light gray) does not use an astrophysical model, but instead calculates the strain signal as a linear combination of sine-Gaussian wavelets [40,41]. These reconstructions have a 94% overlap, as shown in [39]. *Third row:* Residuals after subtracting the filtered numerical relativity waveform from the filtered detector time series. *Bottom row:* A time-frequency representation [42] of the strain data, showing the signal frequency increasing over time.

propagation time, the events have a combined signal-to-noise ratio (SNR) of 24 [45].

Only the LIGO detectors were observing at the time of GW150914. The Virgo detector was being upgraded, and GEO 600, though not sufficiently sensitive to detect this event, was operating but not in observational mode. With only two detectors the source position is primarily determined by the relative arrival time and localized to an area of approximately 600 deg^2 (90% credible region) [39,46].

The basic features of GW150914 point to it being produced by the coalescence of two black holes—i.e., their orbital inspiral and merger, and subsequent final black hole ringdown. Over 0.2 s, the signal increases in frequency and amplitude in about 8 cycles from 35 to 150 Hz, where the amplitude reaches a maximum. The most plausible explanation for this evolution is the inspiral of two orbiting masses, m_1 and m_2, due to gravitational-wave emission. At the lower frequencies, such evolution is characterized by the chirp mass [11]

$$\mathcal{M} = \frac{(m_1 m_2)^{3/5}}{(m_1 + m_2)^{1/5}} = \frac{c^3}{G}\left[\frac{5}{96}\pi^{-8/3} f^{-11/3}\dot{f}\right]^{3/5},$$

where f and $\dot{f}$ are the observed frequency and its time derivative and G and c are the gravitational constant and speed of light. Estimating f and $\dot{f}$ from the data in Fig. 1, we obtain a chirp mass of $\mathcal{M} \simeq 30 M_\odot$, implying that the total mass $M = m_1 + m_2$ is $\gtrsim 70 M_\odot$ in the detector frame. This bounds the sum of the Schwarzschild radii of the binary components to $2GM/c^2 \gtrsim 210$ km. To reach an orbital frequency of 75 Hz (half the gravitational-wave frequency) the objects must have been very close and very compact; equal Newtonian point masses orbiting at this frequency would be only $\simeq 350$ km apart. A pair of neutron stars, while compact, would not have the required mass, while a black hole neutron star binary with the deduced chirp mass would have a very large total mass, and would thus merge at much lower frequency. This leaves black holes as the only known objects compact enough to reach an orbital frequency of 75 Hz without contact. Furthermore, the decay of the waveform after it peaks is consistent with the damped oscillations of a black hole relaxing to a final stationary Kerr configuration. Below, we present a general-relativistic analysis of GW150914; Fig. 2 shows the calculated waveform using the resulting source parameters.

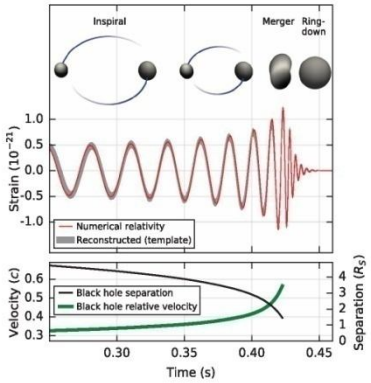

FIG. 2. *Top:* Estimated gravitational-wave strain amplitude from GW150914 projected onto H1. This shows the full bandwidth of the waveforms, without the filtering used for Fig. 1. The inset images show numerical relativity models of the black hole horizons as the black holes coalesce. *Bottom:* The Keplerian effective black hole separation in units of Schwarzschild radii ($R_S = 2GM/c^2$) and the effective relative velocity given by the post-Newtonian parameter $v/c = (GM\pi f/c^3)^{1/3}$, where f is the gravitational-wave frequency calculated with numerical relativity and M is the total mass (value from Table I).

III. DETECTORS

Gravitational-wave astronomy exploits multiple, widely separated detectors to distinguish gravitational waves from local instrumental and environmental noise, to provide source sky localization, and to measure wave polarizations. The LIGO sites each operate a single Advanced LIGO detector [33], a modified Michelson interferometer (see Fig. 3) that measures gravitational-wave strain as a difference in length of its orthogonal arms. Each arm is formed by two mirrors, acting as test masses, separated by $L_x = L_y = L = 4$ km. A passing gravitational wave effectively alters the arm lengths such that the measured difference is $\Delta L(t) = \delta L_x - \delta L_y = h(t)L$, where h is the gravitational-wave strain amplitude projected onto the detector. This differential length variation alters the phase difference between the two light fields returning to the beam splitter, transmitting an optical signal proportional to the gravitational-wave strain to the output photodetector.

To achieve sufficient sensitivity to measure gravitational waves, the detectors include several enhancements to the basic Michelson interferometer. First, each arm contains a resonant optical cavity, formed by its two test mass mirrors, that multiplies the effect of a gravitational wave on the light phase by a factor of 300 [48]. Second, a partially transmissive power-recycling mirror at the input provides additional resonant buildup of the laser light in the interferometer as a whole [49,50]: 20 W of laser input is increased to 700 W incident on the beam splitter, which is further increased to 100 kW circulating in each arm cavity. Third, a partially transmissive signal-recycling mirror at the output optimizes

black hole system in general relativity [94]. A first consistency check involves the mass and spin of the final black hole. In general relativity, the end product of a black hole binary coalescence is a Kerr black hole, which is fully described by its mass and spin. For quasicircular inspirals, these are predicted uniquely by Einstein's equations as a function of the masses and spins of the two progenitor black holes. Using fitting formulas calibrated to numerical relativity simulations [92], we verified that the remnant mass and spin deduced from the early stage of the coalescence and those inferred independently from the late stage are consistent with each other, with no evidence for disagreement from general relativity.

Within the post-Newtonian formalism, the phase of the gravitational waveform during the inspiral can be expressed as a power series in $f^{1/3}$. The coefficients of this expansion can be computed in general relativity. Thus, we can test for consistency with general relativity [95,96] by allowing the coefficients to deviate from the nominal values, and seeing if the resulting waveform is consistent with the data. In this second check [94] we place constraints on these deviations, finding no evidence for violations of general relativity.

Finally, assuming a modified dispersion relation for gravitational waves [97], our observations constrain the Compton wavelength of the graviton to be $\lambda_g > 10^{13}$ km, which could be interpreted as a bound on the graviton mass $m_g < 1.2 \times 10^{-22}$ eV$/c^2$. This improves on Solar System and binary pulsar bounds [98,99] by factors of a few and a thousand, respectively, but does not improve on the model-dependent bounds derived from the dynamics of Galaxy clusters [100] and weak lensing observations [101]. In summary, all three tests are consistent with the predictions of general relativity in the strong-field regime of gravity.

GW150914 demonstrates the existence of stellar-mass black holes more massive than $\approx 25 M_\odot$, and establishes that binary black holes can form in nature and merge within a Hubble time. Binary black holes have been predicted to form both in isolated binaries [102–104] and in dense environments by dynamical interactions [105–107]. The formation of such massive black holes from stellar evolution requires weak massive-star winds, which are possible in stellar environments with metallicity lower than $\approx 1/2$ the solar value [108,109]. Further astrophysical implications of this binary black hole discovery are discussed in [110].

These observational results constrain the rate of stellar-mass binary black hole mergers in the local universe. Using several different models of the underlying binary black hole mass distribution, we obtain rate estimates ranging from 2–400 Gpc^{-3} yr^{-1} in the comoving frame [111–113]. This is consistent with a broad range of rate predictions as reviewed in [114], with only the lowest event rates being excluded.

Binary black hole systems at larger distances contribute to a stochastic background of gravitational waves from the superposition of unresolved systems. Predictions for such a background are presented in [115]. If the signal from such a population were detected, it would provide information about the evolution of such binary systems over the history of the universe.

VII. OUTLOOK

Further details about these results and associated data releases are available at [116]. Analysis results for the entire first observational period will be reported in future publications. Efforts are under way to enhance significantly the global gravitational-wave detector network [117]. These include further commissioning of the Advanced LIGO detectors to reach design sensitivity, which will allow detection of binaries like GW150914 with 3 times higher SNR. Additionally, Advanced Virgo, KAGRA, and a possible third LIGO detector in India [118] will extend the network and significantly improve the position reconstruction and parameter estimation of sources.

VIII. CONCLUSION

The LIGO detectors have observed gravitational waves from the merger of two stellar-mass black holes. The detected waveform matches the predictions of general relativity for the inspiral and merger of a pair of black holes and the ringdown of the resulting single black hole. These observations demonstrate the existence of binary stellar-mass black hole systems. This is the first direct detection of gravitational waves and the first observation of a binary black hole merger.

ACKNOWLEDGMENTS

The authors gratefully acknowledge the support of the United States National Science Foundation (NSF) for the construction and operation of the LIGO Laboratory and Advanced LIGO as well as the Science and Technology Facilities Council (STFC) of the United Kingdom, the Max-Planck Society (MPS), and the State of Niedersachsen, Germany, for support of the construction of Advanced LIGO and construction and operation of the GEO 600 detector. Additional support for Advanced LIGO was provided by the Australian Research Council. The authors gratefully acknowledge the Italian Istituto Nazionale di Fisica Nucleare (INFN), the French Centre National de la Recherche Scientifique (CNRS), and the Foundation for Fundamental Research on Matter supported by the Netherlands Organisation for Scientific Research, for the construction and operation of the Virgo detector, and for the creation and support of the EGO consortium. The authors also gratefully acknowledge research support from these agencies as well as by the Council of Scientific and Industrial Research of India, Department of Science and

Tests of General Relativity with Binary Black Holes from the second LIGO–Virgo Gravitational-Wave Transient Catalog

The LIGO Scientific Collaboration and the Virgo Collaboration

(compiled 29 October 2020)

Gravitational waves enable tests of general relativity in the highly dynamical and strong-field regime. Using events detected by LIGO–Virgo up to 1 October 2019, we evaluate the consistency of the data with predictions from the theory. We first establish that residuals from the best-fit waveform are consistent with detector noise, and that the low- and high-frequency parts of the signals are in agreement. We then consider parametrized modifications to the waveform by varying post-Newtonian and phenomenological coefficients, improving past constraints by factors of ~2; we also find consistency with Kerr black holes when we specifically target signatures of the spin-induced quadrupole moment. Looking for gravitational-wave dispersion, we tighten constraints on Lorentz-violating coefficients by a factor of ~2.6 and bound the mass of the graviton to $m_g \leq 1.76 \times 10^{-23}\ \mathrm{eV}/c^2$ with 90% credibility. We also analyze the properties of the merger remnants by measuring ringdown frequencies and damping times, constraining fractional deviations away from the Kerr frequency to $\delta\hat{f}_{220} = 0.03^{+0.38}_{-0.35}$ for the fundamental quadrupolar mode, and $\delta\hat{f}_{221} = 0.04^{+0.27}_{-0.32}$ for the first overtone; additionally, we find no evidence for postmerger echoes. Finally, we determine that our data are consistent with tensorial polarizations through a template-independent method. When possible, we assess the validity of general relativity based on collections of events analyzed jointly. We find no evidence for new physics beyond general relativity, for black hole mimickers, or for any unaccounted systematics.

I. INTRODUCTION

General relativity (GR) remains our most accurate theory of gravity, having withstood many experimental tests in the Solar System [1] as well as binary pulsar [1, 2], cosmological [3, 4] and gravitational-wave (GW) observations [5–15]. Many of these tests probe regimes where gravitational fields are weak, spacetime curvature is small, and characteristic velocities are not comparable to the speed of light. Observations of compact binary coalescences enable us to test GR in extreme environments of strong gravitational fields, large spacetime curvature, and velocities comparable to the speed of light; high post-Newtonian (PN) order calculations and numerical relativity (NR) simulations are required to accurately model the emitted GW signal [5, 6, 14, 15].

We report results from tests of GR on binary black hole (BBH) signals using the second Gravitational-wave Transient catalog (GWTC-2) [16]. The GWTC-2 catalog includes all observations reported in the first catalog (GWTC-1) [17], covering the first (O1) and second (O2) observing runs, as well as new events identified in the first half of the third observing run (O3a) of the Advanced LIGO and Advanced Virgo detectors [16]. We focus on the most significant signals, requiring them for the GW signal emitted by two coalescing compact objects. Recent NR studies have begun to model astrophysically relevant binary black hole mergers in beyond-GR theories [30–34] and numerous advances have been made deriving the analytical equations of motion and gravitational waveforms in such theories [35–48]. However, it is often unknown whether the full theories are well-posed and a significant amount of work is required before the results can be used in the context of GW data analysis.

The approach taken here is therefore to (i) check the consistency of GR predictions with the data, and (ii) introduce parametrized modifications to GR waveforms in order to constrain the degree to which the deviations from the GR predictions agree with the data. As in [15], the results in this paper should be treated as observational constraints on deviations from GR. Such limits are a quantitative indication of the degree to which the data are described by GR but can also be reinterpreted in the context of a given modified theory of gravity to produce constraints, subject to a number of assumptions [7, 49]. Our analyses do not reveal any inconsistency with GR and the results improve on the previous tests of GR using the BBHs observed in O1 and O2 [5, 6, 8, 13–15].

The analyses performed in this paper can be broken down

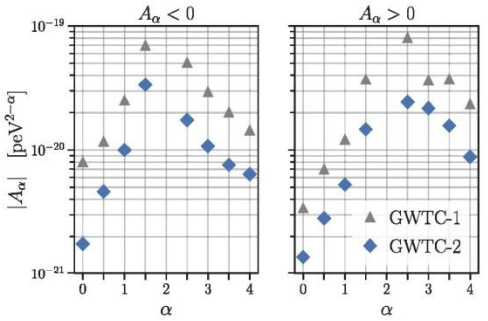

FIG. 11. 90% credible upper bounds on the absolute value of the modified dispersion relation parameter A_α. The upper limits are derived from the distributions in Fig. 12, treating the positive and negative values of A_α separately. Picoelectronvolts provide a convenient scale because 1 peV $\simeq h \times 250$ Hz, where 250 Hz is close to the most sensitive frequencies of the LIGO and Virgo instruments. Marker style distinguishes the new GWTC-2 results from the previous GWTC-1 results in [15].

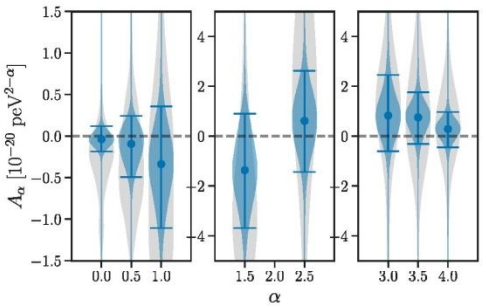

FIG. 12. Violin plots of the full posteriors on the modified dispersion relation parameter A_α calculated from the GWTC-2 events (blue), with the 90% credible interval around the median indicated. For comparison, we also show the GWTC-1 previous measurement (gray), reported in [15].

dispersion relations, we adopt the common phenomenological modification to GR introduced in [185] and applied to LIGO and Virgo data in [8, 15]:

$$E^2 = p^2c^2 + A_\alpha p^\alpha c^\alpha , \tag{6}$$

where A_α and α are phenomenological parameters, and GR is recovered if $A_\alpha = 0$ for all α. To leading order, Eq. (6) may encompass a variety of predictions from different extensions to GR [7, 185–191]; this includes massive gravity for $\alpha = 0$ and $A_\alpha > 0$, with a graviton mass $m_g = A_0^{1/2} c^{-2}$ [186]. As in [15], we consider α values from 0 to 4 in steps of 0.5, excluding $\alpha = 2$, which is degenerate with an overall time delay. A nonzero A_α manifests itself in the data as a frequency-dependent dephasing of the GW signal, which builds up as the wave propagates towards Earth and hence increases with the source comoving distance, potentially enhancing weak GR deviations.

The analysis makes use of a modified version of the IMRPhenomPv2 waveform (checks for systematics using SEOBNRv4HM_ROM were presented in [15]). We use Eq. (3) of [15] to compute the dephasing for a given A_α. This expression was derived in [185] by treating waves emitted at a given time as particles that travel at the particle velocity $v_p = pc^2/E$ associated with the wave's instantaneous frequency. Different dephasings can arise from different prescriptions, e.g., using the group velocity instead, but the corresponding bound on A_α (see Sec. II and Table I).[4] Since we can take A_α and m_g to be universal parameters, results from different events can be easily combined by multiplying the individual likelihoods. Although we only discuss the overall combined results here, individual-event posteriors are available in [53], as for other tests.

We show our results in Table VII and Figs. 11 and 12. Table VII and Fig. 11 present constraints on the allowed amount of dispersion through the 90%-credible upper limits on $|A_\alpha|$, computed separately for $A_\alpha > 0$ and $A_\alpha < 0$. There is noticeable improvement when combining GWTC-2 results with respect to the previous result in [15]. This is the case for both positive and negative amplitudes, meaning that we are more tightly constraining these quantities closer to the nondispersive, GR prediction ($A_\alpha = 0$). The average improvement in the $|A_\alpha|$ upper limits relative to [15] is a factor 2.6, although this fluctuates slightly across α's. Overall, this is consistent with the factor of $\sqrt{31/7} \approx 2.1$ naively expected from the increase in the number of events analyzed.[5]

Upper limits on the A_α parameters can be uncertain due to the difficulty in accurately sampling the long tails of the posteriors. To quantify this uncertainty, we follow a Bayesian bootstrapping procedure [192], as done previously in [8, 15], with 2000 bootstrap realisations for each value of α and sign of A_α. We find that the average width of the 90%-credible interval of the individual-event upper limits is a factor of 0.12 of the reported upper limit itself, i.e., the average uncertainty in the upper limit is 0.12. Out of all upper limits, 9 carry fractional uncertainties larger than 0.5. The most uncertain upper limit is that for GW190828_065509 and $A_4 < 0$, with a fractional uncertainty of 1.7.

Figure 12 shows the overall posterior obtained for negative

TABLE VII. Results for the modified dispersion analysis (Sec. VI). The table shows 90%-credible upper bounds on the graviton mass m_g and the absolute value of the modified dispersion relation parameter A_α, as well as the GR quantiles $Q_{\rm GR}$. The < and > labels denote the upper bound on $|A_\alpha|$ when assuming $A_\alpha < 0$ and > 0, respectively, and $\tilde{A}_\alpha = A_\alpha/\mathrm{eV}^{2-\alpha}$ is dimensionless. Rows compare the GWTC-1 results from [15] to the GWTC-2 results.

	m_g	$\lvert\tilde{A}_0\rvert$			$\lvert\tilde{A}_{0.5}\rvert$			$\lvert\tilde{A}_1\rvert$			$\lvert\tilde{A}_{1.5}\rvert$			$\lvert\tilde{A}_{2.5}\rvert$			$\lvert\tilde{A}_3\rvert$			$\lvert\tilde{A}_{3.5}\rvert$			$\lvert\tilde{A}_4\rvert$		
	$[10^{-23}$ eV$/c^2]$	< $[10^{-45}]$	>	$Q_{\rm GR}$ [%]	< $[10^{-38}]$	>	$Q_{\rm GR}$ [%]	< $[10^{-32}]$	>	$Q_{\rm GR}$ [%]	< $[10^{-26}]$	>	$Q_{\rm GR}$ [%]	< $[10^{-14}]$	>	$Q_{\rm GR}$ [%]	< $[10^{-8}]$	>	$Q_{\rm GR}$ [%]	< $[10^{-2}]$	>	$Q_{\rm GR}$ [%]	< $[10^{4}]$	>	$Q_{\rm GR}$ [%]
GWTC-1	4.70	7.99	3.39	79	1.17	0.70	73	2.51	1.21	70	6.96	3.70	86	5.05	8.01	28	2.94	3.66	25	2.01	3.73	35	1.44	2.34	34
GWTC-2	1.76	1.75	1.37	66	0.46	0.28	66	1.00	0.52	79	3.35	1.47	83	1.74	2.43	31	1.08	2.17	17	0.76	1.57	12	0.64	0.88	25

and positive values of A_α. The enhanced stringency of our measurements relative to our previous GWTC-1 results is also visible here, as seen in the smaller size of the blue violins with respect to the gray, and the fact that the medians (blue circles) are generally closer to the GR value. The latter is also manifested in the GR quantiles $Q_{\rm GR} = P(A_\alpha < 0)$ in Table VII, which tend to be closer to 50% ($Q_{\rm GR} = 50\%$ implies the distribution is centered on the GR value).

From our combined GWTC-2 data, we bound the graviton mass to be $m_g \leq 1.76 \times 10^{-23}\mathrm{eV}/c^2$, with 90% credibility (Table VII). This represents an improvement of a factor of 2.7 relative to [15]. The new measurement is 1.8 times more stringent than the most recent Solar System bound of 3.16×10^{-23} eV$/c^2$, also with 90% credibility [193].

VII. REMNANT PROPERTIES

A. Ringdown

In GR, the remnant object resulting from the coalescence of two astrophysical BHs is a perturbed Kerr BH. This remnant BH will gradually relax to its Kerr stationary state by emitting GWs corresponding to a specific set of characteristic quasi-normal modes (QNMs), whose frequency f and damping time τ depend solely on the BH mass $M_{\rm f}$ and the dimensionless spin $\chi_{\rm f}$. This last stage of the coalescence is known as *ringdown*. The description of the ringdown stage is based on the final state conjecture [194–198] stating that the physical spectrum of QNMs is exclusively determined by the final BH mass and spin (the no-hair conjecture [161, 199–206]) and that the Kerr solution is an attractor of BH spacetimes in astrophysical scenarios.[6]

By analyzing the postmerger signal from a BBH coalescence independently of the preceding inspiral, we can verify the final state conjecture, test the nature of the remnant object (complementary to the searches for GW echoes discussed in Sec. VII B), and estimate directly the remnant mass and spin assuming it is a Kerr BH—which, in turn, allows us to test GR's prediction for the energy and angular momentum emitted during the coalescence (complementary to the IMR consistency test discussed in Sec. IV B, and the postinspiral parameters in Sec. V A). This set of analyses is referred to as *BH spectroscopy* [122, 123, 210–219]. Unlike the IMR consistency test, a ringdown-only analysis is not contaminated by frequency mixing with other phases of the signal and it does not require a large amount of SNR in the inspiral regime (the lack of such SNR is why the IMR consistency test was unable to be applied to GW190521 [82, 83], for instance).

The complex-valued GW waveform during ringdown can be expressed as a superposition of damped sinusoids:

$$h_+(t) - ih_\times(t) = \sum_{\ell=2}^{+\infty}\sum_{m=-\ell}^{\ell}\sum_{n=0}^{+\infty} \mathcal{A}_{\ell mn}\, \exp\left[-\frac{t-t_0}{(1+z)\tau_{\ell mn}}\right] \exp\left[\frac{2\pi i f_{\ell mn}(t-t_0)}{1+z}\right] {}_{-2}S_{\ell mn}(\theta,\phi,\chi_{\rm f}), \tag{7}$$

where z is the cosmological redshift, and the (ℓ, m, n) indices label the QNMs. The angular multipoles are denoted by ℓ and m, while n orders modes of a given (ℓ, m) by decreasing damping time. The frequency and the damping time for each ringdown mode can be computed for a perturbed isolated BH as a function of its mass $M_{\rm f}$ and spin $\chi_{\rm f}$ [220–223]. For each (ℓ, m, n), there are in principle two associated frequencies and damping times: those for a *prograde* mode, with $\mathrm{sgn}(f_{\ell mn}) = \mathrm{sgn}(m)$, and those for a *retrograde* mode, with $\mathrm{sgn}(f_{\ell mn}) \neq \mathrm{sgn}(m)$—retrograde modes are not expected to be relevant [212], so we do not include them in Eq. (7). The frequency and damping time of the $+|m|$ mode are related to those of the $-|m|$ mode by $f_{\ell mn} = -f_{\ell -mn}$ and $\tau_{\ell mn} = \tau_{\ell -mn}$ for $m \neq 0$. The complex amplitudes $\mathcal{A}_{\ell mn}$ characterize the excitation and the phase of each ringdown mode at a reference time t_0, which for a BBH merger can be predicted from numerical simulations [224–226]. In general, $\mathcal{A}_{\ell mn}$ is independent of $\mathcal{A}_{\ell -mn}$.

The angular dependence of the GW waveform is contained in the spin-weighted spheroidal harmonics ${}_{-2}S_{\ell mn}(\theta, \phi, \chi_{\rm f})$, where θ, ϕ are the polar and azimuthal angles in a frame centered on the remnant BH and aligned with its angular mo-

[6] In principle such frequencies and damping times would also depend on the electric charge of the remnant BH. However, for astrophysically relevant scenarios the BH charge is expected to be negligible [207–209].

Journal of Cosmology and Astroparticle Physics
An IOP and SISSA journal

Constraining the range of Yukawa gravity interaction from S2 star orbits II: bounds on graviton mass

A.F. Zakharov,[a,b,c,d,e] **P. Jovanović,**[f] **D. Borka**[g] **and V. Borka Jovanović**[g]

[a]National Astronomical Observatories of Chinese Academy of Sciences, Datun Road 20A, Beijing, 100012 China
[b]Institute of Theoretical and Experimental Physics, 117259 Moscow, Russia
[c]National Research Nuclear University MEPhI (Moscow Engineering Physics Institute), 115409, Moscow, Russia
[d]Bogoliubov Laboratory for Theoretical Physics, JINR, 141980 Dubna, Russia
[e]North Carolina Central University, Durham, NC 27707, U.S.A.
[f]Astronomical Observatory, Volgina 7, 11060 Belgrade, Serbia
[g]Atomic Physics Laboratory (040), Vinča Institute of Nuclear Sciences, University of Belgrade, P.O. Box 522, 11001 Belgrade, Serbia

E-mail: zakharov@itep.ru, pjovanovic@aob.rs, dusborka@vin.bg.ac.rs, vborka@vin.bg.ac.rs

Received May 4, 2016
Accepted May 7, 2016
Published May 20, 2016

Abstract. Recently LIGO collaboration discovered gravitational waves [1] predicted 100 years ago by A. Einstein. Moreover, in the key paper reporting about the discovery, the joint LIGO & VIRGO team presented an upper limit on graviton mass such as $m_g < 1.2 \times 10^{-22} eV$ [1] (see also more details in another LIGO paper [2] dedicated to a data analysis to obtain such a small constraint on a graviton mass). Since the graviton mass limit is so small the authors concluded that their observational data do not show violations of classical general relativity. We consider another opportunity to evaluate a graviton mass from phenomenological consequences of massive gravity and show that an analysis of bright star

JCAP05(2016)045

modification of the Newtonian potential [5, 14]:

$$V(r) = -\frac{GM}{(1+\delta)r}\left[1+\delta e^{-\left(\frac{r}{\lambda}\right)}\right], \tag{1.1}$$

where δ is a universal constant. In our previous paper [35] we found constraints on parameters of Yukawa gravity.

Will considered an opportunity to evaluate a graviton mass analyzing a time delay in electromagnetic waves such as supernova or gamma-ray burst [5], moreover earlier he demonstrated a possibility to constrain a graviton mass from from gravitational wave signal alone [4].

Pulsar timing may be used to evaluate a graviton mass [36]. In the paper it was concluded that, with 90% probability, massless gravitons can be distinguished from gravitons heavier than 3×10^{-22} eV (Compton wavelength $\lambda_g = 4.1\times10^{12}$ km), if bi-weekly observation of 60 pulsars is performed for 5 years with a pulsar rms timing accuracy of 100 ns and if 10 year observation of 300 pulsars with 100 ns timing accuracy would probe graviton masses down to 3×10^{-23} eV ($\lambda_g = 4.1\times10^{13}$ km). These conclusions are based on an analysis of cross-correlation functions of gravitational wave background. An idea to use pulsar timing for gravitational wave detection has been proposed many years ago [37]. An analysis of the cross-correlation function between pulsar timing residuals of pulsar pairs could give an opportunity to detect gravitational waves [38, 39]. If a graviton has a mass it gives an impact on cross-correlation functions [36]. However, as a first step people have to discover stochastic GW signal and only after a detailed analysis of cross-correlation it could help to put constraints on a graviton mass.

Here we show that our previous results concerning the constraints on parameters of Yukawa gravity, presented in the paper [35], can be extended in the way that one could also obtain a graviton mass bounds from the observations of trajectories of bright stars near the Galactic Center. As it is shown below our estimate of a graviton mass is slightly greater than the estimate obtained by the LIGO collaboration with the first detection of gravitational waves from the binary black hole system. However, we would like to note that: a) our estimate is consistent with the LIGO one; b) in principle, with analysis of trajectories of bright stars near the Galactic Center one could obtain such a graviton mass estimate before the LIGO report [1] about the discovery of gravitational waves and their estimate of a graviton mass; c) in the future our estimate may be improved with forthcoming observational facilities.

2 Graviton mass estimates from S2 star orbit

Two groups of observers are monitoring bright stars (including S2 one) to evaluate gravitational potential at the Galactic Center [40–48]. Recently, the astrometric observations of S2 star [49] were used to evaluate parameters of black hole and to test and constrain several models of modified gravity at mpc scales [50–54]. The simulations of the S2 star orbit around the supermassive black hole at the Galactic Centre (GC) in Yukawa gravity [35] and their comparisons with the NTT/VLT astrometric observations of S2 star [49] resulted with the constraints on the range of Yukawa interaction λ, which showed that λ is most likely on the order of several thousand astronomical units. However, it was not possible to obtain the reliable constrains on the universal constant δ because its values $0 < \delta < 1$ were highly correlated to λ, while the values $\delta > 2$ corresponded to a practically fixed $\lambda \sim 5000$–6000 AU

JCAP05(2016)045

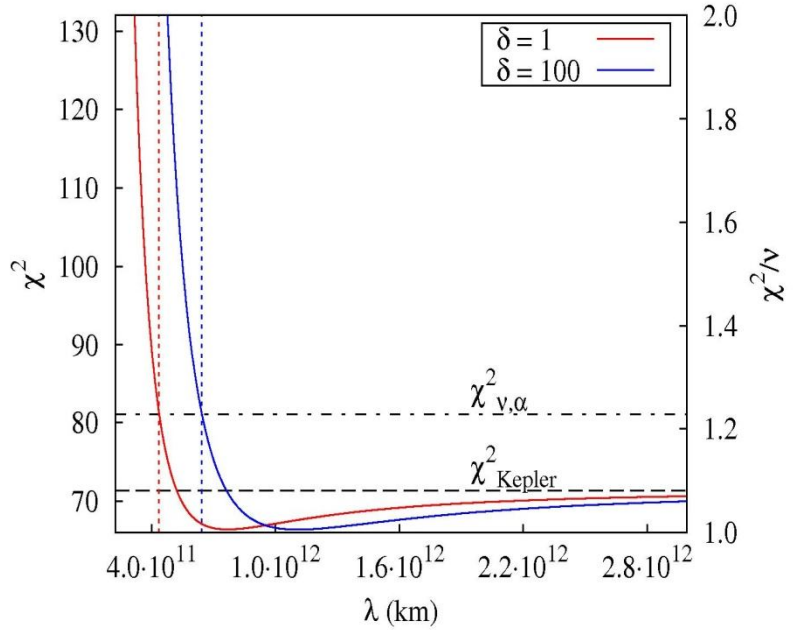
δ = 1
δ = 100
130
120
110
100
90
80
70
χ²
2.0
1.8
1.6
1.4
1.2
1.0
χ²/ν
χ²γ,α
χ²Kepler
4.0·10¹¹
1.0·10¹²
1.6·10¹²
2.2·10¹²
2.8·10¹²
λ (km)

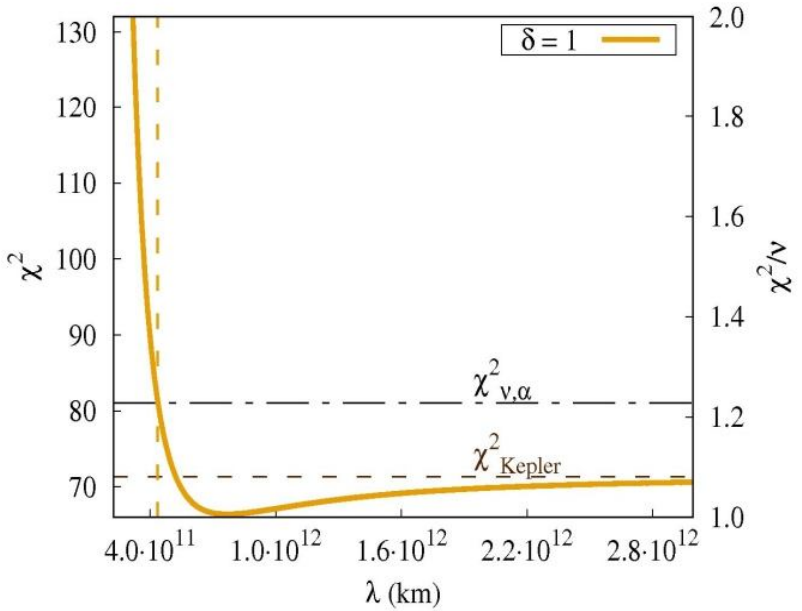
δ = 1
χ²
χ²/ν
χ²ν,α
χ²Kepler
130
120
110
100
90
80
70
2.0
1.8
1.6
1.4
1.2
1.0
4.0·10¹¹
1.0·10¹²
1.6·10¹²
2.2·10¹²
2.8·10¹²
λ (km)

Constraints on graviton mass from S2 trajectory

- AFZ, D. Borka, P. Jovanovic, V. Borka Jovanovic gr-qc: 1605.00913v; JCAP (2016) :
- $\lambda_g > 2900$ AU = 4.3×10^{11} km with P=0.9 or
- $m_g < 2.9 \times 10^{-21}$ eV $= 5.17 \times 10^{-54}$ g
- Hees et al. PRL (2017) slightly improved our estimates with their new data $m_g < 1.6 \times 10^{-21}$ eV (see discussion below)

Impact of our studies

Claudia de Rham, J. Tate Deskins, Andrew J. Tolley, Shuang-Yong Zhou, Graviton Mass Bounds, Reviews in Modern Physics 89, 0250004 (2017).

A. Hees, T. Do, A. M. Ghez, G. D. Martinez, S. Naoz, E. E. Becklin, A. Boehle, S. Chappell, D. Chu, A. Dehghanfar, K. Kosmo, J. R. Lu, K. Matthews, M. R. Morris, S. Sakai, R. Schodel, and G. Witze, Testing General Relativity with stellar orbits around the supermassive black hole in our Galactic center, arXiv:1705.07902v1 [astro-ph.GA], PRL 118, 211101.

A couple of our papers have been quoted in the second paper.

Testing General Relativity with Stellar Orbits around the Supermassive Black Hole in Our Galactic Center

A. Hees,[1*] T. Do,[1] A. M. Ghez,[1†] G. D. Martinez,[1] S. Naoz,[1] E. E. Becklin,[1] A. Boehle,[1] S. Chappell,[1] D. Chu,[1] A. Dehghanfar,[1] K. Kosmo,[1] J. R. Lu,[2] K. Matthews,[3] M. R. Morris,[1] S. Sakai,[1] R. Schödel,[4] and G. Witzel[1]

[1]*Department of Physics and Astronomy, University of California, Los Angeles, California 90095, USA*

[2]*Astronomy Department, University of California, Berkeley, California 94720, USA*

[3]*Division of Physics, Mathematics, and Astronomy, California Institute of Technology, MC 301-17, Pasadena, California 91125, USA*

[4]*Instituto de Astrofísica de Andalucía (CSIC), Glorieta de la Astronomía S/N, 18008 Granada, Spain*

(Received 22 December 2016; revised manuscript received 14 March 2017; published 25 May 2017)

We demonstrate that short-period stars orbiting around the supermassive black hole in our Galactic center can successfully be used to probe the gravitational theory in a strong regime. We use 19 years of observations of the two best measured short-period stars orbiting our Galactic center to constrain a hypothetical fifth force that arises in various scenarios motivated by the development of a unification theory or in some models of dark matter and dark energy. No deviation from general relativity is reported and the fifth force strength is restricted to an upper 95% confidence limit of $|\alpha| < 0.016$ at a length scale of $\lambda = 150$ astronomical units. We also derive a 95% confidence upper limit on a linear drift of the argument of periastron of the short-period star S0-2 of $|\dot{\omega}_{S0\text{-}2}| < 1.6 \times 10^{-3}$ rad/yr, which can be used to constrain various gravitational and astrophysical theories. This analysis provides the first fully self-consistent test of the gravitational theory using orbital dynamic in a strong gravitational regime, that of a supermassive black hole. A sensitivity analysis for future measurements is also presented.

DOI: 10.1103/PhysRevLett.118.211101

The development of a quantum theory of gravitation or of a unification theory generically predicts deviations from general relativity (GR). In addition, observations requiring the introduction of dark matter and dark energy also challenge GR and the standard model of particle physics [1] and are sometimes interpreted as a modification of gravitational theory (see, e.g., Refs. [2,3]). It is thus important to test the gravitational interaction with different types of observations [4]. While GR is thoroughly tested in the Solar System (see, e.g., Refs. [5–8]) and with binary pulsars (see, e.g., Ref. [9]), observations of short-period stars orbiting the supermassive black hole (SMBH) at the center of our Galaxy allow one to probe gravity in a strong field regime unexplored so far, as shown in Fig. 1 (see also Refs. [10,11]). In this Letter, we report two results: (i) a search for a fifth force around our Galactic center and (ii) a constraint on the advance of the periastron of the short-period star S0-2 that can be used to constrain various gravitational and astrophysical theories in our Galactic center. This analysis provides the first fully self-consistent test of the gravitational theory using an orbital dynamic in a strong gravitational regime around a SMBH. The constraints presented in this Letter, resulting from 20 yr of observations, are therefore highly complementary with Solar System or binary pulsar tests of gravitation and open a new window to study gravitation.

One phenomenological framework widely used to search for deviations from GR is the fifth force formalism [13–18], which considers deviations from Newtonian gravity in which the gravitational potential takes the form of a Yukawa potential

$$U = \frac{GM}{r}[1 + \alpha e^{-r/\lambda}], \tag{1}$$

with G the Newton's constant, M the mass of the central body, and r the distance to the central mass. This potential is characterized by two parameters: a length λ and a strength of interaction α. A Yukawa potential appears in several theoretical scenarios, such as unification theories that predict new fundamental interactions with a massive

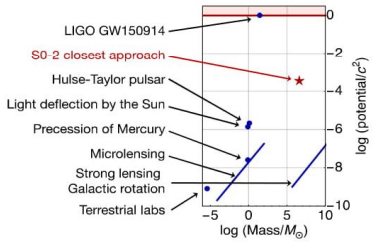

FIG. 1. The gravitational potential probed by different tests of gravitation against the mass of the central body that generates gravity in these tests. Short-period stars, such as S0-2, around our Galactic center explore a new region in this parameter space. The figure is inspired by Ref. [12].

stars are probing space-time in a higher potential and around a central body much more massive than in the other experiments. This is highlighted in the right panel of Fig. 2, where λ is expressed in terms of the gravitational radius of the central body. Furthermore, short-period stars probe the space-time around a SMBH, which is conceptually different from Solar System tests where the space-time curvature is generated by weakly gravitating bodies. Specifically, some nonperturbative effects may arise around strongly gravitating bodies (see, e.g., Ref. [76]). In addition, in models of gravity exhibiting screening mechanisms, deviations from GR may be screened in the Solar System (see, e.g., Ref. [77]). In this context, searches for alternative theories of gravitation in other environments are important.

A specific theoretical model covered by the fifth force framework is a massive graviton. In that context, we found a 90% confidence limit $\lambda > 5000$ A.U. for $\alpha = 1$, which can be interpreted as a lower limit on the graviton's Compton wavelength $\lambda_g > 7.5 \times 10^{11}$ km or, equivalently, as an upper bound on the graviton's mass $m_g < 1.6 \times 10^{-21}$ eV$/c^2$ (see also Ref. [36]). This constraint is one order of magnitude less stringent than the recent bound obtained by LIGO [78], which, nevertheless, does not apply for all models predicting a fifth force.

From an empirical perspective, one of the effects produced by a fifth force is a secular drift of the argument of periastron ω [31,79]. Several theoretical scenarios predict such an effect, which can be constrained by observations. We produced a new orbital fit using a model that includes seven global parameters (the SMBH GM, R_0, and the positions and velocities of the SMBH) and seven orbital parameters for each star, with the additional parameter being a linear drift of the argument of the periastron $\dot{\omega}$. As a result of our fit including the jackknife analysis, we obtained an upper confidence limit on a linear drift of the argument of periastron for S0-2 given by

$$|\dot{\omega}_{\mathrm{S0\text{-}2}}| < 1.7 \times 10^{-3} \text{ rad/yr at } 95\% \text{ C.L.} \quad (3)$$

This limit is currently one order of magnitude larger than the relativistic advance of the periastron $\dot{\omega}_{\mathrm{GR}} = 6\pi GM/[Pc^2 a(1-e^2)] = 1.6 \times 10^{-4}$ rad/yr for S0-2 (with a being the semimajor axis). Nevertheless, the limit from Eq. (3) can be used to derive a preliminary constraint on various theoretical scenarios (astrophysical or modified gravity) that predict an advance of the periastron for short-period stars in the Galactic center like, for example,

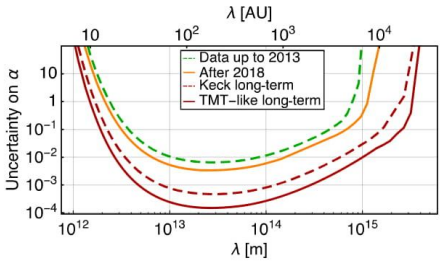

FIG. 3. Statistical uncertainty on the fifth force strength σ_α expected for various observational scenarios: the dashed green (light) line corresponds to the data used in this analysis, the continuous orange (light) line corresponds to data that will be available by the end of 2018. The two red (dark) lines include 16 additional years of observations with two astrometric observations and one spectroscopic observation per year with the following astrometric (spectroscopic) accuracy for an S0-2-like star: current Keck accuracy, 0.5 mas (30 km/s); TMT-like improved accuracy, 15 μas (5 km/s).

improve the current results. Figure 3 shows a sensitivity analysis based on a Fisher matrix approach performed to assess the improvement expected by observations with a TMT-like telescope. We have simulated 16 additional years of data for two scenarios: (i) a scenario where Keck observations are used with an astrometric uncertainty of 0.16 mas, comparable to today's performance, and (ii) a scenario with an improved astrometric uncertainty of 0.015 mas, which corresponds to a TMT-like scenario. Extending the time baseline by one S0-2 period improves the result by a factor of 13, while an improved accuracy brings an additional improvement of a factor of 5. In addition, the discovery of new stars orbiting closer to the SMBH and unbiased measurements of the known faint short-period star S0-102 ($P = 11.5$ yr) [43] would improve this analysis.

In conclusion, we have used 19 yr of observations of S0-2 and S0-38 reported in Ref. [44] to constrain a hypothetical fifth interaction around the SMBH in our Galactic center. The constraints obtained in our analysis are summarized in Fig. 2. Our results complement the ones obtained in the Solar System since they are obtained in a completely different and unexplored strong field regime. We have shown that future observations—and especially the next generation of telescopes—will improve our results substantially. In addition, we have derived a limit on an hypothetical advance of the periastron of the short-period

[35] A. Hees, W. M. Folkner, R. A. Jacobson, and R. S. Park, Constraints on MOND theory from radio tracking data of the Cassini spacecraft, Phys. Rev. D **89**, 102002 (2014); Z.-W. Li, S.-F. Yuan, C. Lu, and Y. Xie, New upper limits on deviation from the inverse-square law of gravity in the solar system: a Yukawa parameterization, Res. Astron. Astrophys. **14**, 139 (2014).

[36] D. Borka, P. Jovanović, V. B. Jovanović, and A. F. Zakharov, Constraining the range of Yukawa gravity interaction from S2 star orbitsJ. Cosmol. Astropart. Phys. 11 (2013) 050; A. F. Zakharov, P. Jovanović, D. Borka, and V. B. Jovanović, Constraining the range of Yukawa gravity interaction from S2 star orbits II: Bounds on graviton mass, J. Cosmol. Astropart. Phys. 05 (2016) 045.

[37] A. M. Ghez, B. L. Klein, M. Morris, and E. E. Becklin, High Proper-Motion Stars in the Vicinity of Sagittarius A*: Evidence for a Supermassive Black Hole at the Center of Our Galaxy, Astrophys. J. **509**, 678 (1998).

[38] A. M. Ghez, M. Morris, E. E. Becklin, A. Tanner, and T. Kremenek, The accelerations of stars orbiting the Milky Way's central black hole, Nature (London) **407**, 349 (2000).

[39] A. M. Ghez, G. Duchêne, K. Matthews, S. D. Hornstein, A. Tanner, J. Larkin, M. Morris, E. E. Becklin, S. Salim, T. Kremenek, D. Thompson, B. T. Soifer, G. Neugebauer, and I. McLean, The First Measurement of Spectral Lines in a Short-Period Star Bound to the Galaxy's Central Black Hole: A Paradox of Youth, Astrophys. J. Lett. **586**, L127 (2003).

[40] A. M. Ghez, S. Salim, S. D. Hornstein, A. Tanner, J. R. Lu, M. Morris, E. E. Becklin, and G. Duchêne, Stellar Orbits around the Galactic Center Black Hole, Astrophys. J. **620**, 744 (2005).

[41] A. M. Ghez, S. D. Hornstein, J. R. Lu, A. Bouchez, D. Le Mignant, M. A. van Dam, P. Wizinowich, K. Matthews, M. Morris, E. E. Becklin, R. D. Campbell, J. C. Y. Chin, S. K. Hartman, E. M. Johansson, R. E. Lafon, P. J. Stomski, and D. M. Summers, The First Laser Guide Star Adaptive Optics Observations of the Galactic Center: Sgr A*'s Infrared Color and the Extended Red Emission in its Vicinity, Astrophys. J. **635**, 1087 (2005).

[42] A. M. Ghez, S. Salim, N. N. Weinberg, J. R. Lu, T. Do, J. K. Dunn, K. Matthews, M. R. Morris, S. Yelda, E. E. Becklin, T. Kremenek, M. Milosavljevic, and J. Naiman, Measuring distance and properties of the Milky Way's central supermassive black hole with stellar orbits, Astrophys. J. **689**, 1044 (2008).

[43] L. Meyer, A. M. Ghez, R. Schödel, S. Yelda, A. Boehle, J. R. Lu, T. Do, M. R. Morris, E. E. Becklin, and K. Matthews, The Shortest-Known–Period Star Orbiting Our Galaxy's Supermassive Black Hole, Science **338**, 84 (2012).

[44] A. Boehle, A. M. Ghez, R. Schödel, L. Meyer, S. Yelda, S. Albers, G. D. Martinez, E. E. Becklin, T. Do, J. R. Lu, K. Matthews, M. R. Morris, B. Sitarski, and G. Witzel, An improved distance and mass estimate for Sgr A* from a multistar orbit analysis, Astrophys. J. **830**, 17 (2016).

[45] R. Genzel, A. Eckart, T. Ott, and F. Eisenhauer, On the nature of the dark mass in the centre of the Milky Way, Mon. Not. R. Astron. Soc. **291**, 219 (1997).

[46] A. Eckart and R. Genzel, Stellar proper motions in the central 0.1 pc of the Galaxy, Mon. Not. R. Astron. Soc. **284**, 576 (1997).

[47] R. Schödel *et al.*, A star in a 15.2-year orbit around the supermassive black hole at the centre of the Milky Way, Nature (London) **419**, 694 (2002).

[48] A. Eckart, R. Genzel, T. Ott, and R. Schödel, Stellar orbits near Sagittarius A*, Mon. Not. R. Astron. Soc. **331**, 917 (2002).

[49] F. Eisenhauer, R. Schödel, R. Genzel, T. Ott, M. Tecza, R. Abuter, A. Eckart, and T. Alexander, A Geometric Determination of the Distance to the Galactic Center, Astrophys. J. Lett. **597**, L121 (2003).

[50] F. Eisenhauer *et al.*, SINFONI in the Galactic Center: Young Stars and Infrared Flares in the Central Light-Month, Astrophys. J. **628**, 246 (2005).

[51] S. Gillessen, F. Eisenhauer, T. K. Fritz, H. Bartko, K. Dodds-Eden, O. Pfuhl, T. Ott, and R. Genzel, The orbit of the star S2 around SgrA* from VLT and Keck data, Astrophys. J. Lett. **707**, L114 (2009).

[52] S. Gillessen, F. Eisenhauer, S. Trippe, T. Alexander, R. Genzel, F. Martins, and T. Ott, Monitoring stellar orbits around the massive black hole in the Galactic center, Astrophys. J. **692**, 1075 (2009).

[53] S. Gillessen, P. M. Plewa, F. Eisenhauer, R. Sari, I. Waisberg, M. Habibi, O. Pfuhl, E. George, J. Dexter, S. von Fellenberg, T. Ott, and R. Genzel, An update on monitoring stellar orbits in the Galactic center, Astrophys. J. **837**, 30 (2017).

[54] T. Alexander, Stellar processes near the massive black hole in the Galactic center, Phys. Rep. **419**, 65 (2005).

[55] M. Jaroszynski, Relativistic effects in proper motions of stars surrounding the Galactic center, Acta Astronaut. **48**, 653 (1998); P. C. Fragile and G. J. Mathews, Reconstruction of Stellar Orbits Close to Sagittarius A*: Possibilities for Testing General Relativity, Astrophys. J. **542**, 328 (2000); G. F. Rubilar and A. Eckart, Periastron shifts of stellar orbits near the Galactic Center, Astron. Astrophys. **374**, 95 (2001); N. N. Weinberg, M. Milosavljević, and A. M. Ghez, Stellar Dynamics at the Galactic Center with an Extremely Large Telescope, Astrophys. J. **622**, 878 (2005); S. Zucker, T. Alexander, S. Gillessen, F. Eisenhauer, and R. Genzel, Probing Post-Newtonian Physics near the Galactic Black Hole with Stellar Redshift Measurements, Astrophys. J. Lett. **639**, L21 (2006); G. V. Kraniotis, Periapsis and gravitomagnetic precessions of stellar orbits in Kerr and Kerr–de Sitter black hole spacetimes, Classical Quantum Gravity **24**, 1775 (2007); C. M. Will, Testing the general relativistic "no-hair" theorems using the Galactic center black hole SgrA* Astrophys. J. Lett. **674**, L25 (2008); D. Merritt, T. Alexander, S. Mikkola, and C. M. Will, Testing properties of the Galactic center black hole using stellar orbits, Phys. Rev. D **81**, 062002 (2010); R. Angélil and P. Saha, Relativistic redshift effects and the galactic-center stars, Astrophys. J. **711**, 157 (2010); R. Angélil, P. Saha, and D. Merritt, Towards relativistic orbit fitting of Galactic center stars and pulsars, Astrophys. J. **720**, 1303 (2010); L. Iorio, Long-term classical and general relativistic effects on the radial velocities of the stars orbiting Sgr A*, Mon. Not. R. Astron. Soc. **411**, 453 (2011); R. Angélil and P. Saha, Galactic-center S stars as a prospective test of the Einstein equivalence principle, Astrophys. J. Lett. **734**, L19 (2011);

Journal of Cosmology and Astroparticle Physics
An IOP and SISSA journal

Constraining the range of Yukawa gravity interaction from S2 star orbits III: improvement expectations for graviton mass bounds

A.F. Zakharov,[a,b,c,d,e,1] **P. Jovanović,**[f] **D. Borka**[g] **and V. Borka Jovanović**[g]

[a]National Astronomical Observatories of Chinese Academy of Sciences, Datun Road 20A, Beijing, 100012 China
[b]Institute of Theoretical and Experimental Physics, 117259 Moscow, Russia
[c]National Research Nuclear University MEPhI (Moscow Engineering Physics Institute), 115409, Moscow, Russia
[d]Bogoliubov Laboratory for Theoretical Physics, JINR, 141980 Dubna, Russia
[e]North Carolina Central University, Durham, NC 27707, U.S.A.
[f]Astronomical Observatory, Volgina 7, P.O. Box 74, 11060 Belgrade, Serbia
[g]Atomic Physics Laboratory (040), Vinča Institute of Nuclear Sciences, University of Belgrade, P.O. Box 522, 11001 Belgrade, Serbia

E-mail: zakharov@itep.ru, pjovanovic@aob.rs, dusborka@vinca.rs, vborka@vinca.rs

Received January 17, 2018
Revised February 14, 2018
Accepted March 9, 2018
Published ???, 2018

[1]Corresponding author.

https://doi.org/xxxxxxx

Graviton mass estimate improvement forecast

Graviton Mass Estimates from Trajectories of Bright Stars near the Galactic Center

We use a modification of the Newtonian potential corresponding to a massive graviton case (Visser, 1998; Will, 1998, 2014):

$$V(r) = -\frac{GM}{(1+\delta)r}\left[1 + \delta e^{-\left(\frac{r}{\lambda}\right)}\right], \tag{5}$$

where δ is a universal constant (we put $\delta = 1$). In our previous studies we found constraints on parameters of Yukawa gravity. As it was described in we used observational data from NTT/VLT. If we wish to find a limiting value for λ_x, so that $\lambda > \lambda_x$ with a probability $P = 1-\alpha$ (where we select $\alpha = 0.1$)

Expectations to constrain the range of Yukawa gravity with future observations

We assume that in future GR predictions about precession angles for bright star orbits around the Galactic Center will be successfully confirmed, therefore, for each star we have a constraint on Λ which can be obtained from the condition for Λ, so that Yukawa gravity induces the same orbital precession as GR. This constraint can be obtained directly from (11) and (17), assuming that $\Delta\varphi_Y = \Delta\varphi_{GR}$. In this way we obtain that:

$$\Lambda \approx \sqrt{\frac{\delta c^2 (a\sqrt{1-e^2})^3}{6(1+\delta)GM}}. \tag{19}$$

As it can be seen from the above expression, taking into account that δ is

universal constant, the corresponding values of Λ in the case of all S-stars depend only on the semi-major axes and eccentricities of their orbits. In order to stay in accordance with (Zakharov et al., 2016), here we will also assume that $\delta = 1$, in which case formula (19) reduces to:

$$\Lambda \approx \frac{c}{2}\sqrt{\frac{(a\sqrt{1-e^2})^3}{3GM}} \approx \sqrt{\frac{(a\sqrt{1-e^2})^3}{6R_S}}, \tag{20}$$

Using Kepler law we could write the previous equation in the following form

$$\Lambda \approx \frac{T}{T_0}\sqrt{\frac{(a_0\sqrt{1-e^2})^3}{6R_S}}. \tag{21}$$

Eur. Phys. J. C (2018) 78:689
https://doi.org/10.1140/epjc/s10052-018-6166-5

THE EUROPEAN PHYSICAL JOURNAL C

Regular Article - Theoretical Physics

Constraints on tidal charge of the supermassive black hole at the Galactic Center with trajectories of bright stars

Alexander F. Zakharov[1,2,3,4,5,a]

[1] National Astronomical Observatories of Chinese Academy of Sciences, 20A Datun Road, Beijing 100012, China
[2] Institute of Theoretical and Experimental Physics, B. Cheremushkinskaya, 25, Moscow 117218, Russia
[3] National Research Nuclear University MEPhI (Moscow Engineering Physics Institute), Kashirskoe highway 31, Moscow 115409, Russia
[4] Joint Institute for Nuclear Research, Dubna, Russia
[5] North Carolina Central University, Durham, NC 27707, USA

Received: 26 June 2018 / Accepted: 20 August 2018 / Published online: 29 August 2018

Abstract As it was pointed out recently in Hees et al. (Phys Rev Lett 118:211101, 2017), observations of stars near the Galactic Center with current and future facilities provide an unique tool to test general relativity (GR) and alternative theories of gravity in a strong gravitational field regime. In particular, the authors showed that the Yukawa gravity could be constrained with Keck and TMT observations. Some time ago, Dadhich et al. (Phys Lett B 487:1, 2001) showed that the Reissner–Nordström metric with a tidal charge is naturally appeared in the framework of Randall–Sundrum model with an extra dimension (Q^2 is called tidal charge and it could be negative in such an approach). Astrophysical consequences of presence of black holes with a tidal charge are considerered, in particular, geodesics and shadows in Kerr–Newman braneworld metric are analyzed in Schee and Stuchlík (Intern J Mod Phys D 18:983, 2009), while profiles of emission lines generated by rings orbiting braneworld Kerr black hole are considered in Schee and Stuchlík (Gen Relat Grav 52:1795, 2009). Possible observational signatures of gravitational lensing in a presence of the Reissner–Nordström black hole with a tidal charge at the Galactic Center are discussed in papers (Bin-Nun in Phys Rev D 81:123011, 2010; Bin-Nun in Phys Rev D 82:064009, 2010; Bin-Nun in Class Quant Grav 28:114003, 2011). Here we are following such an approach and we obtain analytical expressions for orbital precession for Reissner–Nordström–de-Sitter solution in post-Newtonian approximation and discuss opportunities to constrain parameters of the metric from observations of bright stars with current and future astrometric observational facilities such as VLT, Keck, GRAVITY, E-ELT and TMT.

[a] e-mail: zakharov@itep.ru

1 Introduction

The Galactic Center is a very peculiar object. A couple of different models have been suggested for it, including dense cluster of stars [8], fermion ball [9], boson stars [10,11], neutrino balls [12]. Later, some of these models have been constrained with subsequent observations [8]. However, as it was found in computer simulations, sometimes differences for alternative models may be very tiny as it was shown in paper [13] where the authors discussed shadows for boson star and black hole models. The most natural and generally accepted model for the Galactic Center is a supermassive black hole (see, e.g. recent reviews [14–17]). A natural way to evaluate a gravitational potential is to analyze trajectories of photons or test particles moving in the potential. Shapes of shadows forming by photons moving around black holes were discussed in [18–21] (see also [22]). Shadows (dark spots) can not be detected but theoretical models could describe a distribution of bright structures around these dark shadows. Bright structures around shadows are being observing with an improving accuracy of current and forthcoming VLBI facilities in mm-band, including the Event Horizon Telescope [24–27].

To create an adequate theoretical model for the Galactic Center astronomers monitored trajectories of bright stars (or clouds of hot gas) using the largest telescopes VLT and Keck with adaptive optics facilities [28–34]. One could introduce a distance between observational data for trajectories of bright stars and their theoretical models. Practically, such a distance is a measure of quality for a theoretical fit. To test different theoretical models one of the most simple approach is to compare apocenter (pericenter) shifts for theoretical fits and observational data for trajectories. If an apocenter (pericenter) shifts for a theoretical fit exceed apocenter (pericenter)

A&A 615, L15 (2018)
https://doi.org/10.1051/0004-6361/201833052

Astronomy & Astrophysics

LETTER TO THE EDITOR

Detection of the gravitational redshift in the orbit of the star S2 near the Galactic centre massive black hole⋆

GRAVITY Collaboration⋆⋆: R. Abuter[8], A. Amorim[6,14], N. Anugu[7], M. Bauböck[1], M. Benisty[5], J. P. Berger[5,8], N. Blind[10], H. Bonnet[8], W. Brandner[3], A. Buron[1], C. Collin[2], F. Chapron[2], Y. Clénet[2], V. Coudé du Foresto[2], P. T. de Zeeuw[12,1], C. Deen[1], F. Delplancke-Ströbele[8], R. Dembet[8,2], J. Dexter[1], G. Duvert[5], A. Eckart[4,11], F. Eisenhauer[1,⋆⋆⋆], G. Finger[8], N. M. Förster Schreiber[1], P. Fédou[2], P. Garcia[7,14], R. Garcia Lopez[15,3], F. Gao[1], E. Gendron[2], R. Genzel[1,13], S. Gillessen[1], P. Gordo[6,14], M. Habibi[1], X. Haubois[9], M. Haug[8], F. Haußmann[1], Th. Henning[3], S. Hippler[3], M. Horrobin[4], Z. Hubert[2,3], N. Hubin[8], A. Jimenez Rosales[1], L. Jochum[8], L. Jocou[5], A. Kaufer[9], S. Kellner[11], S. Kendrew[16,3], P. Kervella[2], Y. Kok[1], M. Kulas[3], S. Lacour[2], V. Lapeyrère[2], B. Lazareff[5], J.-B. Le Bouquin[5], P. Léna[2], M. Lippa[1], R. Lenzen[3], A. Mérand[8], E. Müler[8,3], U. Neumann[3], T. Ott[1], L. Palanca[9], T. Paumard[2], L. Pasquini[8], K. Perraut[5], G. Perrin[2], O. Pfuhl[1], P. M. Plewa[1], S. Rabien[1], A. Ramírez[9], J. Ramos[3], C. Rau[1], G. Rodríguez-Coira[2], R.-R. Rohloff[3], G. Rousset[2], J. Sanchez-Bermudez[9,3], S. Scheithauer[3], M. Schöller[8], N. Schuler[9], J. Spyromilio[8], O. Straub[2], C. Straubmeier[4], E. Sturm[1], L. J. Tacconi[1], K. R. W. Tristram[9], F. Vincent[2], S. von Fellenberg[1], I. Wank[4], I. Waisberg[1], F. Widmann[1], E. Wieprecht[1], M. Wiest[4], E. Wiezorrek[1], J. Woillez[8], S. Yazici[1,4], D. Ziegler[2], and G. Zins[9]

(Affiliations can be found after the references)

Received 26 June 2018 / Accepted 29 June 2018

ABSTRACT

The highly elliptical, 16-year-period orbit of the star S2 around the massive black hole candidate Sgr A* is a sensitive probe of the gravitational field in the Galactic centre. Near pericentre at 120 AU ≈ 1400 Schwarzschild radii, the star has an orbital speed of ≈7650 km s^{-1}, such that the first-order effects of Special and General Relativity have now become detectable with current capabilities. Over the past 26 years, we have monitored the radial velocity and motion on the sky of S2, mainly with the SINFONI and NACO adaptive optics instruments on the ESO Very Large Telescope, and since 2016 and leading up to the pericentre approach in May 2018, with the four-telescope interferometric beam-combiner instrument GRAVITY. From data up to and including pericentre, we robustly detect the combined gravitational redshift and relativistic transverse Doppler effect for S2 of $z = \Delta\lambda/\lambda \approx 200\,\mathrm{km\,s^{-1}}/c$ with different statistical analysis methods. When parameterising the post-Newtonian contribution from these effects by a factor f, with $f = 0$ and $f = 1$ corresponding to the Newtonian and general relativistic limits, respectively, we find from posterior fitting with different weighting schemes $f = 0.90 \pm 0.09|_{\mathrm{stat}} \pm 0.15|_{\mathrm{sys}}$. The S2 data are inconsistent with pure Newtonian dynamics.

Key words. Galaxy: center – gravitation – black hole physics

1. Introduction

General Relativity (GR) so far has passed all experimental tests with flying colours (Einstein 1916; Will 2014). The most stringent are tests that employ solar mass pulsars in binary systems (Kramer et al. 2006), and gravitational waves from 10 to 30 $M_\odot$ black hole in-spiral events (Abbott et al. 2016a,b,c). These tests cover a wide range of field strengths and include the strong curvature limit (Fig. A.2). At much lower field strength, Earth laboratories probe planetary masses that are about a factor 10^6 lower than the stellar mass scale. For massive black hole (MBH) candidates with masses of $10^{6-10}\,M_\odot$, only indirect evidence for GR effects has been reported, such as relativistically broadened, redshifted iron Kα line emission in nearby active galaxies (Tanaka et al. 1995; Fabian et al. 2000). The closest MBH is at the centre of the Milky Way ($R_0 \approx 8$ kpc, $M_\bullet \approx 4 \times 10^6\,M_\odot$), and its Schwarzschild radius subtends the largest angle on the sky of all known MBHs ($R_\mathrm{S} \approx 10\,\mu$as ≈ 0.08 AU). It is coincident with a very compact, variable X-ray, infrared, and radio source, Sgr A*, which in turn is surrounded by a very dense cluster of orbiting young and old stars. Radio and infrared observations have provided detailed information on the distribution, kinematics, and physical properties of this nuclear star cluster and of the hot, warm, and cold interstellar gas interspersed in it (cf. Genzel et al. 2010; Morris et al. 2012; Falcke & Markoff 2013). High-resolution near-infrared (NIR) speckle and adaptive optics (AO) assisted imaging and spectroscopy of the nuclear star cluster over the past 26 years, mainly by two groups in Europe (the

⋆ This paper is dedicated to Tal Alexander, who passed away about a week before the pericentre approach of S2.

⋆⋆ GRAVITY is developed in a collaboration by the Max Planck Institute for extraterrestrial Physics, LESIA of Paris Observatory/CNRS/Sorbonne Université/Univ. Paris Diderot and IPAG of Université Grenoble Alpes/CNRS, the Max Planck Institute for Astronomy, the University of Cologne, the CENTRA – Centro de Astrofisica e Gravitação, and the European Southern Observatory.

⋆⋆⋆ Corresponding author: F. Eisenhauer
e-mail: eisenhau@mpe.mpg.de

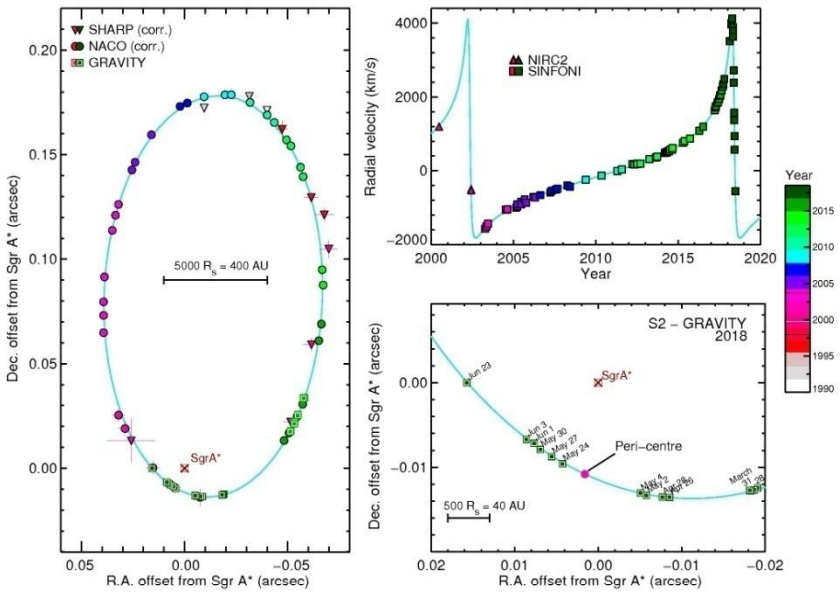

Fig. 2. Summary of the observational results of monitoring the S2 – Sgr A* orbit from 1992 to 2018. *Left*: projected orbit of the star S2 on the sky (J2000) relative to the position of the compact radio source Sgr A* (brown crossed square at the origin). Triangles and circles (and 1 σ uncertainties) denote the position measurements with SHARP at the NTT and NACO at the VLT, colour-coded for time (colour bar on the right side). All data points are corrected for the best-fit zero-point (x_0, y_0) and drifts $(\dot{x}_0, \dot{y}_0)$ of the coordinate system relative to Sgr A* (see Plewa et al. 2015). Green squares mark the GRAVITY measurements. The *bottom right panel* shows a zoom around pericentre in 2018. *Top right*: radial velocity of S2 as a function of time (squares: SINFONI/NACO at the VLT; triangles: NIRC2 at Keck). S2 reached pericentre of its orbit at the end of April 2002, and then again on May 19th, 2018 (MJD 58257.67). The data before 2017 are taken from Ghez et al. (2008), Boehle et al. (2016), Chu et al. (2018), and Gillessen et al. (2017, 2009b). The 2017/2018 NACO/SINFONI and GRAVITY data are presented here for the first time. The cyan curve shows the best-fitting S2 orbit to all these data, including the effects of General and Special Relativity.

and 26 additional spectroscopy epochs with SINFONI using the 25 mas pix^{-1} scale and the combined $H + K$-band grating with a spectral resolution of $R \approx 1500$.

For more details on the data analysis of all three instruments, we refer to Appendix A.

3. Results

3.1. Relativistic corrections

The left panel of Fig. 2 shows the combined single-telescope and interferometric astrometry of the 1992–2018 sky-projected orbital motion of S2, where the zero point is the position of the central mass and of Sgr A*. All NACO points were corrected for a zero-point offset and drift in RA/Dec, which are obtained from the orbit fit. The bottom right panel zooms into the 2018 section of the orbit around pericentre measured with GRAVITY. The zoom demonstrates the hundred-fold improvement of astrometry between SHARP in the 1990s (≈4 mas precision) and NACO in the 2000s (≈0.5 mas) to GRAVITY in 2018 (as small as ≈30 μas). While the motion on the sky of S2 could be detected with NACO over a month, the GRAVITY observations detect the motion of the star from day to day. The upper right panel of Fig. 2 displays the radial velocity measurements with SINFONI at the VLT and NIRC2 at Keck in the 1992–2018 period.

At pericentre $R_{\rm peri}$, S2 moves with a total space velocity of ≈7650 km s^{-1}, or $\beta = v/c = 2.55 \times 10^{-2}$. This means that the first-order parameterised post-Newtonian correction terms (PPN(1)), due to Special and General Relativity, beyond the orbital Doppler and Rømer effects, are within reach of current measurement precision, PPN(1) $\sim \beta^2 \sim (R_{\rm S}/R_{\rm peri}) \sim 6.5 \times 10^{-4}$. These terms can be parameterised spectroscopically as (e.g. Misner et al. 1973; Alexander 2005; Zucker et al. 2006).

$$z = \frac{\Delta\lambda}{\lambda} = B_0 + B_{0.5}\beta + B_1\beta^2 + O(\beta^3), \quad (1)$$

where the PPN(1)$_z$ term $B_1 = B_{1,\rm tD} + B_{1,\rm gr}$, with $B_{1,\rm tD} = B_{1,\rm gr} = 0.5$, and $\beta^2 = [R_{\rm S}(1+e)]/[2a(1-e)] = 6.51 \times 10^{-4}$ for S2. Here a is the semi-major axis and e is the eccentricity of the S2 orbit. $B_{0.5}\beta$ is the Newtonian Doppler shift.

Equation (1) indicates that PPN(1)$_z$ consists in equal terms of the special relativistic transverse Doppler effect ($B_{1,\rm tD}$) and the general relativistic gravitational redshift ($B_{1,\rm gr}$), totalling ≈200 km s^{-1} redshift at pericentre, while at apocentre, it amounts

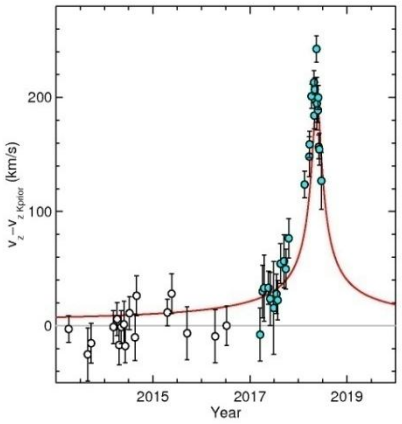

Fig. 3. Residual velocity $c\Delta z = c(z_{GR} - z_K)$ for the best fitting prior Keplerian K_{prior} ($f = 0$, grey) and the same orbit with $f = 1$ (red GR_{prior}). K_{prior} was constructed from all 1992–2018 astrometric data with NACO & GRAVITY and the SINFONI data between 2004 and 2016 (open black circles). The 2017/2018 SINFONI data points (black circles with cyan shading) can then be added to test if the spectroscopic data around pericentre follow K_{prior} or the GR_{prior} predicted from K_{prior}. The new data points near and up to pericentre, where the β^2 effects in radial velocity are expected to be important, fall close to the predicted GR_{prior} curve, and exclude the Keplerian prior orbit.

to only 6 km s^{-1}. If the total orbital redshift z_{tot} is separated into a Newtonian/Kepler part z_K and a GR correction, one can write $z_{tot} = z_K + f\,(z_{GR} - z_K)$, where f is zero for purely Newtonian physics and unity for GR. In the following we show the residuals $\Delta z = z_{GR} - z_K$. The Keplerian part of the orbit is at $\Delta z = 0$, and the PPN(1)$_z$ corrections appear as an excess.

3.2. Analysis with prior Kepler orbit

We define a prior orbit K_{prior} by excluding those data for which the PPN(1)$_z$ corrections matter. For K_{prior} we use the entire 1992–2018 SHARP/NACO and GRAVITY data and the SINFONI data from 2004 up to the end of 2016. We then obtained K_{prior} as described in Gillessen et al. (2017), which requires a simultaneous fit of 13 parameters. The Rømer delay is included in the calculation. The resulting orbit is a modest update of Gillessen et al. (2017). Using this as the prior orbit, we then added the radial velocities from 2017 and 2018 (Fig. 3). The 26 residual 2017/2018 spectroscopic data relative to K_{prior} clearly do not follow the best-fitting Keplerian orbit derived from all previous 51 spectroscopic and 196 positions in the past 26 years (grey line in Fig. 3), but instead follow the $f = 1$ (i.e. GR(K_{prior})) version of K_{prior} (red line in Fig. 3). This test is fair: GR-corrections should only be detectable with our measurement errors within ±1 year of pericentre.

This a priori test demonstrates that the spectroscopic data around the pericenter passage are inconsistent with Newtonian dynamics and consistent with GR. However, both K_{prior} ($\chi^2_r = 21$) and GR(K_{prior}) ($\chi^2_r = 8$) are poor fits to the data.

3.3. Posterior analysis

Because of the uncertainties in the parameters of K_{prior}, in particular, in the strongly correlated mass and distance, a more conservative approach is to determine the best-fit value of the parameter f a posteriori, including all data and fitting for the optimum values of all parameters. In carrying out the fitting, it is essential to realise that the inferred measurement uncertainties are dominated by systematic effects, especially when evidence from three or more very different measurement techniques is combined (see Appendix A.6 for a more detailed discussion). In particular the NACO measurements are subject to correlated systematic errors, for example from unrecognised confusion events (Plewa & Sari 2018), which typically last for one year and are comparable in size to the statistical errors. We therefore downsampled the NACO data into 100 bins with equal path lengths along the projected orbit (Fig. 4, middle) and gave these data in addition a lower weight of 0.5. Depending on exactly which weighting or averaging scheme was chosen, the posterior analysis including all data between 1992 and 2018 yielded f values between 0.85 and 1.09. With a weighting of 0.5 of the NACO data, we find $f = 0.90 \pm 0.09$ (Fig. 4). GR ($f = 1$) is favoured over pure Newtonian physics ($f = 0$) at the $\approx 10\,\sigma$ level.

The error on f is derived from the posterior probability distributions (Fig. 4, bottom) of a Markov chain Monte Carlo (MCMC) analysis. Fig. A.1 shows the full set of correlation plots and probability distributions for the fit parameters. The distributions are compact and all parameters are well determined. The best-fit values and uncertainties are given Table A.1.

The superb GRAVITY astrometry demonstrably improves the quality of the fits and is crucial for overcoming the source confusion between Sgr A* and S2 near pericentre. A minimal detection of PPN(1)$_z$ (Eq. (1)) is provided by a combination using only NACO and SINFONI data ($f_{NACO+SINFONI} = 0.71 \pm 0.19$, $3.6\,\sigma$), but the inclusion of the GRAVITY data very significantly improves the precision and significance of the fitted parameters: the improvement reaches a factor of 2–3.

A still more demanding test is to search for any Keplerian fit to all data and determine whether its goodness of fit is significantly poorer than the goodness of fit of the best-fitting GR-orbit. For linear models the formula presented in Andrae et al. (2010) can be used to estimate the significance. However, the value for the degrees of freedom (d.o.f.) is not well defined for non-linear models (Andrae et al. 2010). In our case, we have two models that only differ significantly over a very critical short time-span given the uncertainties in the underlying data. We therefore used the number of those data points as d.o.f. for which the two models predict significant differences. The difference in χ^2 yields a formal significance of $5\,\sigma$ or greater in favour of the relativistic model.

For further comments on a Bayesian analysis of our data, see Appendix A.9.

4. Discussion

We have reported the first direct detection of the PPN(1) gravitational redshift parameter around the MBH in the Galactic centre from a data set that extends up to and includes the pericentre approach in May 2018. Three different analysis methods of our data suggest that this detection favours the post-Newtonian model with robust significance. Further improvement of our results is expected as our monitoring continues post pericentre. Still, there are reasons to be cautious about the significance of these early results, mainly because of the systematic

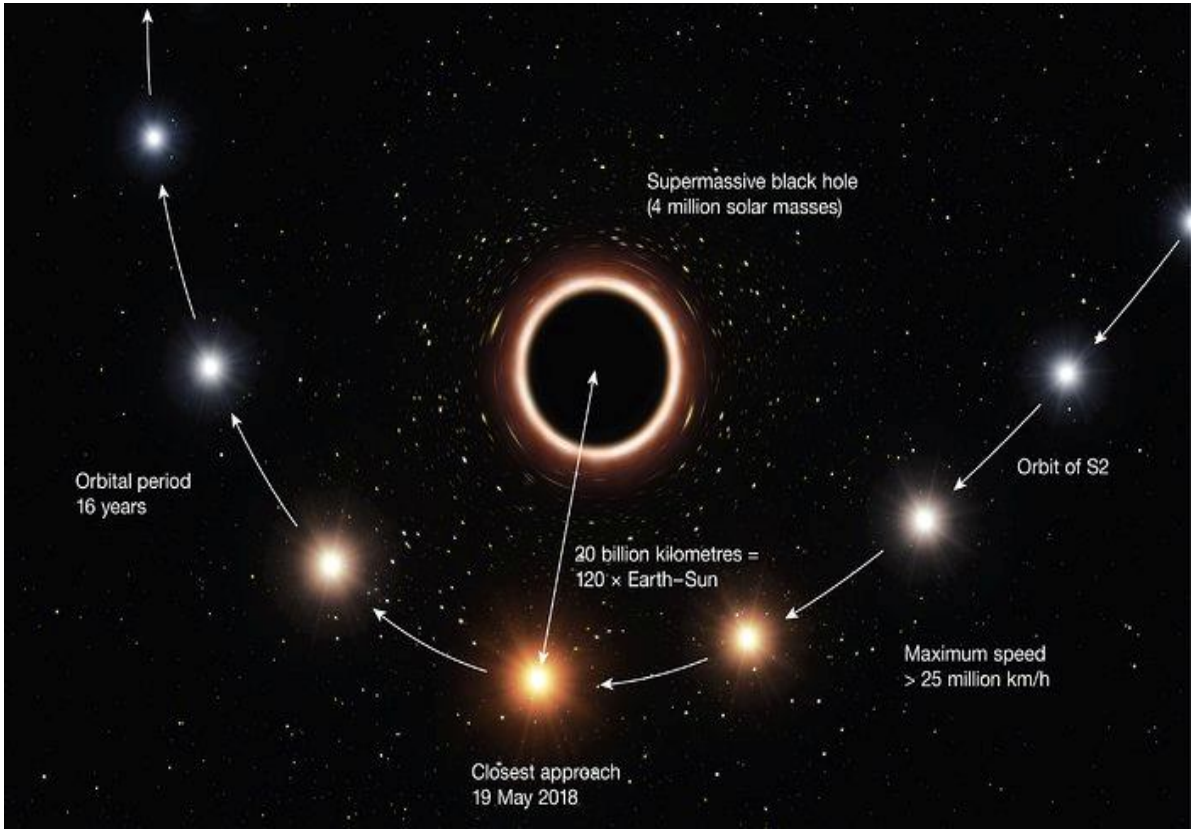
Supermassive black hole
(4 million solar masses)
Orbital period
16 years
Orbit of S2
20 billion kilometres =
120 × Earth–Sun
Maximum speed
> 25 million km/h
Closest approach
19 May 2018

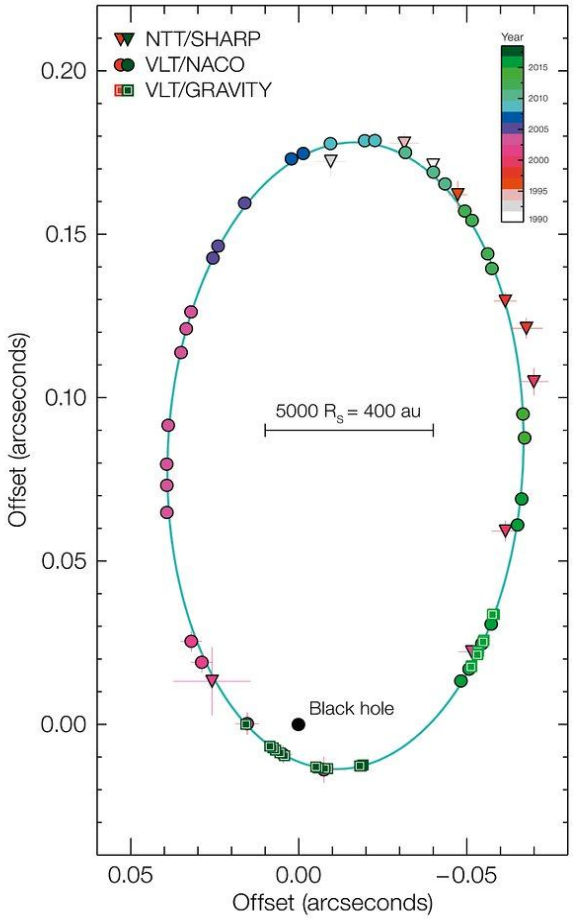
NTT/SHARP
VLT/NACO
VLT/GRAVITY
Year
2015
2010
2005
2000
1995
1990
0.20
0.15
0.10
0.05
0.00
Offset (arcseconds)
5000 R$_S$ = 400 au
Black hole
0.05
0.00
−0.05
Offset (arcseconds)

GRAVITY result about PN(1) correction for gravitational redshift

- For orbital precession f=0.94 ± 0.09 (2018)
- R = 8178 ± 13stat. ± 22sys. parsecs
- Mass = 4.154 ± 0.014*10^6 solar masses
  f = 1.04±0.05
- **Gravity Collaboration 2019, A&A, 625, L10**
-

REPORT

GRAVITATION

Relativistic redshift of the star S0-2 orbiting the Galactic Center supermassive black hole

Tuan Do[1]*, Aurelien Hees[2,1], Andrea Ghez[1], Gregory D. Martinez[1], Devin S. Chu[1], Siyao Jia[3], Shoko Sakai[1], Jessica R. Lu[3], Abhimat K. Gautam[1], Kelly Kosmo O'Neil[1], Eric E. Becklin[1,4], Mark R. Morris[1], Keith Matthews[5], Shogo Nishiyama[6], Randy Campbell[7], Samantha Chappell[1], Zhuo Chen[1], Anna Ciurlo[1], Arezu Dehghanfar[1,8], Eulalia Gallego-Cano[9], Wolfgang E. Kerzendorf[10,11,12,13], James E. Lyke[7], Smadar Naoz[1,14], Hiromi Saida[15], Rainer Schödel[9], Masaaki Takahashi[16], Yohsuke Takamori[17], Gunther Witzel[1,18], Peter Wizinowich[7]

The general theory of relativity predicts that a star passing close to a supermassive black hole should exhibit a relativistic redshift. In this study, we used observations of the Galactic Center star S0-2 to test this prediction. We combined existing spectroscopic and astrometric measurements from 1995–2017, which cover S0-2's 16-year orbit, with measurements from March to September 2018, which cover three events during S0-2's closest approach to the black hole. We detected a combination of special relativistic and gravitational redshift, quantified using the redshift parameter Υ. Our result, $\Upsilon = 0.88 \pm 0.17$, is consistent with general relativity ($\Upsilon = 1$) and excludes a Newtonian model ($\Upsilon = 0$) with a statistical significance of 5σ.

General relativity (GR) has been thoroughly tested in weak gravitational fields in the Solar System (*1*), with binary pulsars (*2*) and with measurements of gravitational waves from stellar-mass black hole binaries (*3*, *4*). Observations of short-period stars in our Galactic Center (GC) (*5*–*8*) allow GR to be tested in a different regime (*9*): the strong field near a supermassive black hole (SMBH) (*10*, *11*). The star S0-2 (also known as S2) has a 16-year orbit around Sagittarius A* (Sgr A*), the SMBH at the center of the Milky Way. In 2018 May, S0-2 reached its point of closest approach, at a distance of 120 astronomical units with a velocity reaching 2.7% of the speed of light. Within a 6-month interval of that date, the star also passed through its maximum and minimum velocity (in March and September, respectively) along the line of sight, spanning 6000 km s^{-1} in radial velocity (RV) (Fig. 1). Here we present observations of all three events combined with data from 1995–2017 (Fig. 2).

During 2018, the close proximity of S0-2 to the SMBH caused the relativistic redshift, which is the combination of the transverse Doppler shift from special relativity and the gravitational redshift from GR. This deviation from a Keplerian orbit was predicted to reach 200 km s^{-1} (Fig. 3) and is detectable with current telescopes. The GRAVITY collaboration (*9*) previously reported a similar measurement. Our measurements are complementary in the following ways: (i) We took a complete set of independent measurements with three additional months of data, doubling the time baseline for the year of closest approach and including the third turning point (RV minimum) in September 2018. (ii) We used three different spectroscopic instruments in 2018, enabling us to probe the presence of instrumental biases. (iii) To test for bias in the result, we analyzed the systematic errors that may arise from an experiment spanning more than 20 years. (iv) We publicly released the stellar measurements and the posterior probability distributions.

We used a total of 45 astrometric positional measurements (spanning 24 years) and 115 RVs (18 years) to fit the orbit of S0-2. Of these, 11 are new astrometric measurements of S0-2 from 2016 to 2018 and 28 are new RV measurements from 2017 and 2018 (Fig. 1). Astrometric measurements were obtained at the W. M. Keck Observatory by using speckle imaging (a technique to overcome blurring from the atmosphere by taking very short exposures and combining the images with software) from 1995–2005 and adaptive optics (AO) imaging (*12*) from 2005–2018. RV measurements were obtained from the W. M. Keck Observatory, Gemini North Telescope, and Subaru Telescope. All of our RV observations were taken using AO. We supplement our observations with previously reported RVs from Keck from 2000 (*7*) and the Very Large Telescope from 2003–2016 (*8*). This work includes data from two imaging instruments and six spectroscopic instruments (*13*).

We scheduled our 2018 observations using a tool designed to maximize the sensitivity of the experiment to the redshift signal (*13*). We predicted that, given the existing data (1995–2017), spectroscopic measurements at the RV maximum and minimum in 2018 would provide the most sensitivity and thus would be ideal for detecting the relativistic redshift (Fig. 3). Although they are less sensitive to the effect of the redshift, imaging observations of the sky position of S0-2 in 2018 also slightly improve the measurement of the relativistic redshift.

The RVs of S0-2 are measured by fitting a physical model (which includes properties of the star, such as its effective temperature, surface gravity, and rotational velocity in addition to RV) to its observed spectrum (*13*). The same procedure is applied to the new and archival observations; for the latter, this spectroscopic method improves the precision by a factor of 1.7 compared with previous analyses (*14*, *15*).

We also characterized additional sources of uncertainties beyond the uncertainties in the fitted model. (i) The wavelength solution, which transforms locations on the detector to vacuum wavelengths, was characterized by comparing the observed wavelengths of atmospheric OH emission lines in the spectra of S0-2 and in observations of blank sky to their known vacuum wavelengths. This comparison shows the uncertainty of the wavelength solution of the spectroscopic instruments to be ~2 km s^{-1}, with some observations from 2002–2004 having lower accuracy between 2 and 26 km s^{-1}. (ii) Reexamination

[1]Department of Physics and Astronomy, University of California, Los Angeles, CA 90095, USA. [2]Sytèmes de Référence Temps Espace, Observatoire de Paris, Université Paris-Sciences-et-Lettres, Centre National de la Recherche Scientifique, Sorbonne Université, Laboratoire National de Métrologie et d'Essais, 61 Avenue de l'Observatoire, 75014 Paris, France. [3]Department of Astronomy, University of California, Berkeley, CA 94720, USA. [4]Universities Space Research Association/Stratospheric Observatory for Infrared Astronomy, NASA Ames Research Center, Mail Stop N232-12, Moffet Field, CA 94035, USA. [5]Division of Physics, Mathematics, and Astronomy, California Institute of Technology, MC 301-17, Pasadena, CA 91125, USA. [6]Faculty of Education, Miyagi University of Education, 149 Aramaki-aza-aoba, Aoba-ku, Sendai, Miyagi 980-0845, Japan. [7]W. M. Keck Observatory, 65-1120 Mamalahoa Highway, Kamuela, HI 96743, USA. [8]Institut de Planétologie et d'Astrophysique de Grenoble, 414 Rue de la Piscine, 38400 Saint-Martin-d'Héres, France. [9]Instituto de Astrofísica de Andalucía, Consejo Superior de Investigaciones Científicas, Glorieta de la Astronomía S/N, 18008 Granada, Spain. [10]European Southern Observatory, Karl-Schwarzschild-Straße 2,85748 Garching bei München, Germany. [11]Center for Cosmology and Particle Physics, New York University, 726 Broadway, New York, NY 10003, USA. [12]Department of Physics and Astronomy, Michigan State University, East Lansing, MI 48824, USA. [13]Department of Computational Mathematics, Science, and Engineering, Michigan State University, East Lansing, MI 48824, USA. [14]Mani L. Bhaumik Institute for Theoretical Physics, Department of Physics and Astronomy, University of California, Los Angeles, CA 90095, USA. [15]Faculty of Liberal Arts, Daido University, 10-3 Takiharu-cho, Minami-ku, Nagoya, Aichi 457-8530, Japan. [16]Department of Physics and Astronomy, Aichi University of Education, 1 Hirosawa, Igaya-cho, Kariya, Aichi 448-8542, Japan. [17]National Institute of Technology, Wakayama College, 77 Noshima, Nada-cho, Gobo, Wakayama 644-0023, Japan. [18]Max Planck Institute for Radio Astronomy, Auf dem Hügel 69, D-53121 Bonn, Germany.
*Corresponding author. Email: tdo@astro.ucla.edu

Keck group: Do et al., Science 365, 664–668 (2019) 16 August 2019

- f= 0.88 ± 0.17, is consistent with general relativity (f = 1) and excludes a Newtonian model (f = 0) with a statistical significance of 5 σ.

Scalar field effects on the orbit of S2 star

The GRAVITY Collaboration: A. Amorim,[1,4] M. Bauböck,[5] M. Benisty,[6] J.-P. Berger,[5] Y. Clénet,[7] V. Coudé du Forest,[7] T. de Zeeuw,[8,5] J. Dexter,[5] G. Duvert,[6] A. Eckart,[9] F. Eisenhauer,[5] Miguel C. Ferreira,[1]★ F. Gao,[5] Paulo J.V. Garcia,[1,2,3]† E. Gendron,[7] R. Genzel,[5,10] S. Gillessen,[5] P. Gordo,[1,4] M. Habibi,[5] M. Horrobin,[9] A. Jimenez-Rosales,[5] L. Jocou,[6] P. Kervella,[7] S. Lacour,[7,5] J.-B. Le Bouquin, P. Léna,[7] T. Ott,[5] M. Pössel,[11] T. Paumard,[7] K. Perraut,[6] G. Perrin,[7] O. Pfuhl,[5] G. Rodriguez Coira,[7] G. Rousset,[7] O. Straub,[5] C. Straubmeier,[9] E. Sturm,[5] F. Vincent,[7] S. von Fellenberg,[5] I. Waisberg[5] and F. Widmann[5]

[1] *CENTRA, Centro de Astrofísica e Gravitação, Instituto Superior Técnico, Avenida Rovisco Pais 1, 1049 Lisboa, Portugal*
[2] *Universidade do Porto, Faculdade de Engenharia, Rua Dr. Roberto Frias, 4200-465 Porto, Portugal*
[3] *European Southern Observatory, Casilla 19001, Santiago 19, Chile*
[4] *Universidade de Lisboa - Faculdade de Ciências, Campo Grande, 1749-016 Lisboa, Portugal*
[5] *Max Planck Institute for Extraterrestrial Physics (MPE), Giessenbachstr.1, 85748 Garching, Germany*
[6] *Univ. Grenoble Alpes, CNRS, IPAG, 38000 Grenoble, France*
[7] *LESIA, Observatoire de Paris, Université PSL, CNRS, Sorbonne Université, Université de Paris, 5 place Jules Janssen, 92195 Meudon, France*
[8] *Sterrewacht Leiden, Leiden University, Postbus 9513, 2300 RA Leiden, The Netherlands*
[9] *Physikalisches Institut, Universität zu Köln, Zülpicher Str. 77, 50937 Köln, Germany*
[10] *Departments of Physics and Astronomy, Le Conte Hall, University of California, Berkeley, CA 94720, USA*
[11] *Max Planck Institute for Astronomy (MPIA) and Haus der Astronomie, Königstuhl 17, D-69117 Heidelberg, Germany*

Accepted XXX. Received YYY; in original form ZZZ

ABSTRACT

Precise measurements of the S-stars orbiting SgrA* have set strong constraints on the nature of the compact object at the centre of the Milky Way. The presence of a black hole in that region is well established, but its neighboring environment is still an open debate. In that respect, the existence of dark matter in that central region may be detectable due to its strong signatures on the orbits of stars: the main effect is a Newtonian precession which will affect the overall pericentre shift of S2, the latter being a target measurement of the GRAVITY instrument. The exact nature of this dark matter (e.g., stellar dark remnants or diffuse dark matter) is unknown. This article assumes it to be an scalar field of toroidal distribution, associated with ultra-light dark matter particles, surrounding the Kerr black hole. Such a field is a form of "hair" expected in the context of superradiance, a mechanism that extracts rotational energy from the black hole. Orbital signatures for the S2 star are computed and shown to be detectable by GRAVITY. The scalar field can be constrained because the variation of orbital elements depends both on the relative mass of the scalar field to the black hole and on the field mass coupling parameter.

Key words: black hole physics – celestial mechanics – dark matter – gravitation – Galaxy: centre – quasars: supermassive black holes

★ Corresponding author, e-mail: mcferreira@tecnico.ulisboa.pt
† Corresponding author, e-mail: pgarcia@fe.up.pt

Results from nine (!) our papers were used

Table 2. Literature computing extensions/alternatives to GR effects in the orbits of the S-stars.

extension/alternative	results/comments	reference
charged non-rotating black holes	Upper limit to black hole charge from S2 precession upper limit.	De Laurentis et al. (2018a), Iorio (2012), Zakharov (2018)
charged rotating black holes and plasma effects	upper limits from black hole mass, spin and local magnetic field	Zajaček et al. (2018)
fermion ball	Ruled out by Ghez et al. (2005) and Gravity Collaboration et al. (2018a).	Munyaneza & Viollier (2002)
boson "star"	Effects much smaller than GR at S2 orbit, only relevant at a few tens of Schwarzschild radii.	Amaro-Seoane et al. (2010),Boshkayev & Malafarina (2019),Grould et al. (2017a)
Yukawa potential	Upper limits on potential parameters and graviton mass from S2 precession upper limit.	Borka et al. (2013), Hees et al. (2017), Zakharov et al. (2016), Zakharov et al. (2018)
Einstein-Maxwell-Dilaton-Axion gravity	Effects smaller than 10^{-3} of GR for S2, need pulsars or inner stars for further tests.	De Laurentis et al. (2018a)
Brans-Dicke theory	Effects smaller than 10^{-3} of GR for S2, need pulsars or inner stars for further tests.	De Laurentis et al. (2018a), Kalita (2018)
$f(R)$ gravity	Effects smaller than 10^{-3} of GR for S2, need pulsars or inner stars for further tests.	Capozziello et al. (2014), De Laurentis et al. (2018a), De Laurentis et al. (2018b), Kalita (2018)
nonlocal gravity	Precession compatible with observational upper limit, of the order of GR prediction	Dialektopoulos et al. (2019)
scalar tensor gravity	Precession is 13× GR value, ruled out by Hees et al. (2017).	Borka Jovanović et al. (2019)
$f(R, \phi)$ gravity	Best fit precession prediction for S2 is 20× GR value, ruled out by Hees et al. (2017).	Capozziello et al. (2014)
hybrid gravity	Best fit precession prediction too high, ruled out by Hees et al. (2017).	Borka et al. (2016)
R^n gravity	When compared with Hees et al. (2017) upper value, the GR value ($n = 1$) is recovered to $< 1\%$, or smaller if extended mass distributions are present.	Borka et al. (2012), Zakharov et al. (2014)
quadratic Einstein-Gauss-Bonnet gravity	Derive expressions for gravitational redshift in function of theory coupling parameters (scalar/matter & scalar/Gauss-Bonnet invariant).	Hees et al. (2019)
dark matter profiles (See Table 1 for dark matter + black hole studies.)	Dark matter mass required to explain TeV emission compatible with orbital upper limits. Limits on spatial distribution of non-annihilating dark matter.	de Paolis et al. (2011), Hall & Gondolo (2006), Iorio (2013), Lacroix (2018),Zakharov et al. (2007)
scalar fields and ultralight dark matter	Upper limits on scalar field mass (1% of black hole) for particles of mass 4×10^{-19} eV/c^2	Bar et al. (2019)

black holes. To study this possibility, we will analyse the solutions to the Klein-Gordon equation in a Kerr space time. We will follow the analytic results of Detweiler (1980) and then translate the scalar field solution in an effective gravitational potential which can then be treated with the usual perturbation analysis of Keplerian orbits. In this section we will be using Planck units ($\hbar = c = G = 1$) unless otherwise

is the mass of the scalar field. The principle of least action results in the Einstein-Klein-Gordon system of equations

$$\begin{cases} G^{\alpha\beta} = & 8\pi T^{\alpha\beta} \\ \nabla_\alpha \nabla^\alpha \Psi = & \mu^2 \Psi \end{cases} \tag{2}$$

where $G_{\alpha\beta}$ is the Einstein tensor, ∇_α represents the covariant derivative and

Relativistic precession of S2 (see the cover page of the Bergman's book)

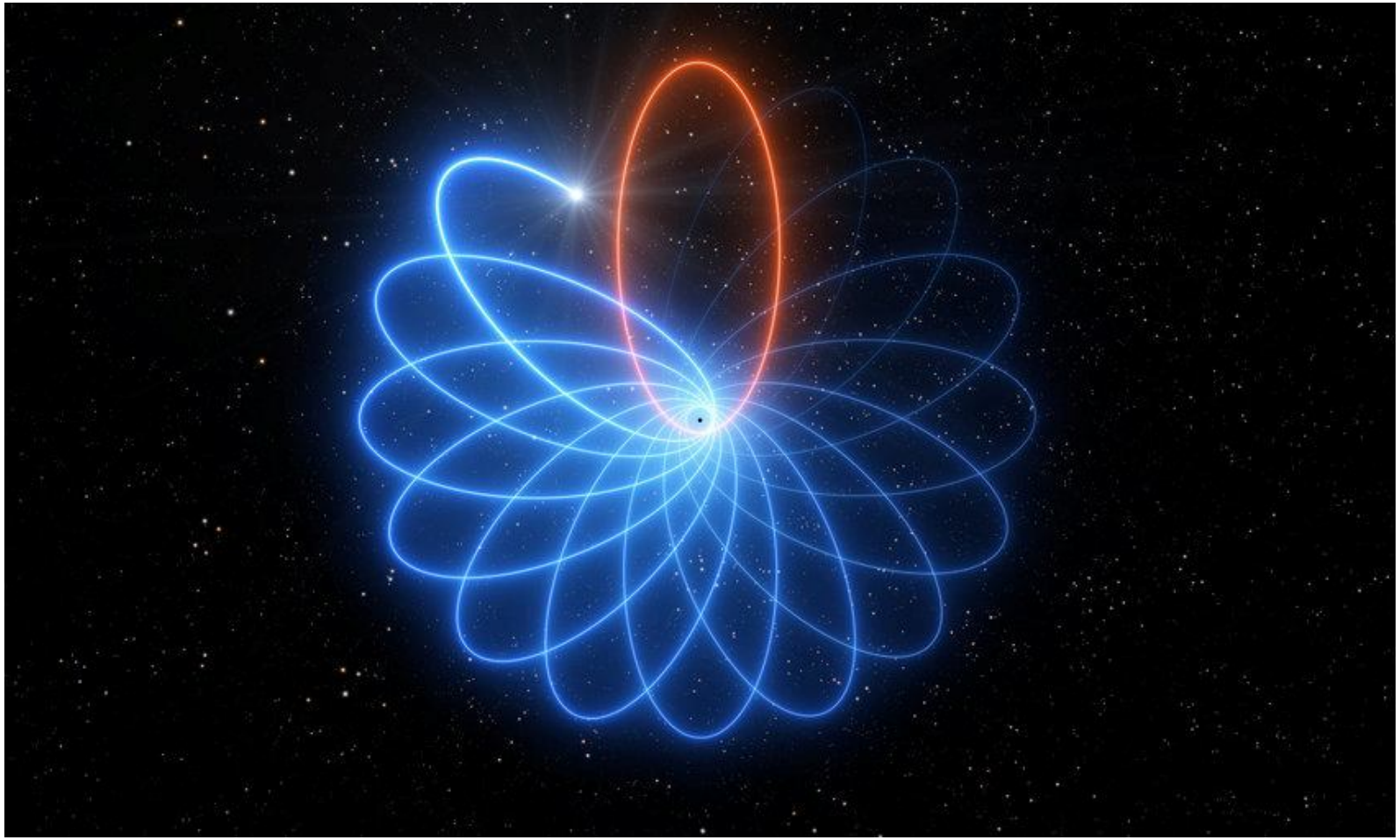

A&A 636, L5 (2020)
https://doi.org/10.1051/0004-6361/202037813

Astronomy & Astrophysics

LETTER TO THE EDITOR

Detection of the Schwarzschild precession in the orbit of the star S2 near the Galactic centre massive black hole

GRAVITY Collaboration:* R. Abuter[8], A. Amorim[6,13], M. Bauböck[1], J. P. Berger[5,8], H. Bonnet[8], W. Brandner[3], V. Cardoso[13,15], Y. Clénet[2], P. T. de Zeeuw[11,1], J. Dexter[14,1], A. Eckart[4,10,**], F. Eisenhauer[1], N. M. Förster Schreiber[1], P. Garcia[7,13], F. Gao[1], E. Gendron[2], R. Genzel[1,12,**], S. Gillessen[1,**], M. Habibi[1], X. Haubois[9], T. Henning[3], S. Hippler[3], M. Horrobin[4], A. Jiménez-Rosales[1], L. Jochum[9], L. Jocou[5], A. Kaufer[9], P. Kervella[2], S. Lacour[2], V. Lapeyrère[2], J.-B. Le Bouquin[5], P. Léna[2], M. Nowak[17,2], T. Ott[1], T. Paumard[2], K. Perraut[5], G. Perrin[2], O. Pfuhl[8,1], G. Rodríguez-Coira[2], J. Shangguan[1], S. Scheithauer[3], J. Stadler[1], O. Straub[1], C. Straubmeier[4], E. Sturm[1], L. J. Tacconi[1], F. Vincent[2], S. von Fellenberg[1], I. Waisberg[16,1], F. Widmann[1], E. Wieprecht[1], E. Wiezorrek[1], J. Woillez[8], S. Yazici[1,4], and G. Zins[9]

(Affiliations can be found after the references)

Received 25 February 2020 / Accepted 4 March 2020

ABSTRACT

The star S2 orbiting the compact radio source Sgr A* is a precision probe of the gravitational field around the closest massive black hole (candidate). Over the last 2.7 decades we have monitored the star's radial velocity and motion on the sky, mainly with the SINFONI and NACO adaptive optics (AO) instruments on the ESO VLT, and since 2017, with the four-telescope interferometric beam combiner instrument GRAVITY. In this Letter we report the first detection of the General Relativity (GR) Schwarzschild Precession (SP) in S2's orbit. Owing to its highly elliptical orbit ($e = 0.88$), S2's SP is mainly a kink between the pre-and post-pericentre directions of motion $\approx \pm 1$ year around pericentre passage, relative to the corresponding *Kepler* orbit. The superb 2017−2019 astrometry of GRAVITY defines the pericentre passage and outgoing direction. The incoming direction is anchored by 118 NACO-AO measurements of S2's position in the infrared reference frame, with an additional 75 direct measurements of the S2-Sgr A* separation during bright states ("flares") of Sgr A*. Our 14-parameter model fits for the distance, central mass, the position and motion of the reference frame of the AO astrometry relative to the mass, the six parameters of the orbit, as well as a dimensionless parameter $f_{\rm SP}$ for the SP ($f_{\rm SP} = 0$ for Newton and 1 for GR). From data up to the end of 2019 we robustly detect the SP of S2, $\delta\phi \approx 12'$ per orbital period. From posterior fitting and MCMC Bayesian analysis with different weighting schemes and bootstrapping we find $f_{\rm SP} = 1.10 \pm 0.19$. The S2 data are fully consistent with GR. Any extended mass inside S2's orbit cannot exceed ≈0.1% of the central mass. Any compact third mass inside the central arcsecond must be less than about 1000 $M_\odot$.

Key words. black hole physics – Galaxy: nucleus – gravitation – relativistic processes

1. Introduction

Testing GR and the massive black hole paradigm. The theory of General Relativity (GR) continues to pass all experimental tests with flying colours (Einstein 1916; Will 2014). High-precision laboratory and Solar System experiments, and observations of solar-mass pulsars in binary systems (Kramer et al. 2006; Kramer 2016) have confirmed GR in the low-curvature regime. Gravitational waves from several stellar mass, black hole (sBH) candidate in-spirals with LIGO (Abbott et al. 2016) have tested the strong-curvature limit.

General Relativity predicts black holes, that is, space-time solutions with a non-spinning or spinning central singularity cloaked by a communication barrier, an event horizon (cf. Schwarzschild 1916; Kerr 1965). The LIGO measurements currently provide the best evidence that the compact in-spiralling binaries are indeed merging sBHs, but see Cardoso & Pani (2019).

Following the discovery of quasars (Schmidt 1963), evidence has been growing that most massive galaxies harbour a central compact mass, perhaps in the form of a massive black hole (MBH: 10^6–$10^{10}\,M_\odot$, Lynden-Bell & Rees 1971; Kormendy & Ho 2013; McConnell & Ma 2013). Are these compact mass concentrations truly MBHs, as predicted by GR? Evidence in favour comes from relativistically broadened, redshifted iron Kα line emission in nearby Seyfert galaxies (Tanaka et al. 1995; Fabian et al. 2000), from stellar or gas motions very close to them (e.g., Moran et al. 1999), and high resolution millimetre imaging (Event Horizon Telescope Collaboration 2019).

The nearest MBH candidate is at the centre of the Milky Way ($R_0 \approx 8$ kpc, $M_\bullet \approx 4 \times 10^6\,M_\odot$, Genzel et al. 2010; Ghez et al. 2008). It is coincident with a very compact and variable X-ray, infrared, and radio source, Sgr A*, which in turn is surrounded by a very dense cluster of orbiting young and old stars. Radio and infrared observations have provided detailed information on the

* GRAVITY is developed in a collaboration by the Max Planck Institute for extraterrestrial Physics, LESIA of Observatoire de Paris/Université PSL/CNRS/Sorbonne Université/Université de Paris and IPAG of Université Grenoble Alpes/CNRS, the Max Planck Institute for Astronomy, the University of Cologne, the CENTRA - Centro de Astrofisica e Gravitação, and the European Southern Observatory.

** Corresponding authors: R. Genzel, e-mail: genzel@mpe.mpg.de; S. Gillessen, e-mail: ste@mpe.mpg.de; and A. Eckart, e-mail: eckart@ph1.uni-koeln.de.

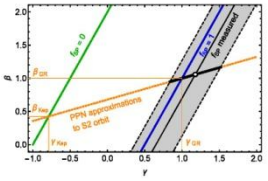

Fig. C.1. Interpretation of our measurement in the plane of the PPN parameters β and γ. Our value for f_{SP} and its uncertainty are represented by the black line and grey band. The GR value $f_{SP} = 1$ is the blue line, and the Newtonian value $f_{SP} = 0$ is the green line. The best approximations to the orbits by PPN parameters are shown by the orange dotted line. Assuming GR is a PPN theory, our measurement corresponds to the white circle at the intersection point and the uncertainties are the adjacent black thick lines.

our constraint in the plane spanned by β and γ. Because there is no exact representation of the Keplerian orbit in the PPN formalism, we instead seek the PPN orbit that most closely resembles the Keplerian orbit. This depends on the eccentricity, and for S2, we find $\gamma_{Kep} = -0.78762$ and $\beta_{Kep} = 0.42476$. Changing f_{SP} corresponds to moving along a line from $(\gamma_{Kep}, \beta_{Kep})$ to $(\gamma_{GR}, \beta_{GR})$. With this, we find $\beta = 1.05 \pm 0.11$ and $\gamma = 1.18 \pm 0.34$, and the two are fully correlated.

Appendix D: Astrophysical implications

Distributed mass component inside the orbit of S2. An extended mass component would create retrograde Newtonian precession. Our data strongly constrain such a component. For simplicity we use spherically symmetric distributions of the extended mass. Using a Plummer (1911) profile with a scale parameter of 0.3 arcsec (Mouawad et al. 2005) and fitting for the normalisation of that mass component assuming $f_{SP} = 1$ shows that $(0.00 \pm 0.10)\%$ of the central mass could be in such an extended configuration. Changing the radius parameter to 0.2 or 0.4 arcsec yields $(-0.02 \pm 0.09)\%$ or $(0.01 \pm 0.11)\%$. Using instead a power-law profile with logarithmic slope between −1.4 and −2 results in a mass estimate of $(-0.03 \pm 0.07)\%$. Overall, we estimate that for typical density profiles the extended mass component cannot exceed 0.1%, or $\approx 4000\,M_\odot$ (1σ limits). For comparison, modelling of the star cluster suggests that the total stellar content within the apocentre of S2 is $<1000\,M_\odot$, and the mass of stellar black holes within that radius is $80–340\,M_\odot$ (Fig. D.1, cf. Genzel et al. 2010; Alexander 2017; Baumgardt et al. 2018). We conclude that the expected stellar content within the S2 orbit is too small to significantly affect the SP.

Merritt et al. (2010) investigated for which configurations the Newtonian precession due to an extended mass component in the form of individual stellar mass objects exceeds the effects of spin and quadrupole moment of the MBH. They addressed a range of masses between 1 and $10^3\,M_\odot$ in the central milli-parsec. The above limits translate into a limit of $\approx 200\,M_\odot$ in that radial range. Figure 1 of Merritt et al. (2010) shows that for S2 itself, our limit on the extended mass would lead to perturbations almost on par with the expected spin effects for a maximally spinning MBH, giving some hope that the spin of Sgr A* can eventually be detected from S2 despite its large orbital radius. Zhang

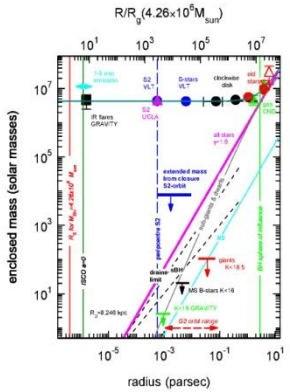

Fig. D.1. Constraints on the enclosed mass in the central 10 pc of the Galaxy. The blue crossed circle, the pink triangle, and the black crossed rectangles are estimates of the enclosed mass within the S2 orbit, other S-stars and the massive star discs (Paumard et al. 2006; Bartko et al. 2009; Yelda et al. 2014). The red filled circles, the red crossed rectangle, and red open triangles denote mass measurements from late-type stars. Green triangles are mass estimates from rotating gas in the circum-nuclear disc (see Genzel et al. 2010 for details). The filled black rectangle comes from the clockwise loop-motions of synchrotron near-infrared flares (GRAVITY Collaboration 2018b). The cyan double arrow denotes current VLBI estimates of the 3 mm size of Sgr A* (Issaoun et al. 2019). The continuous magenta line shows the total mass from all stars and stellar remnants (Alexander 2017). The grey line marks the distribution of $K < 18.5$ sub-giants and dwarfs from Schödel et al. (2018). The black dashed lines and the cyan line indicate the distribution of stellar black holes and neutron stars from theoretical simulations of Alexander (2017) and Baumgardt et al. (2018), which span a range of roughly a factor 5. Red, black and green upper limits denote upper limits on giants, main-sequence B stars and $K < 19$ GRAVITY sources. The Schwarzschild radius of a $4.26 \times 10^6\,M_\odot$ black hole and the innermost stable circular orbit radius for a non-spinning black hole are given by red vertical lines. The pericentre radius of S2 is the dashed vertical blue line and the sphere of influence of the black hole is given by the vertical green line. The blue horizontal line denotes the 2σ upper limit of any extended mass around Sgr A* obtained from the lack of retrograde precession in the S2 orbit (see text).

& Iorio (2017) cautioned, however, that already the Newtonian perturbation from S55/S0-102 (Meyer et al. 2012; Gillessen et al. 2017) might hide the spin's signature. For stars on shorter period orbits or with higher eccentricities, detecting the higher order effects of the metric is easier; and stellar perturbations have a different observational signature than the effect of the metric.

A second massive object in the GC. The presence of an intermediate mass black hole (IMBH) orbiting Sgr A* inside the orbit of S2 is constrained by our measurements. Gualandris et al. (2010) explored a grid of three-body simulations with an

Appendix E: Details of the fit

Table E.1. Best-fit orbit parameters.

Parameter	Value	Fit error	MCMC error	Unit
f_{SP}	1.10	0.19	0.21	
f_{RS}	1	Fixed	Fixed	
$M_\bullet$	4.261	0.012	0.012	$10^6\,M_\odot$
R_0	8246.7	9.3	9.3	pc
a	125.058	0.041	0.044	mas
e	0.884649	0.000066	0.000079	
i	134.567	0.033	0.033	°
ω	66.263	0.031	0.030	°
Ω	228.171	0.031	0.031	°
P	16.0455	0.0013	0.0013	yr
t_{peri}	2018.37900	0.00016	0.00017	yr
x_0	−0.90	0.14	0.15	mas
y_0	0.07	0.12	0.11	mas
vx_0	0.080	0.010	0.010	mas yr^{-1}
vy_0	0.0341	0.0096	0.0096	mas yr^{-1}
vz_0	−1.6	1.4	1.4	km s^{-1}

Notes. The orbital parameters are to be interpreted as the osculating orbital parameters. The argument of periapsis ω and the time of pericentre passage t_{peri} are given for the epoch of last apocentre in 2010.

In Table E.1 we report the best-fitting parameters of our 14-parameter fit, together with the formal fit errors and the 1σ confidence intervals from the MCMC. The two approaches agree because our fit is well behaved. There is a single minimum for χ^2, and the posterior distribution is close to a 14-dimensional Gaussian (Fig. E.3), with significant correlations, however. Figure E.1 shows the posterior for f_{SP}.

In Fig. E.2 we show selected correlation plots from the posterior distribution, which are worth discussing in the context of f_{SP}. The strongest correlation for f_{SP} is with the pericentre time. This is not surprising, given the discussion in Appendix B, where we showed that near pericentre the SP acts like a shift in time. The second strongest correlation for f_{SP} is with the RA offset of the coordinate system. This explains why including the NACO flare data helps determining f_{SP}: the flares essentially measure the offset of the coordinate system.

The parameter f_{SP} is also weakly correlated with the semi-major axis a and it is anti-correlated with the eccentricity e of the orbit. The former can be understood in the following way: If the orbit were slightly larger on sky, a stronger precession term would be required in order to achieve the same amount of kink (in mas on sky) at pericentre. The latter is understood similarly: A higher eccentricity leads to a narrower orbit figure, and hence less of the precession term would be needed. Interestingly, f_{SP} is almost uncorrelated with the argument of periapsis ω (i.e. the angle describing the orientation of the orbital ellipse in its plane), despite that the SP changes exactly that parameter.

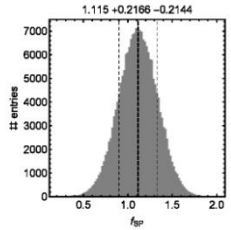

Fig. E.1. Result of the MCMC modelling of our data, showing the posterior distribution of the Schwarzschild parameter f_{SP}.

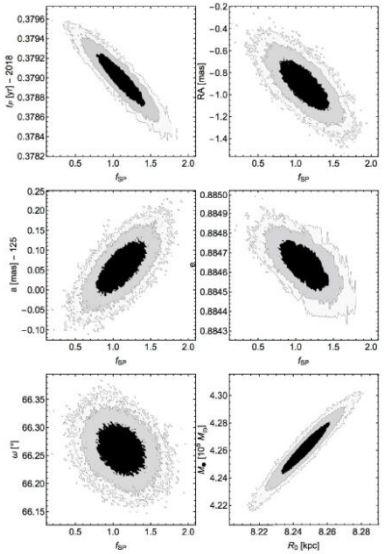

Fig. E.2. Selected parameter correlations from the 14-dimensional posterior distribution as determined from MCMC modelling.

The strongest correlation between any two parameters for our fit is the well known degeneracy between mass $M_\bullet$ and distance R_0 (Ghez et al. 2008; Gillessen et al. 2009a, 2017; Boehle et al. 2016; GRAVITY Collaboration 2018a, 2019). The parameter f_{SP} is only very weakly correlated with R_0.

Editors' Suggestion | Featured in Physics

Search for a Variation of the Fine Structure Constant around the Supermassive Black Hole in Our Galactic Center

A. Hees,[1,*] T. Do,[2] B. M. Roberts,[1,3] A. M. Ghez,[2] S. Nishiyama,[4] R. O. Bentley,[2] A. K. Gautam,[2] S. Jia,[5] T. Kara,[4] J. R. Lu,[5] H. Saida,[6] S. Sakai,[2] M. Takahashi,[7] and Y. Takamori[8]

[1]*SYRTE, Observatoire de Paris, Université PSL, CNRS, Sorbonne Université, LNE, 61 avenue de l'Observatoire 75014 Paris, France*

[2]*Department of Physics and Astronomy, University of California, Los Angeles, California 90095, USA*

[3]*School of Mathematics and Physics, The University of Queensland, Brisbane, Queensland 4072, Australia*

[4]*Miyagi University of Education, 149 Aramaki-aza-aoba, Aoba-ku, Sendai, Miyagi 980-0845, Japan*

[5]*Astronomy Department, University of California, Berkeley, California 94720, USA*

[6]*Daido University, 10-3 Takiharu-cho, Minami-ku, Nagoya, Aichi 457-8530, Japan*

[7]*Aichi University of Education, 1 Hirosawa, Igaya-cho, Kariya, Aichi 448-8542, Japan*

[8]*National Institute of Technology, Wakayama College, 77 Noshima, Nada-cho, Gobo, Wakayama 644-0023, Japan*

(Received 21 December 2019; accepted 23 January 2020; published 26 February 2020)

Searching for space-time variations of the constants of Nature is a promising way to search for new physics beyond general relativity and the standard model motivated by unification theories and models of dark matter and dark energy. We propose a new way to search for a variation of the fine-structure constant using measurements of late-type evolved giant stars from the S star cluster orbiting the supermassive black hole in our Galactic Center. A measurement of the difference between distinct absorption lines (with different sensitivity to the fine structure constant) from a star leads to a direct estimate of a variation of the fine structure constant between the star's location and Earth. Using spectroscopic measurements of five stars, we obtain a constraint on the relative variation of the fine structure constant below 10^{-5}. This is the first time a varying constant of nature is searched for around a black hole and in a high gravitational potential. This analysis shows new ways the monitoring of stars in the Galactic Center can be used to probe fundamental physics.

DOI: 10.1103/PhysRevLett.124.081101

The current understanding of our Universe is based on the theory of general relativity (GR) and on the standard model (SM) of particle physics. While both theories have been extremely successful, they are expected to break down at a certain point. In particular, a breaking of the Einstein equivalence principle is expected in various unification scenarios [1,2], in higher dimensional theories [3], and by some models of dark matter [4,5] and dark energy [6,7]. On a more philosophical note, the "principle of absence of absolute structure" led to many developments of extensions of physics where the constants of physics become dynamical entities, explicitly breaking the equivalence principle (see the discussion in section 2 of [8]).

One way to test the equivalence principle is to search for space-time variations of the constants of nature such as the fine structure constant α, the mass of fermions and the quantum chromodynamics energy scale (see [9] for a review of the tests of GR and [10] for a review of the search for varying constants). Various experiments using atomic clocks have provided stringent constraints on linear drifts of the constants of nature at the level of 10^{-16} yr^{-1} [11–18], on a dependency of the constants of nature to the Sun gravitational potential at the level of 10^{-7} [14–16,19,20] or on harmonic variations of the constants of nature [21]. A time variation of α has also been searched for using measurements of quasar absorption spectra [22] providing constraint on $\Delta\alpha/\alpha$ at the level of 10^{-6} for a cosmological redshift up to $z \sim 3$. A variation of α has also been constrained at the level of 10^{-3} for $z \sim 10^3$ using cosmic microwave background measurements [23] and at a similar level for $z \sim 10^{10}$ by a big bang nucleosynthesis analysis [24]. Finally, a dependency of α on the gravitational potential has also been searched for using absorption lines from a white dwarf [25]. Although many searches for a variation of α have been performed, the question of its constancy around a black hole and around a supermassive body remains totally open.

The motion of the short-period stars (S stars) orbiting around the $4 \times 10^6\ M_\odot$ supermassive black hole (SMBH) at the center of our Galaxy has been monitored for 25 years by two experiments: one carried out at the Keck Observatory [26–28] and the other with the New Technology Telescope (NTT) and with the Very Large Telescope (VLT) [29–31]. Recently, these measurements have opened a new window to probe fundamental physics around a SMBH. Measurements of the short-period star

A. Gilbert, S. Gillessen, M. Horrobin, S. Trippe, H. Bonnet, C. Dumas, N. Hubin, A. Kaufer, M. Kissler-Patig, G. Monnet, S. Ströbele, T. Szeifert, A. Eckart, R. Schödel, and S. Zucker, Astrophys. J. **628**, 246 (2005); S. Gillessen, F. Eisenhauer, T. K. Fritz, H. Bartko, K. Dodds-Eden, O. Pfuhl, T. Ott, and R. Genzel, Astrophys. J. Lett. **707**, L114 (2009); S. Gillessen, F. Eisenhauer, S. Trippe, T. Alexander, R. Genzel, F. Martins, and T. Ott, Astrophys. J. **692**, 1075 (2009); S. Gillessen, P. M. Plewa, F. Eisenhauer, R. Sari, I. Waisberg, M. Habibi, O. Pfuhl, E. George, J. Dexter, S. von Fellenberg, T. Ott, and R. Genzel, Astrophys. J. **837**, 30 (2017); R. Abuter *et al.* (Gravity Collaboration), Astron. Astrophys. **625**, L10 (2019).

[30] R. Abuter *et al.* (Gravity Collaboration), Astron. Astrophys. **615**, L15 (2018).

[31] A. Amorim *et al.* (Gravity Collaboration), Phys. Rev. Lett. **122**, 101102 (2019).

[32] D. Borka, P. Jovanović, V. Borka Jovanović, and A. F. Zakharov, J. Cosmol. Astropart. Phys. 11 (2013) 050; A. F. Zakharov, P. Jovanović, D. Borka, and V. Borka Jovanović, J. Cosmol. Astropart. Phys. 05 (2016) 045; 04 (2018) 050.

[33] K. Hinterbichler and J. Khoury, Phys. Rev. Lett. **104**, 231301 (2010); K. Hinterbichler, J. Khoury, A. Levy, and A. Matas, Phys. Rev. D **84**, 103521 (2011).

[34] A. I. Vainshtein, Phys. Lett. B **39**, 393 (1972); C. Deffayet, G. Dvali, G. Gabadadze, and A. Vainshtein, Phys. Rev. D **65**, 044026 (2002).

[35] D. D. Doneva and S. S. Yazadjiev, Phys. Rev. Lett. **120**, 131103 (2018); G. Antoniou, A. Bakopoulos, and P. Kanti, Phys. Rev. Lett. **120**, 131102 (2018); H. O. Silva, J. Sakstein, L. Gualtieri, T. P. Sotiriou, and E. Berti, Phys. Rev. Lett. **120**, 131104 (2018).

[36] T. Do, J. R. Lu, A. M. Ghez, M. R. Morris, S. Yelda, G. D. Martinez, S. A. Wright, and K. Matthews, Astrophys. J. **764**, 154 (2013).

[37] S. Nishiyama, H. Saida, Y. Takamori, M. Takahashi, R. Schödel, F. Najarro, S. Hamano, M. Omiya, M. Tamura, M. Takahashi, H. Gorin, S. Nagatomo, and T. Nagata, Publ. Astron. Soc. Jpn. **70**, 74 (2018).

[38] H. Saida, S. Nishiyama, T. Ohgami, Y. Takamori, M. Takahashi, Y. Minowa, F. Najarro, S. Hamano, M. Omiya, A. Iwamatsu, M. Takahashi, H. Gorin, T. Kara, A. Koyama, Y. Ohashi, M. Tamura, S. Nagatomo, T. Zenko, and T. Nagata, Publ. Astron. Soc. Jpn. **71**, 126 (2019).

[39] T. Do, W. Kerzendorf, Q. Konopacky, J. M. Marcinik, A. Ghez, J. R. Lu, and M. R. Morris, Astrophys. J. Lett. **855**, L5 (2018).

[40] See the Supplemental Material at http://link.aps.org/supplemental/10.1103/PhysRevLett.124.081101 for the detailed calculation of the atomic transitions, for the data and for a details presentation of the methodology used in this analysis, which includes Refs. [26,28,37,39,41–69].

[41] V. A. Dzuba, V. V. Flambaum, and M. G. Kozlov, Phys. Rev. A **54**, 3948 (1996); V. A. Dzuba and W. R. Johnson, Phys. Rev. A **57**, 2459 (1998).

[42] J. C. Berengut, Phys. Rev. A **94**, 012502 (2016).

[43] V. A. Dzuba, J. C. Berengut, C. Harabati, and V. V. Flambaum, Phys. Rev. A **95**, 012503 (2017).

[44] A. J. Geddes, L. V. Skripnikov, A. Borschevsky, J. C. Berengut, V. V. Flambaum, and T. P. Rakitzis, Phys. Rev. A **98**, 022508 (2018).

[45] E. V. Kahl and J. C. Berengut, Comput. Phys. Commun. **238**, 232 (2019).

[46] A. Kramida, Y. Ralchenko, J. Reader, and (The NIST ASD Team 2018), NIST Atomic Spectra Database (ver. 5.6.1), http://physics.nist.gov/asd (2019).

[47] Z. Chen, E. Gallego-Cano, T. Do, G. Witzel, A. M. Ghez, R. Schödel, B. N. Sitarski, E. E. Becklin, J. Lu, M. R. Morris, A. Dehghanfar, A. K. Gautam, A. Hees, M. W. Hosek, Jr., S. Jia, A. C. Mangian, and K. Matthews, Astrophys. J. Lett. **882**, L28 (2019).

[48] S. Jia, J. R. Lu, S. Sakai, A. K. Gautam, T. Do, M. W. Hosek, Jr., M. Service, A. M. Ghez, E. Gallego-Cano, R. Schödel, A. Hees, M. R. Morris, E. Becklin, and K. Matthews, Astrophys. J. **873**, 9 (2019).

[49] S. Sakai, J. R. Lu, A. Ghez, S. Jia, T. Do, G. Witzel, A. K. Gautam, A. Hees, E. Becklin, K. Matthews, and M. W. Hosek, Jr., Astrophys. J. **873**, 65 (2019).

[50] M. J. Reid, K. M. Menten, S. Trippe, T. Ott, and R. Genzel, Astrophys. J. **659**, 378 (2007).

[51] J. C. Berengut, V. A. Dzuba, V. V. Flambaum, and A. Ong, Phys. Rev. Lett. **109**, 070802 (2012).

[52] M. S. Safronova, Ann. Phys. (N.Y.) **531**, 1800364 (2019).

[53] M. G. Kozlov and D. Budker, Ann. Phys. (N.Y.) **531**, 1800254 (2018).

[54] V. A. Dzuba, V. V. Flambaum, and M. G. Kozlov, Phys. Rev. A **99**, 032501 (2019).

[55] B. G. C. Lackenby, V. A. Dzuba, and V. V. Flambaum Phys. Rev. A **99**, 042509 (2019).

[56] J. C. Berengut, V. V. Flambaum, and M. G. Kozlov, Phys. Rev. A **73**, 012504 (2006).

[57] J. C. Berengut, V. V. Flambaum, and M. G. Kozlov, J. Phys. B **41**, 235702 (2008).

[58] V. A. Dzuba, Phys. Rev. A **71**, 032512 (2005).

[59] V. V. Flambaum and V. A. Dzuba, Can. J. Phys. **87**, 25 (2009).

[60] V. A. Dzuba and V. V. Flambaum, Phys. Rev. A **77**, 012515 (2008).

[61] V. A. Dzuba, V. V. Flambaum, P. G. Silvestrov, and O. P. Sushkov, J. Phys. B **20**, 1399 (1987).

[62] V. A. Dzuba, V. V. Flambaum, and O. P. Sushkov, Phys. Lett. A **140**, 493 (1989).

[63] J. C. Berengut, V. A. Dzuba, V. V. Flambaum, and M. V. Marchenko, Phys. Rev. A **70**, 064101 (2004).

[64] M. Støstad, T. Do, N. Murray, J. R. Lu, S. Yelda, and A. Ghez, Astrophys. J. **808**, 106 (2015).

[65] R. Schödel, S. Yelda, A. Ghez, J. H. Girard, L. Labadie, R. Rebolo, A. Pérez-Garrido, and M. R. Morris, Mon. Not. R. Astron. Soc. **429**, 1367 (2013).

[66] E. Diolaiti, O. Bendinelli, D. Bonaccini, L. Close, D. Currie, and G. Parmeggiani, Astron. Astrophys. **147**, 335 (2000).

[67] P. L. Wizinowich, D. Le Mignant, A. H. Bouchez, R. D. Campbell, J. C. Y. Chin, A. R. Contos, M. A. van Dam, S. K. Hartman, E. M. Johansson, R. E. Lafon, H. Lewis, P. J. Stomski, D. M. Summers, C. G. Brown, P. M. Danforth, C. E. Max, and D. M. Pennington, Publ. Astron. Soc. Pac. **118**, 297 (2006).

2021 Review of Particle Physics.
P.A. Zyla *et al.* (Particle Data Group), Prog. Theor. Exp. Phys. 2020, 083C01 (2020) and 2021 update

graviton MASS

INSPIRE search

It is likely that the graviton is massless. More than fifty years ago Van Dam and Veltman (VAN DAM 1970), Iwasaki (IWASAKI 1970), and Zakharov (ZAKHAROV 1970) almost simultaneously showed that in the linear approximation a theory with a finite graviton mass does not approach GR as the mass approaches zero. Attempts have been made to evade this "vDVZ discontinuity" by invoking modified gravity or nonlinear theory by De Rahm (DE-RHAM 2017) and others. More recently, the analysis of gravitational-wave dispersion has led to bounds that are largely independent of the underlying model, even if not the strongest. We quote the best of these as our best limit.

Experimental limits have been set based on a Yukawa potential (YUKA), dispersion relation (DISP), or other modified gravity theories (MGRV).

The following conversions are useful. 1 eV = 1.783×10^{-36} g = $1.957 \times 10^{-6} m_e$, $\lambda_{\hbar} = (1.973 \times 10^{-7}$ m)x(1 eV/m_g).

VALUE (eV)		*DOCUMENT ID*		*TECN*	*COMMENT*
$< 5 \times 10^{-23}$	1	ABBOTT	2019	DISP	LIGO Virgo catalog GWTC-1
• • • We do not use the following data for averages, fits, limits, etc. • • •					
$< 3.2 \times 10^{-23}$	2	BERNUS	2020	YUKA	Planetary ephemeris INPOP19a
$< 2 \times 10^{-24}$	3	SHAO	2020	DISP	Binary pulsar Galileon radiation
$< 7 \times 10^{-23}$	4	BERNUS	2018	YUKA	Planetary ephemeris INPOP17b
$< 3.1 \times 10^{-20}$	5	MIAO	2018	DISP	Binary pulsar orbital decay rate
$< 1.4 \times 10^{-29}$	6	DESAI	2018	YUKA	Gal cluster Abell 1689
$< 5 \times 10^{-30}$	7	GUPTA	2018	YUKA	Using SPT-SZ
$< 3 \times 10^{-30}$	7	GUPTA	2018	YUKA	Using Planck all-sky SZ
$< 1.3 \times 10^{-29}$	7	GUPTA	2018	YUKA	Using redMaPPer SDSS-DR8
$< 6 \times 10^{-30}$	8	RANA	2018	YUKA	Weak lensing in massive clusters
$< 8 \times 10^{-30}$	9	RANA	2018	YUKA	SZ effect in massive clusters
$< 1.0 \times 10^{-23}$	10	WILL	2018	YUKA	Perihelion advances of planets
$< 7 \times 10^{-23}$	1	ABBOTT	2017	DISP	Combined dispersion limit from three BH mergers
$< 1.2 \times 10^{-22}$	1	ABBOTT	2016	DISP	Combined dispersion limit from two BH mergers
$< 3.9 \times 10^{-21}$	11	ZAKHAROV	2016	YUKA	S2 star orbit
$< 5 \times 10^{-23}$	12	BRITO	2013	MGRV	Spinning black holes bounds
$< 6 \times 10^{-32}$	13	GRUZINOV	2005	MGRV	Solar System observations
$< 6 \times 10^{-32}$	14	CHOUDHURY	2004	YUKA	Weak gravitational lensing
$< 9.0 \times 10^{-34}$	15	GERSHTEIN	2004	MGRV	From Ω_{tot} value assuming RTG
$< 8 \times 10^{-20}$	16,17	FINN	2002	DISP	Binary pulsar orbital period decrease
$< 7 \times 10^{-23}$		TALMADGE	1988	YUKA	Solar system planetary astrometric data
$< 1.3 \times 10^{-29}$	18	GOLDHABER	1974	YUKA	Rich clusters
$< 7 \times 10^{-26}$		HARE	1973	YUKA	Galaxy
$< 8 \times 10^{4}$		HARE	1973	YUKA	2γ decay

VALUE (eV)	DOCUMENT ID	TECN	COMMENT

[1] ABBOTT 2019 , ABBOTT 2017 , and ABBOTT 2016 limits assume a dispersion relation for gravitational waves modified relative to GR.

[2] BERNUS 2020 use the latest solution of the ephemeris INPOP (19a) in order to improve the constraint in BERNUS 2018 on the existence of a Yukawa suppression to the Newtonian potential, generically associated to a gravitons mass.

[3] SHAO 2020 sets limit, 95% CL, based on non-observation of excess gravitational radiation in 14 well-timed binary pulsars in the context of the cubic Galileon model.

[4] BERNUS 2018 use the planetary ephemeris INPOP 17b to constraint the existence of a Yukawa suppression to the Newtonian potential, generically associated to a gravitons mass.

[5] MIAO 2019 90% CL limit is based on orbital period decay rates of 8 binary pulsars using a Bayesian prior uniform in graviton mass. Limit becomes $< 5.2 \times 10^{-21}$ eV for a prior uniform in $\ln(m_g)$.

[6] DESAI 2018 limit based on dynamical mass models of galaxy cluster Abell 1689.

[7] GUPTA 2018 obtains graviton mass limits using stacked clusters from 3 disparate surveys.

[8] RANA 2018 limit, 68% CL, obtained using weak lensing mass profiles out to the radius at which the cluster density falls to 200 times the critical density of the Universe. Limit is based on the fractional change between Newtonian and Yukawa accelerations for the 50 most massive galaxy clusters in the Local Cluster Substructure Survey. Limits for other CL's and other density cuts are also given.

[9] RANA 2018 limit, 68% CL, obtained using mass measurements via the SZ effect out to the radius at which the cluster density falls to 500 times the critical density of the Universe for 182 optically confirmed galaxy clusters in an Atacama Cosmology Telescope survey. Limits for other CL's and other density cuts are also given.

[10] WILL 2018 limit from perihelion advances of the planets, notably Earth, Mars, and Saturn. Alternate analysis yields $< 6 \times 10^{-24}$.

[11] ZAKHAROV 2016 constrains range of Yukawa gravity interaction from S2 star orbit about black hole at Galactic center. The limit is $< 2.9 \times 10^{-21}$ eV for $\delta = 100$.

[12] BRITO 2013 explore massive graviton (spin-2) fluctuations around rotating black holes.

[13] GRUZINOV 2005 uses the DGP model (DVALI 2000) showing that non-perturbative effects restore continuity with Einstein's equations as the gravition mass approaches zero, then bases his limit on Solar System observations.

[14] CHOUDHURY 2004 concludes from a study of weak-lensing data that masses heavier than about the inverse of 100 Mpc seem to be ruled out if the gravitation field has the Yukawa form.

[15] GERSHTEIN 2004 use non-Einstein field relativistic theory of gravity (RTG), with a massive graviton, to obtain the 95% CL mass limit implied by the value of $\Omega_{tot} = 1.02 \pm 0.02$ current at the time of publication.

[16] FINN 2002 analyze the orbital decay rates of PSR B1913+16 and PSR B1534+12 with a possible graviton mass as a parameter. The combined frequentist mass limit is at 90% CL.

[17] As of 2020, limits on $\dot{P}/P$ are now about 0.1% (see T. Damour, "Experimental tests of gravitational theory," in this *Review*).

[18] GOLDHABER 1974 establish this limit considering the binding of galactic clusters, corrected to Planck $h_0 = 0.67$.

References:

BERNUS	2020	PR D102 021501	Constraint on the Yukawa suppression of the Newtonian potential from the planetary ephemeris INPOP19a
SHAO	2020	PR D102 024068	New Graviton Mass Bound from Binary Pulsars
ABBOTT	2019	PR D100 104036	Tests of General Relativity with the Binary Black Hole Signals from the LIGO-Virgo Catalog GWTC-1
BERNUS	2018	PRL 123 161103	Constraining the mass of the graviton with the planetary ephemeris INPOP
MIAO	2019	PR D99 123016	Bounding the mass of graviton in a dynamic regime with binary pulsars
DESAI	2018	PL B778 325	Limit on graviton mass from galaxy cluster Abell 1689
GUPTA	2018	ANP 399 85	Limit on graviton mass using stacked galaxy cluster catalogs from SPT-SZ, Planck-SZ and SDSS-redMaPPer
RANA	2018	PL B781 220	Bounds on graviton mass using weak lensing and SZ effect in galaxy clusters
WILL	2018	CQG 35 17LT01	Solar system versus gravitational-wave bounds on the graviton mass
ABBOTT	2017	PRL 118 221101	GW170104. Observation of a 50-Solar-Mass Binary Black Hole Coalescence at Redshift 0.2
ABBOTT	2016	PRL 116 061102	Observation of Gravitational Waves from a Binary Black Hole Merger
ZAKHAROV	2016	JCAP 1605 045	Constraining the range of Yukawa gravity interaction from S2 star orbits II. Bounds on graviton mass
BRITO	2013	PR D88 023514	Massive Spin-2 Fields on Black Hole Spacetimes. Instability of the Schwarzschild and Kerr Solutions and Bounds on the Graviton Mass

An alternative potential for elliptical trajectories

Monthly Notices of the ROYAL ASTRONOMICAL SOCIETY

MNRAS **505,** L64–L68 (2021) https://doi.org/10.1093/mnrasl/slab051
Advance Access publication 2021 May 20

Hinting a dark matter nature of Sgr A∗ via the S-stars

E. A. Becerra-Vergara,[1,2,3★] C. R. Argüelles,[1,2,4] A. Krut,[1,2] J. A. Rueda[1,2,5,6★] and R. Ruffini[1,2,5,6★]

[1]*ICRANet, Piazza della Repubblica 10, I-65122 Pescara, Italy*
[2]*ICRA, Dip. di Fisica, Sapienza Università di Roma, P.le Aldo Moro 5, I-00185 Rome, Italy*
[3]*GIRG, Escuela de Física, Universidad Industrial de Santander, 680002 Bucaramanga, Colombia*
[4]*Fac. de Ciencias Astron. y Geofísicas, Universidad Nacional de La Plata, Paseo del Bosque, B1900FWA La Plata, Argentina*
[5]*ICRANet-Ferrara, Dip. di Fisica e Scienze della Terra, Università degli Studi di Ferrara, Via Saragat 1, I-44122 Ferrara, Italy*
[6]*INAF, Istituto de Astrofisica e Planetologia Spaziali, Via Fosso del Cavaliere 100, I-00133 Rome, Italy*

Accepted 2021 May 12. Received 2021 May 12; in original form 2021 March 1

ABSTRACT

The motion data of the S-stars around the Galactic Centre gathered in the last 28 yr imply that Sgr A∗ hosts a supermassive compact object of about $4 \times 10^6\,M_\odot$, a result awarded with the Nobel Prize in Physics 2020. A non-rotating black hole (BH) nature of Sgr A∗ has been uncritically adopted since the S-star orbits agree with Schwarzschild geometry geodesics. The orbit of S2 has served as a test of general relativity predictions such as the gravitational redshift and the relativistic precession. The central BH model is, however, challenged by the G2 post-peripassage motion and by the lack of observations on event-horizon-scale distances robustly pointing to its univocal presence. We have recently shown that the S2 and G2 astrometry data are better fitted by geodesics in the spacetime of a self-gravitating dark matter *core–halo* distribution of 56 keV-fermions, '*darkinos*', which also explains the outer halo Galactic rotation curves. This letter confirms and extends this conclusion using the astrometry data of the 17 best-resolved S-stars, thereby strengthening the alternative nature of Sgr A∗ as a dense core of darkinos.

Key words: Elementary particles – Dark matter.

1 INTRODUCTION

The gravitational potential in the Galactic centre (GC) is dominated by a supermassive compact object, Sagittarius A∗ (Sgr A∗), long thought to be a massive black hole (BH) of $\approx 4 \times 10^6\,M_\odot$ (Ghez et al. 2005, 2008; Genzel, Eisenhauer & Gillessen 2010; Gravity Collaboration 2018b). From the observational viewpoint, this inference on the nature of Sgr A∗ mainly comes from the nearly Keplerian orbits of tens of stars belonging to the S-star cluster (Gillessen et al. 2009a, 2017), whose motions are well described by geodesics in the Schwarzschild spacetime geometry. The most important S-cluster member is S2 which, with an orbital period of about 16 yr and a pericentre of about 1500 Schwarzschild radii, has the most compact orbit around Sgr A∗. The S2 orbit data have allowed to test general relativity predictions such as the relativistic redshift (see e.g. Gravity Collaboration 2018a; Do et al. 2019) and precession (see e.g. Parsa et al. 2017; Gravity Collaboration 2020). However, not every news is good for the BH model; it is challenged by the G2 motion which cannot be explained by any geodesics in the BH geometry (Plewa et al. 2017; Gillessen et al. 2019), as well as by very scarce data at event-horizon-scale distances from Sgr A∗, robustly pointing to a univocal central BH presence (see e.g. Yuan & Narayan 2014; Bouffard et al. 2019).

In view of the above, we have dived into the possibility of an alternative nature for Sgr A∗ based on the fermionic dark matter (DM) profile predicted by the Ruffini–Argüelles–Rueda (RAR) model (Ruffini, Argüelles & Rueda 2015; Argüelles et al. 2018). In the RAR model, the DM distribution in galaxies is obtained from the general relativity field equations, assuming it as a self-gravitating system of fermions at finite temperature in equilibrium and distributed in phase space according to the Fermi–Dirac statistics including a particle energy cut-off that gives to the configuration, a finite size (see Argüelles et al. 2018, for more details). We hereafter refer to these neutral, massive DM fermions as '*darkinos*'. The RAR model leads to a *dense core–diluted halo* density profile in which the darkinos are: (1) in a quantum degenerate regime within the nearly uniform core, (2) followed by an intermediate quantum-classical regime in the density fall-off and plateau phase, and (3) finally in a Boltzmann regime in the outer halo that follows a power-law density ending with a nearly exponential cut-off defining the galaxy border. There is a bunch of astrophysical consequences of the *core–halo* profile of darkinos derived from the RAR model. In Argüelles et al. (2018), it has been shown that it explains the rotation curves of the Milky Way outer halo. In Argüelles et al. (2019), this agreement has been shown to apply as well to other galaxy types ranging from dwarfs to big ellipticals and galaxy clusters. These results have further enticed attention on the darkinos microphysics, e.g. their self-interactions (Argüelles et al. 2016; Yunis et al. 2020a) and interaction with neutrinos (Penacchioni, Civitarese & Argüelles 2020) as well as in their macrophysics, e.g. their lensing properties (Gómez et al. 2016), their influence in the dynamics of binaries (Gómez & Rueda 2017), their halo formation and stability on cosmological time-scales (Argüelles et al. 2020), and their role in the large- and small-scale structure formation (Yunis, Argüelles & López Nacir 2020b).

★ E-mail: eduar.becerra@icranet.org (EAB-V); jorge.rueda@icra.it (JAR); ruffini@icra.it (RR)

A&A 641, A34 (2020)
https://doi.org/10.1051/0004-6361/201935990

Astronomy & Astrophysics

Geodesic motion of S2 and G2 as a test of the fermionic dark matter nature of our Galactic core

E. A. Becerra-Vergara[1,2,3], C. R. Argüelles[1,2,4], A. Krut[1,2], J. A. Rueda[1,2,5,6,7], and R. Ruffini[1,2,5,6,8]

[1] ICRANet, Piazza della Repubblica 10, 65122 Pescara, Italy
e-mail: eduar.becerra@icranet.org
[2] ICRA, Dipartimento di Fisica, Sapienza Università di Roma, P.le Aldo Moro 5, 00185 Rome, Italy
e-mail: jorge.rueda@icra.it, ruffini@icra.it
[3] Grupo de Investigación en Relatividad y Gravitación, Escuela de Física, Universidad Industrial de Santander, A. A. 678, Bucaramanga 680002, Colombia
[4] Facultad de Ciencias Astronómicas y Geofísicas, Universidad Nacional de La Plata, Paseo del Bosque, B1900FWA La Plata, Argentina
[5] ICRANet-Ferrara, Dipartimento di Fisica e Scienze della Terra, Università degli Studi di Ferrara, Via Saragat 1, 44122 Ferrara, Italy
[6] Dipartimento di Fisica e Scienze della Terra, Università degli Studi di Ferrara, Via Saragat 1, 44122 Ferrara, Italy
[7] INAF, Istituto de Astrofisica e Planetologia Spaziali, Via Fosso del Cavaliere 100, 00133 Rome, Italy
[8] INAF, Viale del Parco Mellini 84, 00136 Rome, Italy

Received 30 May 2019 / Accepted 22 July 2020

ABSTRACT

The motion of S-stars around the Galactic center implies that the central gravitational potential is dominated by a compact source, Sagittarius A* (Sgr A*), which has a mass of about $4 \times 10^6\,M_\odot$ and is traditionally assumed to be a massive black hole (BH). The explanation of the multiyear accurate astrometric data of the S2 star around Sgr A*, including the relativistic redshift that has recently been verified, is particularly important for this hypothesis and for any alternative model. Another relevant object is G2, whose most recent observational data challenge the scenario of a massive BH: its post-pericenter radial velocity is lower than expected from a Keplerian orbit around the putative massive BH. This scenario has traditionally been reconciled by introducing a drag force on G2 by an accretion flow. As an alternative to the central BH scenario, we here demonstrate that the observed motion of both S2 and G2 is explained in terms of the *dense core – diluted halo* fermionic dark matter (DM) profile, obtained from the fully relativistic Ruffini-Argüelles-Rueda (RAR) model. It has previously been shown that for fermion masses 48–345 keV, the RAR-DM profile accurately fits the rotation curves of the Milky Way halo. We here show that the solely gravitational potential of such a DM profile for a fermion mass of 56 keV explains (1) all the available time-dependent data of the position (orbit) and line-of-sight radial velocity (redshift function z) of S2, (2) the combination of the special and general relativistic redshift measured for S2, (3) the currently available data on the orbit and z of G2, and (4) its post-pericenter passage deceleration without introducing a drag force. For both objects, we find that the RAR model fits the data better than the BH scenario: the mean of reduced chi-squares of the time-dependent orbit and z data are $\langle\tilde{\chi}^2\rangle_{\rm S2,RAR} \approx 3.1$ and $\langle\tilde{\chi}^2\rangle_{\rm S2,BH} \approx 3.3$ for S2 and $\langle\tilde{\chi}^2\rangle_{\rm G2,RAR} \approx 20$ and $\langle\tilde{\chi}^2\rangle_{\rm G2,BH} \approx 41$ for G2. The fit of the corresponding z data shows that while for S2 we find comparable fits, that is, $\tilde{\chi}^2_{z,\rm RAR} \approx 1.28$ and $\tilde{\chi}^2_{z,\rm BH} \approx 1.04$, for G2 the RAR model alone can produce an excellent fit of the data, that is, $\tilde{\chi}^2_{z,\rm RAR} \approx 1.0$ and $\tilde{\chi}^2_{z,\rm BH} \approx 26$. In addition, the critical mass for gravitational collapse of a degenerate 56 keV-fermion DM core into a BH is $\sim 10^8\,M_\odot$. This result may provide the initial seed for the formation of the observed central supermassive BH in active galaxies, such as M 87.

Key words. Galaxy: center – Galaxy: kinematics and dynamics – Galaxy: structure – dark matter – elementary particles

1. Introduction

The monitoring of the motion of the so-called S-stars near the Galactic center over the past decades has revealed that the gravitational potential in which they move is dominated by a massive compact source at the center, Sagittarius A* (Sgr A*; Gillessen et al. 2009, 2017). The S-star dynamics implies a mass for Sgr A* of $\approx 4.1 \times 10^6\,M_\odot$, which is traditionally associated in the literature with a massive black hole (BH; Gravity Collaboration 2018a; Ghez et al. 2008; Genzel et al. 2010).

Of the objects that move near and around Sgr A*, S2 and G2 are the most interesting. The star S2 describes an elliptical orbit that is focused on Sgr A* and has a period of 16.05 yr and the second closest pericenter of the S-stars, $r_{p(S2)} \approx 0.6$ mpc (Gillessen et al. 2009, 2017). The S2 orbit constrains the Sgr A* mass best, but its pericenter at $\sim 1500\,r_{\rm Sch}$ from Sgr A* is too far to univocally infer a putative massive BH of Schwarzschild radius $r_{\rm Sch} = 2GM_{\rm BH}/c^2$, where $M_{\rm BH}$ is its mass.

The most recent measurements of the motion of G2 after the peripassage around Sgr A* represent a further challenge for the hypothesis of a massive BH. The G2 radial velocity is lower than that from a Keplerian motion around the massive BH, which has been reconciled by introducing the action of a drag force exerted by an accretion flow (Plewa et al. 2017; Gillessen et al. 2019).

Our aim here is to show that the *dense core – diluted halo* DM density distribution of a general relativistic system of 56 keV fermions, following the extended Ruffini-Argüelles-Rueda (RAR) model (Argüelles et al. 2018, 2019a) instead explains the orbits of S2 and G2 without invoking the massive BH or a drag force. We use the most complete data of

the S2 orbit over the last 26 yr (Gillessen et al. 2017; Gravity Collaboration 2018b), including the recent data released by Do et al. (2019), and the four-year data of the G2 motion after its pericenter passage (Gillessen et al. 2019).

2. Ruffini-Argüelles-Rueda model of dark matter

The Ruffini-Argüelles-Rueda (RAR) model equilibrium equations consist of the Einstein equations in spherical symmetry for a perfect fluid energy-momentum tensor. Pressure and density are given by Fermi-Dirac statistics, and the closure relations are determined by the Klein and Tolman conditions of thermodynamic equilibrium (Ruffini et al. 2015). The solution to this system of equations leads to a continuous and novel *dense core – diluted halo* DM profile from the center all the way to the galactic halo (see Siutsou et al. 2015; Argüelles et al. 2016; Mavromatos et al. 2017, for its applications). Similar *core-halo* profiles with applications to fermionic DM were also obtained in Bilic et al. (2002) and more recently in Chavanis et al. (2015) from a statistical approach within Newtonian gravity.

The above corresponds to the original version of the RAR model, with a unique family of density profile solutions that behaves as $\rho(r) \propto r^{-2}$ at large radial distances from the center. This treatment was extended in Argüelles et al. (2018), by introducing a cutoff in momentum space in the distribution function (DF; i.e., accounting for particle-escape effects) that allows defining the galaxy border (see Appendix A). This extension of the RAR model was successfully applied to explain the Milky Way rotation curve, as shown in Fig. 1, implying a more general *dense core – diluted halo* behavior for the DM distribution as follows:

– A DM core with radius r_c (defined at the first maximum of the twice-peaked rotation curve), whose value is shown to be inversely proportional to the particle mass m, in which the density is nearly uniform. This central core is supported against gravity by the fermion degeneracy pressure, and general relativistic effects are appreciable.

– Then, there is an intermediate region characterized by a sharply decreasing density where quantum corrections are still important, followed by an extended and diluted plateau. This region extends until the halo scale-length r_h is achieved (defined at the second maximum of the rotation curve).

– Finally, the DM density reaches a Boltzmann regime supported by thermal pressure with negligible general relativistic effects, and shows a behavior $\rho \propto r^{-n}$ with $n > 2$ that is due to the phase-space distribution cutof. This leads to a DM halo bounded in radius (i.e., $\rho \approx 0$ occurs when the particle escape energy approaches zero).

As was explicitly shown in Argüelles et al. (2019b,a, 2018), this type of *dense core – diluted halo* density profile suggests that the DM might explain the mass of the dark compact object in Sgr A* as well as the halo mass. It applies not only to the Milky Way, but also to other galactic structures from dwarfs and ellipticals to galaxy clusters (Argüelles et al. 2019a). Specifically, a Milky Way analysis (Argüelles et al. 2018) has shown that this DM profile can indeed explain the dynamics of the closest S-cluster stars (including S2) around Sgr A*, all the way to the halo rotation curve without changing the baryonic bulge-disk components. The analysis of the S-stars was made through a simplified circular velocity analysis in general relativity, constraining the allowed fermion mass to $mc^2 \approx 50$–345 keV. We extend this analysis by fully reconstructing the geodesic of the object in full general relativity, and apply it to S2 and G2. Figure 1 shows the DM density profile and its contribution to the rotation curve for the Milky Way for 56 keV DM fermions.

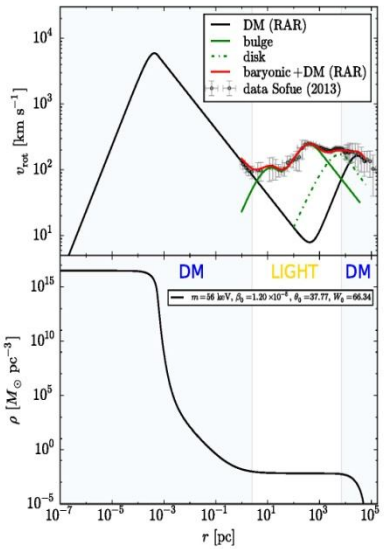

Fig. 1. Milky Way rotation curve and DM density profile from the extended RAR model with a core mass of $M_c = M(r_c) = 3.5 \times 10^6\, M_\odot$. *Top*: DM (black) and baryonic (bulge + disk) contribution to the rotation curve v_{rot} (total in red). *Bottom*: DM density profile. The baryonic model and the data are taken from Sofue (2013). The parameters of the extended RAR model in this case are fermion mass $mc^2 = 56$ keV, temperature parameter $\beta_0 = 1.1977 \times 10^{-5}$, degeneracy parameter $\theta_0 = 37.7656$, and energy cutoff parameter $W_0 = 66.3407$. For the RAR model fitting of the Milky Way, we follow Argüelles et al. (2018); see also Appendix A.

3. Orbit and radial velocity of S2 and G2

To obtain the S2 or G2 positions (orbit) and the corresponding line-of-sight radial velocity (i.e., the redshift function; see Appendix B) at each time, we solved the equations of motion for a test particle (see Appendix C) in the gravitational field produced by two possible scenarii that we describe below.

1. A central Schwarzschild massive BH. Gravity Collaboration (2018b) reported a BH mass of $M_{BH} = 4.1 \times 10^6\, M_\odot$ from the fit of the most recent measurements of the position and velocity of S2. The more recent analysis by Do et al. (2019) reported a BH mass of $3.975 \times 10^6\, M_\odot$. These works used a second-order post-Newtonian (2PN) model to describe the object motion. In order to compare and contrast the BH and the DM-RAR hypotheses on the same ground, that is, using the same analysis method and treatment, we performed our own fit of the data for the BH case using a full general relativistic modeling by solving the equations of motion in the Schwarzschild metric (see Appendix C). From our analysis of S2, we obtain model parameters that are very similar (but not

PERGAMON

Progress in Particle and Nuclear Physics 48 (2002) 291–300

Progress in Particle and Nuclear Physics

http://www.elsevier.com/locate/npe

The Dynamics of Stars Near Sgr A* and Dark Matter at the Center and in the Halo of the Galaxy

N. BILIĆ†, F. MUNYANEZA, G. B. TUPPER and R. D. VIOLLIER‡

Institute of Theoretical Physics and Astrophysics,

Department of Physics, University of Cape Town, Private Bag, Rondebosch 7701, South Africa

November 26, 2001

Abstract

After a discussion of the properties of degenerate fermion balls, we analyze the orbits of the star S0-1, which has the smallest projected distance to Sgr A*, in the supermassive black hole as well as in the fermion ball scenarios of the Galactic center. It is shown that both scenarios are consistent with the data, as measured during the last six years by Genzel et al. and Ghez et al. We then consider a self-gravitating ideal fermion gas at nonzero temperature as a model for the Galactic halo. The Galactic halo of mass $\sim 2 \times 10^{12} M_\odot$ enclosed within a radius of $\sim$ 200 kpc implies the existence of a supermassive compact dark object at the Galactic center that is in hydrostatic and thermal equilibrium with the halo. The central object has a maximal mass of $\sim 2.3 \times 10^6 M_\odot$ within a minimal radius of $\sim$ 18 mpc or $\sim$ 21 light-days for fermion masses $\sim$ 15 keV. We thus conclude that both the supermassive compact dark object and the halo could be made of the same weakly interacting $\sim$ 15 keV particle.

1. Introduction

In the past, self-gravitating neutrino matter has been suggested as a model for quasars, with neutrino masses in the $0.2\text{keV} \lesssim m \lesssim 0.5\text{MeV}$ range [1]. More recently, supermassive compact objects consisting of weakly interacting degenerate fermionic matter, with fermion masses in the $10 \lesssim m/\text{keV} \lesssim 20$ range, have been proposed [2, 3, 4, 5, 6] as an alternative to the supermassive black holes that are believed to reside at the centers of many galaxies.

So far the masses of $\sim$ 20 supermassive compact dark objects at the galactic centers have been measured [7]. The most massive compact dark object ever observed is located at the center of M87 in the Virgo cluster, and it has a mass of $\sim 3 \times 10^9 M_\odot$ [8]. If we identify this object of maximal mass with a degenerate fermion ball at the Oppenheimer-Volkoff (OV) limit [9], i.e., $M_{\rm OV} = 0.54 M_{\rm Pl}^3 m^{-2} g^{-1/2} \simeq 3 \times 10^9 M_\odot$ [4], where $M_{\rm Pl} = \sqrt{\hbar c/G}$, this allows us to fix the fermion mass to $m \simeq 15$ keV for a spin and particle-antiparticle degeneracy factor of $g = 2$. Such a relativistic object would have a radius of $R_{\rm OV} = 4.45 R_{\rm S} \simeq 1.5$ light-days, where $R_{\rm S}$ is the Schwarzschild radius of the mass $M_{\rm OV}$. It would thus be virtually indistinguishable from a black hole of the same mass, as the closest stable orbit around a black hole has a radius of 3 $R_{\rm S}$ anyway.

Near the lower end of the observed mass range is the compact dark object located at the Galactic center [10] with a mass of $M_c \simeq 2.6 \times 10^6 M_\odot$. Interpreting this object as a degenerate fermion ball consisting of $m \simeq 15$ keV and $g = 2$ fermions, the radius is $R_c \simeq 21$ light-days $\simeq 7 \times 10^4 R_{\rm S}$ [2], $R_{\rm S}$ being the Schwarzschild radius of the mass M_c. Such a nonrelativistic object is far from being a black

†Permanent address: Rudjer Bošković Institute, P.O. Box 180, 10002 Zagreb, Croatia; Email: bilic@thphys.irb.hr

‡Email: viollier@physci.uct.ac.za

0146-6410/02/$ - see front matter
PII: S0146-6410(02)00136-9

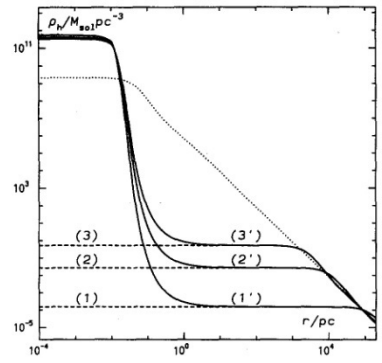

Figure 5: The density profile of the halo for $\eta_0 = 0$ (dotted line) and for the six η_0-values discussed in the text. Configurations with negative η_0 ((1)-(3)) are depicted by the dashed and those with positive η_0 ((1')-(3')) by the solid line.

For fixed N, there is a range of α where the Thomas-Fermi equation has multiple solutions. For example, for $N = 2\times10^{12}$ and $\alpha = 4\times10^{6}$ we find six solutions, which we denote by (1), (2), (3), (3'), (2'), and (1') corresponding to the values η_0 = -30.53, -25.35, -22.39, 29.28, 33.38, and 40.48, respectively. In Fig. 5 we plot the density profiles. For negative central value η_0, for which the degeneracy parameter is negative everywhere, the system behaves basically as a Maxwell-Boltzmann isothermal sphere. Positive values of the central degeneracy parameter η_0 are characterized by a pronounced central core of mass of about $2.5 \times 10^6 M_\odot$ within a radius of about 20 mpc. The presence of the core is obviously due to the degeneracy pressure. A similar structure was obtained in collisionless stellar systems modeled as a nonrelativistic Fermi gas [23].

Fig. 5 shows two important features. First, a galactic halo at a given temperature may or may not have a central core depending whether the central degeneracy papameter η_0 is positive or negative. Second, the closer to zero η_0 is, the smaller the radius at which the r^{-2} asymptotic behavior of the density begins. The flattening of the Galactic rotation curve begins in the range $1 \lesssim r/\mathrm{kpc} \lesssim 10$, hence the solution (3') most likely describes the Galactic halo. This may be verified by calculating the rotation curves in our model. We know already from our estimate (4) that our model yields the correct asymptotic circular velocity of 220 km/s. In order to make a more realistic comparison with the observed Galactic rotation curve, we must include two additional matter components: the bulge and the disk. The bulge is modeled as a spherically symmetric matter distribution of the form [25]

$$\rho_b(s) = \frac{e^{-hs}}{2s^3}\int_0^\infty du \frac{e^{-hsu}}{[(u+1)^8-1]^{1/2}}, \tag{12}$$

where $s = (r/r_0)^1/4$, r_0 is the effective radius of the bulge and h is a parameter. We adopt $r_0 = 2.67$ kpc and h yielding a bulge mass $M_b = 1.5\times10^{10}M_\odot$ [26]. In Fig. 6 the mass of halo and bulge enclosed within a given radius is plotted for various η_0. The data points, indicated by squares, are the mass

Monthly Notices
of the
ROYAL ASTRONOMICAL SOCIETY

MNRAS **451,** 622–628 (2015) doi:10.1093/mnras/stv1016

On the core-halo distribution of dark matter in galaxies

R. Ruffini,[1,2⋆] C. R. Argüelles[2⋆] and J. A. Rueda[1,2⋆]

[1]*Dipartimento di Fisica and ICRA, Sapienza Università di Roma, Piazzale Aldo Moro 5, I-00185 Rome, Italy*
[2]*ICRANet, Piazza della Repubblica 10, I-65122 Pescara, Italy*

Accepted 2015 May 4. Received 2015 April 30; in original form 2015 March 31

ABSTRACT

We investigate the distribution of dark matter in galaxies by solving the equations of equilibrium of a self-gravitating system of massive fermions ('inos') at selected temperatures and degeneracy parameters within general relativity. Our most general solutions show, as a function of the radius, a segregation of three physical regimes: (1) an inner core of almost constant density governed by degenerate quantum statistics; (2) an intermediate region with a sharply decreasing density distribution followed by an extended plateau, implying quantum corrections; (3) an asymptotic, $\rho \propto r^{-2}$ classical Boltzmann regime fulfilling, as an eigenvalue problem, a fixed value of the flat rotation curves. This eigenvalue problem determines, for each value of the central degeneracy parameter, the mass of the ino as well as the radius and mass of the inner quantum core. Consequences of this alternative approach to the central and halo regions of galaxies, ranging from dwarf to big spirals, for SgrA*, as well as for the existing estimates of the ino mass, are outlined.

Key words: methods: numerical – galaxies: haloes – galaxies: nuclei – galaxies: structure – dark matter.

1 INTRODUCTION

The problem of identifying the masses and the fundamental interactions of the dark matter particles is currently one of the most fundamental issues in physics and astrophysics. The first astrophysical and cosmological constraints on the mass of the dark matter particle appeared in Cowsik & McClelland (1972), Weinberg (1972), Gott et al. (1974), Lee & Weinberg (1977), and Tremaine & Gunn (1979). As we will show, some inferences on the dark matter particle mass can be derived from general considerations based solely on quantum statistics and gravitational interactions on galaxy scales.

An important open issue in astrophysics is the description of the dark matter in terms of collisionless massive particles. Attempts have been presented to put constraints on its phase-space density by knowing its evolution from the cosmological decoupling until the approximate time of virialization of a dark matter halo. Phenomenological attempts have been proposed in the past in terms of Maxwellian-like, Fermi–Dirac-like or Bose–Einstein-like distribution functions. Since the 80's all the way up to the present, the problem of modelling the distribution of dark matter in terms of self-gravitating quantum particles has been extensively studied and contrasted against galactic observables. In Ruffini & Stella (1983), Viollier, Trautmann & Tupper (1993), Chavanis & Sommeria (1998), Bilic et al. (2002), Chavanis (2002a), Boyanovsky, de Vega & Sanchez (2008), Argüelles et al. (2013), Ruffini et al. (2013), Destri, de Vega & Sanchez (2013), Argüelles & Ruffini (2014), Argüelles et al. (2014), de Vega, Salucci & Sanchez (2014), Siutsou, Argüelles & Ruffini (2015), and references therein, this problem was studied by considering Fermi–Dirac statistics in different regimes, from the fully degenerate to the dilute one, and for different fermion masses going from few eV to keV. Instead, in Sin (1994), Hu, Barkana & Gruzinov (2000), Böhmer & Harko (2007), Boyanovsky et al. (2008), Spivey, Musielak & Fry (2013), and Harko (2014) the same problem was analysed in terms of Bose–Einstein condensates with particle masses from 10^{-25} eV up to few eV.

Attempts of studying galactic structures in terms of fundamental physical principles such as thermodynamics and statistical physics, has been long considered (e.g. Binney & Tremaine 2008) since galaxies present many quasi-universal self-organized properties such as: the constant mean surface density at one-halo scalelength for luminous and dark matter (Gentile et al. 2009); the Fundamental Plane of galaxies (Djorgovski & Davis 1987; Jorgensen, Franx & Kjaergaard 1996); or the fact that dark matter haloes can be well fitted by many different but similar profiles that resemble isothermal equilibrium spheres (e.g. de Blok et al. 2008; Chemin, de Blok & Mamon 2011; de Vega et al. 2014). Within the statistical and thermodynamical approach, the most subtle problem is the one of understanding the complex processes of relaxation which take place before a galactic halo enters in the steady states we observe. In the context of this paper, we will deal only with the (quasi) relaxed states of galaxies, and do not worry about the previous relaxation

⋆ E-mail: ruffini@icra.it (RR); carlos.arguelles@icranet.org (CRA); jorge.rueda@icra.it (JAR)

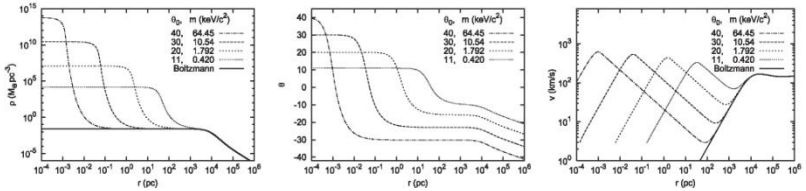

Figure 1. Mass density (left-hand panel), degeneracy parameter (central panel), and rotation velocity curves (right-hand panel) for specific ino masses m and central degeneracies θ_0 fulfilling the observational constraints (8). The density solutions are contrasted with a Boltzmannian isothermal sphere with the same halo properties. All the configurations, for any value of θ_0 and corresponding m, converge for $r \gtrsim r_{\rm h}$ to the classical Boltzmannian isothermal distribution. It is clear how the Boltzmann distribution, is as it should be, independent of m. Interestingly, when the value $M_{\rm c}(r \lesssim 10^{-2}\ {\rm pc}) \sim 10^6\ {\rm M}_\odot$ (i.e. $m \sim 10\ {\rm keV}/c^2$) is chosen as the one of more astrophysical interest, the onset of the classical Boltzmann regime takes place at distances of $r \gtrsim$ few 10^2 pc, in consistency with the observed cored nature of the innermost resolved regions in spiral galaxies as analysed in (de Blok et al. 2008).

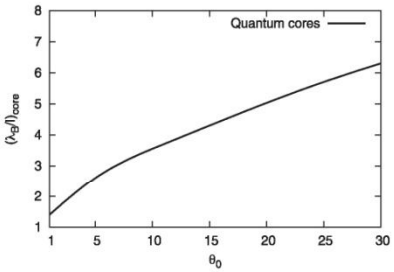

Figure 2. The less degenerate quantum cores in agreement with the halo observables (8) corresponds to $\theta_0 \approx 10$ ($\lambda_{\rm B} \sim 3 l_{\rm c}$). These cores are the ones which achieve the largest sizes, of order $\sim 10^1$ pc, and implying the lowest ino masses in the sub-keV region.

Table 1. Core properties for different equilibrium configurations fulfilling the halo parameters (8) of spiral galaxies.

θ_0	m (keV/c^2)	$r_{\rm c}$ (pc)	$M_{\rm c}$(M$_\odot$)	$v_{\rm c}$ (km s^{-1})	$\theta_{\rm c}$
11	0.420	3.3×10^1	8.5×10^8	3.3×10^2	2.1
25	4.323	2.5×10^{-1}	1.4×10^7	4.9×10^2	5.5
30	10.540	4.0×10^{-2}	2.7×10^6	5.4×10^2	6.7
40	64.450	1.0×10^{-3}	8.9×10^4	6.2×10^2	8.9
58.4	2.0×10^3	9.3×10^{-7}	1.2×10^2	7.5×10^2	14.4
98.5	3.2×10^6	3.2×10^{-13}	7.2×10^{-5}	9.8×10^2	21.4

as well as the numerical implications of β_0 and θ_0, they are given at the end of this section.

We define the core mass, the circular velocity at $r_{\rm c}$, and the core degeneracy as $M_{\rm c} = M(r_{\rm c})$, $v_{\rm c} = v(r_{\rm c})$ and $\theta_{\rm c} = \theta(r_{\rm c})$, respectively. In Table 1, we show the core properties of the equilibrium configurations in spiral galaxies, for a wide range of (θ_0, m). For any selected value of θ_0, we obtain the correspondent ino mass m to fulfil the halo properties (8), after the above eigenvalue problem of β_0 is solved.

It is clear from Table 1 and Fig. 1 that the mass of the core $M_{\rm c}$ is strongly dependent on the ino mass, and that the maximum space-density in the core is considerably larger than the maximum value considered in (Tremaine & Gunn 1979) for a Maxwellian distribution. Interestingly, as can be seen from Fig. 1, the less degenerate quantum cores in agreement with the halo observables (8), are the ones with the largest sizes, of the order of halo-distance-scales. In this limit, the fermion mass acquires a sub-keV minimum value which is larger, but comparable, than the corresponding sub-keV bound in (Tremaine & Gunn 1979), for the same halo observables. Indeed, their formula gives a lower limit $m \approx 0.05\ {\rm keV}/c^2$ when using the proper value for the King radius, $r_{\rm K} \simeq 8.5$ kpc, as obtained from $\sigma = \sqrt{2/5} v_{\rm h}$ and $\rho_0 = 2.5 \times 10^{-2}\ {\rm M}_\odot\ {\rm pc}^{-3}$, which are the associated values to the Boltzmannian density profile of Fig. 1. This small difference is formally understood by the following fact: while their conclusions are reached by adopting the maximum phase-space density, $Q^{\rm h}_{\rm max} \sim \rho_0^{\rm h} m^{-4} \sigma_{\rm h}^{-3}$, at the centre of a halo described by a Maxwellian distribution; in our model the maximum phase-space density is reached at the centre of the dense quantum core described by Fermi–Dirac statistics, $Q^{\rm c}_{\rm max} \sim \rho_0^{\rm c} m^{-4} \sigma_{\rm c}^{-3}$ (where lower and upper index c reads for the central core). An entire new family of solutions exists for larger values of central phase-space occupation numbers, always in agreement with the halo observables (see Fig. 1). Now, since these phase-space values, by the Liouville's theorem, can never exceed the maximum primordial phase-space density at decoupling, $Q^{\rm u}_{\rm max}$, we have $Q^{\rm h,c}_{\rm max} < Q^{\rm u}_{\rm max}$. Then, considering that all our quantum solutions satisfy $Q^{\rm c}_{\rm max} > Q^{\rm h}_{\rm max}$, it directly implies larger values of our ino mass with respect to the Tremaine and Gunn limit. Nevertheless, as we have quantitatively shown above, e.g. for the case of typical spiral galaxies, the two limits become comparable for our less degenerate ($\theta_0 \approx 10$) quantum cores in agreement with the used halo observables (8).

In the case of a typical spiral galaxy, for an ino mass of $m \sim 10\ {\rm keV}/c^2$, and a temperature parameter $\beta_0 \sim 10^{-7}$, obtained from the observed halo rotation velocity $v_{\rm h}$, the de Broglie wavelength $\lambda_{\rm B}$ is higher than the interparticle mean-distance in the core $l_{\rm c}$, see Fig. 2, safely justifying the quantum-statistical treatment applied here.

If we turn to the issue of an alternative interpretation to the black hole on SgrA*, we conclude that a compact degenerate core mass $M_{\rm c} \sim 4 \times 10^6\ {\rm M}_\odot$ is definitely possible corresponding to an ino of $m \sim 10\ {\rm keV}/c^2$ (see Table 1). However, the core radius of our configuration is larger by a factor of $\sim 10^2$ than the one obtained with the closest observed star to Sgr A*, i.e. the S2 star (Gillessen et al. 2009). Nevertheless, for an ino mass of $m \sim 10\ {\rm keV}/c^2$ ($\theta_0 = 30$), the very low temperature of the dense quantum core is already a small fraction of the Fermi energy (i.e. $\lambda_{\rm B} > l$), where additional

Bertrand's theorem

There are only two central potentials where all bounded orbits are closed and elliptical (L&L, Mechanics; Arnold, 1989)

$U_{OH}(r) = a\, r^2 \; (a>0)$ (harmonic oscillator potential)

and

$U_N(r) = -\, k/r$ (Newtonian potential)

Graduate Texts in Mathematics

V. I. Arnold

Mathematical Methods of Classical Mechanics

Second Edition

Springer-Verlag

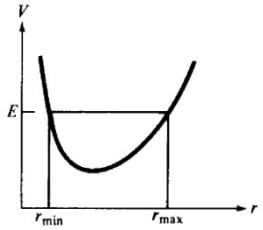

Figure 31 Graph of the effective potential energy

i.e., $\dot{r} = 0$. Therefore, the velocity of the moving point, in general, is not equal to zero since $\dot{\varphi} \neq 0$ for $M \neq 0$.

The inequality $V(r) \leq E$ gives one or several annular regions in the plane:

$$0 \leq r_{min} \leq r \leq r_{max} \leq \infty.$$

If $0 \leq r_{min} < r_{max} < \infty$, then the motion is bounded and takes place inside the ring between the circles of radius r_{min} and r_{max}.

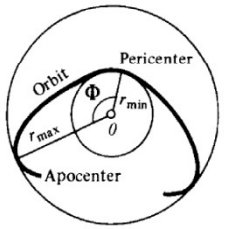

Figure 32 Orbit of a point in a central field

The shape of an orbit is shown in Figure 32. The angle φ varies monotonically while r oscillates periodically between r_{min} and r_{max}. The points where $r = r_{min}$ are called *pericentral*, and where $r = r_{max}$, *apocentral* (if the center is the earth—perigee and apogee; if it is the sun—perihelion and aphelion; if it is the moon—perilune and apolune).

Each of the rays leading from the center to the apocenter or to the pericenter is an axis of symmetry of the orbit.

In general, the orbit is not closed: the angle between the successive pericenters and apocenters is given by the integral

$$\Phi = \int_{r_{min}}^{r_{max}} \frac{M/r^2\, dr}{\sqrt{2(E - V(r))}}.$$

The angle between two successive pericenters is twice as big.

The smallest angle between apocenter and pericenter

- $\Phi_{OH}=\pi/2$
- $\Phi_{N}=\pi$

If astronomers monitor quasi-elliptical trajectories of stars with high eccentricities it is very easy to distinguish $U_{OH}(r)$ and $U_{N}(r)$ potentials since in the case of the RAR potential stars centers of ellipses should coincide with the Galactic Center while in the case of the Newtonian potential stars foci of the ellipses coincide with the Center. Orbital periods of stars moving in the harmonic oscillator potential are constant and they do not depend on semi-major axis. Even in the case if the Galactic Center position is not accurately known in respect to quasi-elliptical trajectories, a set of trajectories with high eccentricity clearly showed that the Newtonian potential is preferable and stars are moving around a common focus but not around a common center (Zakharov, 2021)

The most important conclusions

- C. Will (1986,1993): “Was Einstein right?”
- T. Damour (1994): “Was Einstein 100% right?”
- C. Will(2020): “Is Einstein still right?”
- Taking into account all experiments and observations
- (including observations of bright stars near BH@GC) at the moment one could say “Einstein was 100% right”
- It has been proven that $4*10^6$ $M_\odot$ is located inside 40 A.U. (Solar system size)
- We put several small bricks in the Great Wall of knowledge about BH @ GC

- 2019: Observers operating largest telescopes with AO use our ideas to constrain parameters of alternative theories of gravity
- 2020: GRAVITY showed that precession of S2 star follows GR predictions
- 2020: Keck constraints on fine structure constant

Main conclusions

- The gravity law near the BH @ GC has to follow GR (at least at the first PN-approximation). It leads from S2 precession and gravitational redshift the near pericenter passage
- We found graviton mass constraints which are comparable with LIGO's ones
- The observers working with largest telescopes with AO (Keck, VLT, GRAVITY, TMT, E-ELT) follow our ideas to improve current graviton mass constraints with current and forthcoming facilities. The current graviton mass LIGO constraint will be outperformed with current GRAVITY observation (private comm.)
- The observers use our ideas to constrain parameters of alternative theories of gravity with observations of bright stars near GC

• Conclusions

- Studies of great mathematicians (Kolmogorov, Penrose…) could have a giant practical impact in physics and technology
- Trajectories of bright stars or bright spots around massive BHs are very important tool for an evaluation of BH parameters
- Trajectories of bright stars or bright spots around massive BHs can be used to obtain constraints on alternative theories of gravity (f(R) theory, for instance)
- Constraints on Yukawa potential has been found
- Constraints of graviton mass have been obtained (they are consistent with LIGO ones)
- Perspectives to improve the current graviton mass estimates with future observations (VLT, Keck, GRAVITY, E-ELT, TMT) are discussed
- If an accuracy of the observations will be improved one should not need to observe entire quasi-elliptical orbit to test gravitational potential
- Constraints of tidal charge have been obtained
- The harmonic oscillator potential $U_{OH}(r)$ is not suitable for GC

- Thanks for your kind attention!
-